Targeting murine alveolarization using an *ex vivo* approach of isolated ventilated and perfused neonatal lungs

Inaugural Dissertation
submitted to the
Faculty of Medicine
in partial fulfillment of the requirements
for the PhD-Degree
of the Faculties of Veterinary Medicine and Medicine
of the Justus Liebig University Giessen

by
Reshma Jamal
Born in
Chennai, India

Giessen,2024

From the Max Planck Institute for Heart and Lung Research
Director: Prof. Dr. Werner Seeger
of the Faculty of Medicine of the Justus Liebig University Giessen

Supervisor and Examination Reviewer: Prof. Dr. Werner Seeger
Second Examination Reviewer and Committee Member: Prof. Dr. Peter Koenig
Examination Chair : Prof. Dr. Norbert Weissmann
Examination Vice Chair / Co-Supervisor: Prof. Dr. Ivan Manzini
Date of Doctoral Defense: 16 August 2024

1. Introduction

1.1. Comparative anatomy of mouse and human lungs

Lungs are the central organs of the respiratory system. Lungs provide the essential function of gas exchange for the survival of all cells in the body and to maintain homeostasis. Respiration happens through inhalation of oxygen from the atmosphere which enters the bloodstream and release of carbon dioxide from the blood stream to the alveoli and airways through expiration (Glenny & Petersson,2014). Lungs are organized into two zones (A) The conducting zone – It starts right from the nasal passage extending to the distal bronchioles and carries air into the lungs. (B) The respiratory zone – It includes respiratory bronchioles and alveoli which are the sites of gas exchange (Bailey,2021) (Figure 1).

Trachea serves as a principal tube which branches into two primary bronchi which further splits into secondary bronchi and further divide into several generations of bronchioles. In humans, the respiratory tree branches into 23 generation whereas in mice the respiratory tree branches into 13 generations (Bates & Irvin,2003). In mice, respiratory bronchioles are absent and the bronchioles directly open into alveoli unlike in humans, where respiratory bronchioles are present. The respiratory zone consists of millions of alveolar sacs which comprise the lung parenchyma and act as functional tissue taking up the maximum portion of the total lung volume (90%) (Ochs & Knudsen,2018). The bronchial tree is non-cartilaginous in mice when compared to humans where it is cartilaginous (Pan et al.,2019).

The total lung capacity of mice is 1 ml. Mice lungs consist of five lobes in the right and only one single lobe in the left. The blood-gas barrier in the mice is 0.32 μm thick (Bates & Irvin,2003) and plays an important role in gas exchange. Respiration rate of mice is high (250-350bpm) which is due to their high metabolic rate. Mouse lungs are known to have a very thin respiratory epithelium and a large airway lumen. The number of alveoli in adult mouse lung is approximately 2.31×10^6 alveoli. The alveolar and capillary surface area were calculated to be about 82.2 cm^2 and 124 cm^2 respectively considering the shrinkage of the organ during tissue processing steps (Knust et al.,2009). The lungs work in association with the heart, transporting blood from the heart to the lungs via the pulmonary artery. The pulmonary artery transports deoxygenated blood to the lungs where the gas exchange takes place through alveolar units. Oxygen disperses through the epithelium of the alveoli into the blood by surrounding capillaries and the oxygenated blood is taken by the pulmonary veins into the heart (Bailey,2021).

The mechanical properties of the lungs are crucial to assess the overall efficiency of the respiratory system (Faffe & Zin,2009). Elasticity of the lungs are well maintained by connective tissue components like collagen and elastin as a part of extracellular matrix (Bates,2009).
In-depth analysis of anatomy and physiology of mice will pave way to thorough understanding of various diseases and translate the results to find potential therapeutic drug targets in humans (Törmänen & Johnson,2019).

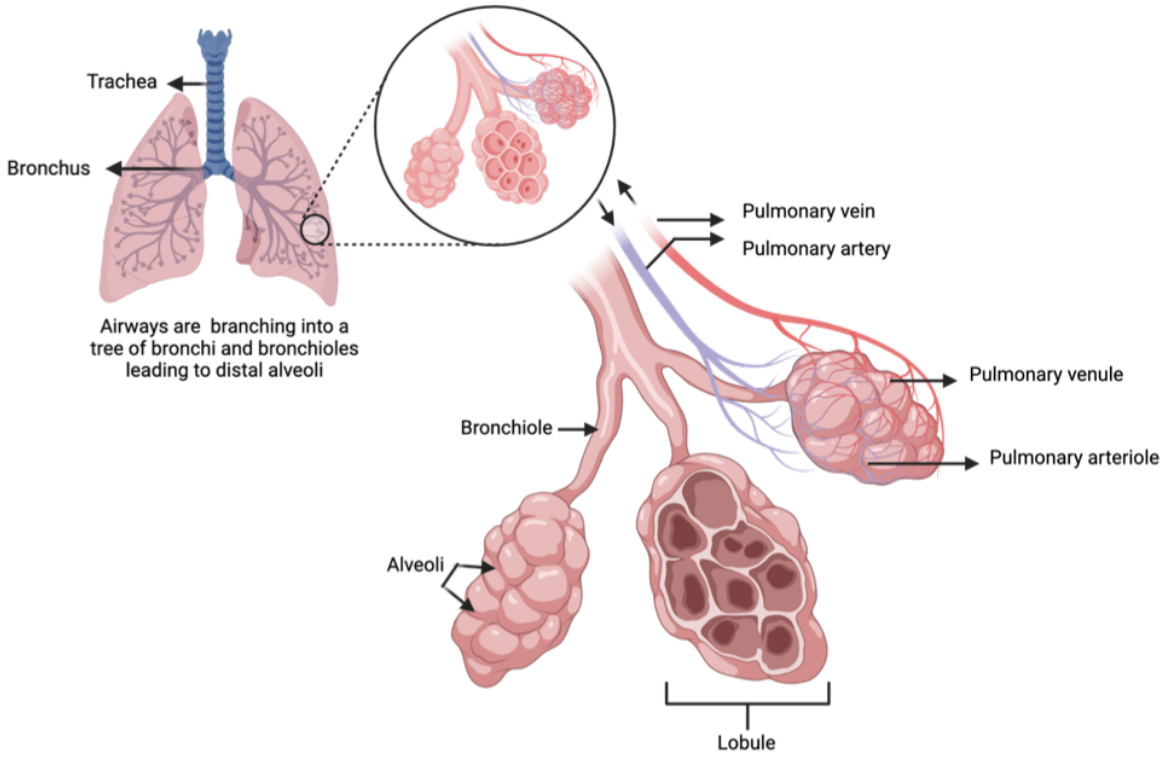

Figure 1: Schematic representation of the lungs showing the distal alveolar gas exchange unit. Lungs are the organs of respiration with the central function of gas exchange which takes place in the alveoli, the distal units of the lungs. The capillary network of the alveoli carries deoxygenated blood through the pulmonary artery to the alveoli and oxygenated blood through the pulmonary vein from the alveoli to the body. Illustration created with BioRender.com (Adapted from Atlas of Anatomy, Gilroy et al.,2008).

1.2 Stages of lung development

As an organ of gas exchange, lungs possess tree like branches which originate from a tiny lung bud during the embryonic stage and continues to outgrow and branch by the phenomenon of branching morphogenesis. The distal region of the lung undergoes expansion of the gas exchange area by the process of forming new alveolar walls (septa) allowing the formation and maturation of new alveolar sacs. This process is called alveolarization (Schittny,2017).

Lung development is classified into 5 different stages:

A. Embryonic stage
B. Pseudoglandular stage
C. Canalicular stage
D. Saccular stage
E. Alveolar stage

These stages have their own timelines in mice and humans as listed below (Table 1): (Burri,1999)

Table 1 : Stages of lung development in mice and humans. E : Embryonic day, P : Postnatal day

Stage No.	**Developmental stage**	**Mice**	**Humans**
1	Embryonic stage	E8-9.5	Week 3-7
2	Pseudoglandular stage	E9.5-16.5	Week 7-17
3	Canalicular stage	E16.5-17.5	Week 17-27
4	Saccular stage	E17.5-PN5	Week 27- 36
5	Alveolar stage	P5-P30	Week 36- approx. 7-10 years

During the **embryonic stage**, lung bud originates from the foregut endoderm and paves way for the onset of lung formation. The lung bud extends in ventral and caudal direction and remains initially as an open connection with the foregut . This foregut during development gets separated and forms the esophagus (Burri,1999). The lung bud then divides into the right and left primary bronchial buds (Figure 2). The upper/stem part of the lung bud forms into trachea and larynx (Schittny et al.,1998). In humans, by the fifth week of gestation the primary bronchial bud gives rise to three secondary bronchial buds which in turn give rise to ten tertiary bronchial buds in the embryonic phase of development (Moore at al.,2016).

The **pseudoglandular stage** is significantly marked by the process of branching morphogenesis (Figure 2 (Schittny et al.,2008). In mice, there occurs approximately thirteen generations of branching of the bronchial tree leading into the terminal bronchioles. The epithelial cells lining

the airways differentiate into various cell types, and the lung tissue starts to resemble a glandular structure (Moore et al.,2016).

The **canalicular stage** is characterized by the establishment of capillary network. The terminal bronchioles further divide into respiratory bronchioles. These structures are the precursors to the alveolar sacs and are crucial for establishing the future gas exchange area. The close association of capillaries with the developing alveoli begins, setting up the functional respiratory membrane. (Sadler,2012).

In the **saccular phase**, the respiratory bronchioles give rise to a final generation of terminal bronchioles which open up into the primitive sac shaped alveoli which are lined with alveolar epithelial cells type I and type II cells. Type II alveolar epithelial cells produce surfactants. These are the substance that reduces surface tension within the alveoli, preventing their collapse and aiding in their expansion during breathing. The capillary network around the alveolar sacs becomes more dense and well-integrated, enhancing the potential for efficient gas exchange.(Vrachnis et al., 2013).

The **alveolar phase** of lung development is characterized by the formation and maturation of new alveoli which continues to develop until the early adulthood. In humans and mice, secondary septa formation happens during bulk alveolarization after which occurs the maturation of alveoli (Figure 2). Immature alveoli have a double capillary bed which later turns into a single capillary bed (Caduff et al.,1986). During this stage, new septa are formed from the already existing septa by the process of secondary septation.

In mice, bulk alveolarization occurs between P5 to P10 where major secondary septation occurs and new alveoli are formed (Schittny & Mund, 2008).

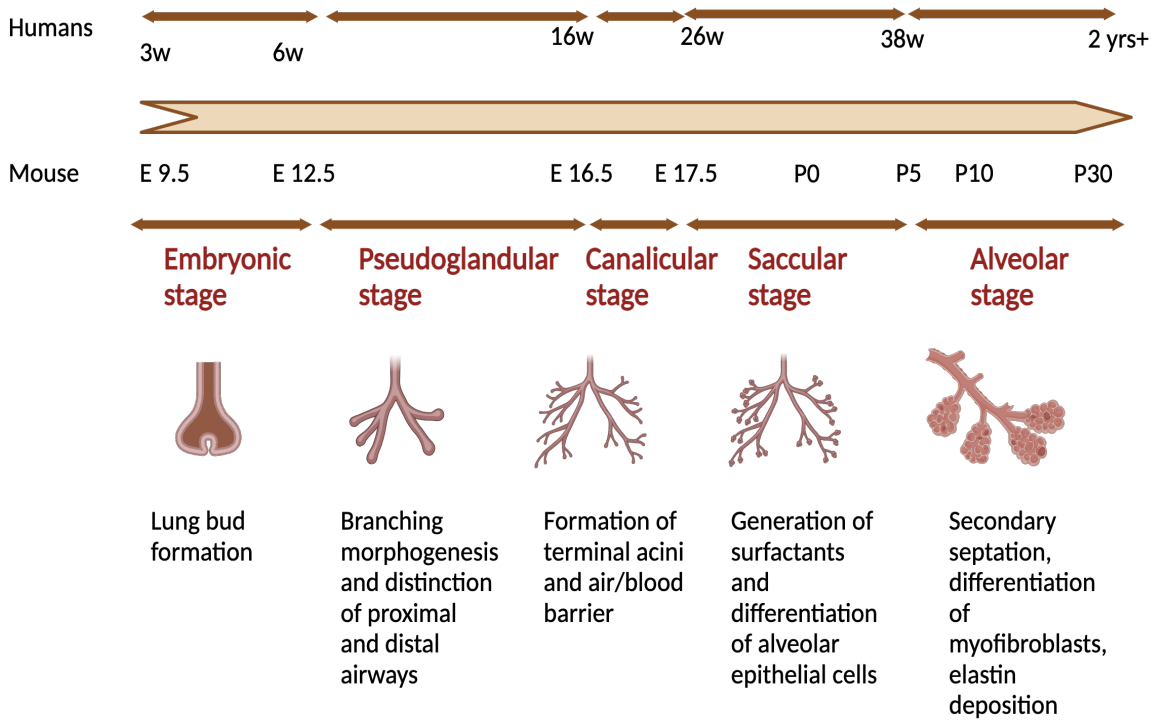

Figure 2: Schematic representation of different stages of lung development and their respective timelines in mice and humans. This figure illustrates the progression of lung development through different stages, from the initial formation of lung bud structure to the establishment of mature alveoli capable of effective gas exchange. E – embryonic, P- postnatal, w-weeks. Illustration created with Biorender.com (Adapted from Iliodromiti et al., 2013).

Hematoxylin and eosin-stained (H&E) lung sections representing secondary septation enabling clear visualization of the developing and mature alveolar structures. during the process of alveolarization are depicted in Figure 3.

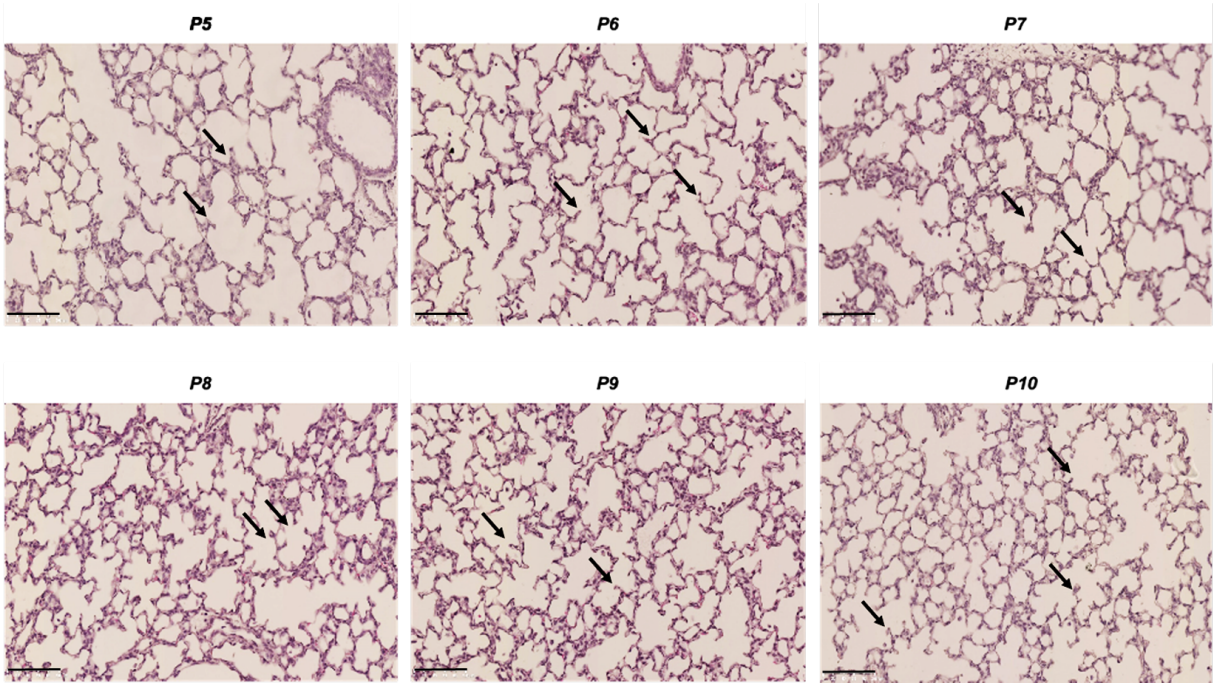

Figure 3: **Secondary septation in mice during the process of alveolarization**. Representative images of lung sections from postnatal mice of age 5 days to 10 days. H and E staining was performed on 3µm paraffin sections. Arrows in the figure point out to secondary septa. P-postnatal. Scale bar: 100 µm.

1.3 Cellular composition of the distal lung

Postnatal development of the lungs involves alveoli formation by secondary septation enabling efficient gas exchange (Boyden et al.,1965). Several studies have been conducted to gain deep insights into cells involved during alveolarization and secondary septa formation during development and in the process of lung regeneration after injury (Barkaukas et al.,2013). Alveolar air-blood barrier is created by a respiratory membrane consisting of alveolar epithelial cell and a capillary endothelial cell (Swan et al.,2011) The thin, squamous, alveolar type I epithelial cells cover approximately 96% of the internal region of the alveoli and play a major role in gas exchange. These thin-walled cells enable diffusion of gases. Alveolar type I cells communicate with alveolar type II epithelial cells to secrete surfactant proteins in response to the stretch stimuli (Howatt et al.,1965). The surfactants include a mixture of phospholipids and proteins produced by alveolar epithelial type II cells. Alveolar epithelial type II cells contain organelles called lamellar bodies where the surfactants are stored. There are four different surfactant proteins SP-A, SP-B, SP-C and SP-D (Agassandian et al.,2013, Kasper et al.,2017). Lung interstitial cells are mesenchymal cells and participate in alveologenesis. Alveolar mesenchymal cells play an important role in lung development by interacting with other different cell types to promote septation (Zepp et al.,2017). Lung mesenchymal cells include, adventitial fibroblasts, lipofibroblasts, myofibroblasts, smooth muscle cells in regions of airways, vasculature and pericytes (Torday et al.,1995). Myofibroblasts express smooth muscle actin and are involved in the development of secondary crests and act as a source of elastin at the tips of the secondary septa (Burri et al.,1974, Dickie et al.,2008). Lung lipofibroblasts are known to provide triglycerides for surfactant synthesis and serve as important source of retinoic acid (Al Alam et al.,2015). Elastin fibers accumulate at the septal crests causing the formation of septum. Fibroblast growth factor (FGF) and Platelet-derived growth factor A (PDGF-A) play an important role in lung development and secondary septa formation (Lindahl et al.,1997).

Pulmonary endothelial cells and alveolar epithelial type I cells share a common basement membrane and are conjoined by tight junctions forming a barrier to prevent fluid infiltration into the alveoli (Herriges et al.,2014). Pulmonary endothelial cells are highly heterogeneous and play an important role in lung angiogenesis forming the pulmonary vasculature (Eldridge et al.,2019)

Tissue resident alveolar macrophages facilitate phagocytosis and engulf microbes with lysosomes and destroy pathogens. Macrophages clear up foreign particles which escape via the mucus to the upper respiratory tract (Naeem et al.,2022).

1.4 Lung diseases affecting the alveolar structure in neonates and adults

Newborn babies who are born prematurely have difficulty in breathing and cause diseases like bronchopulmonary dysplasia (BPD), neonatal respiratory distress syndrome (NRDS), meconium aspiration syndrome (Gallacher DJ et al.,2016).

Neonatal respiratory distress syndrome in preterm infants occurs due to insufficient surfactants in lungs. Surfactants produced by alveolar epithelial type II cells aids in reducing surface tension thereby increasing the gas exchange. Insufficient surfactants results in increased respiratory effort by newborn preterm infants for lungs to expand during breathing and cause alveolar collapse (Ghafoor et al.,2003). Life-saving treatments such as mechanical ventilation and/or oxygen supplementation can, however, cause acute and chronic lung injury, resulting in Bronchopulmonary dysplasia, a neonatal chronic lung disease, that is characterized by hyper inflated lungs, impaired alveolarization as well as vasculature development (Jobe et al.,2001). In addition to prematurity-related chronic lung disease or VILI, there several other acute and chronic conditions beyond infancy causing lung diseases. Several pulmonary diseases affect the alveolar structure in adults. Their impact is either transient or permanent.

Examples of **acute lung diseases** include (i) Pneumonia-It is the inflammation of the alveoli, causing the air sacs to fill with fluid or pus. Severe pneumonia can result in fibrotic damage. Both viral and bacterial pneumonia impact alveolar function (Gaitonde et al.,2019, Cunha,2001). (ii) Acute bronchitis-It is the inflammation of the bronchial lining leading to increased mucus production and cough. Acute bronchitis manifests as inflammation without evidence of pneumonia and typically affects individuals without underlying chronic obstructive pulmonary disease (COPD) (Adams et al.,1999).

Examples of **chronic lung diseases** include (i) Chronic Obstructive Pulmonary Disease (COPD) – A group of progressive lung diseases that cause airflow obstruction and breathing difficulties. Subtypes of COPD include A) Emphysema : It is characterized by the destruction of alveolar walls, leading to enlarged air spaces and reduced gas exchange (Vogelmeier et al.,2020) B) Chronic bronchitis : It is characterized by chronic inflammation of the bronchial tubes and excessive mucus production. (Janssen et al.,2019). (ii) Pulmonary fibrosis -These are diseases affecting the interstitium of the lung. Fibrosis of the lung causes thickening and stiffening of the tissue resulting in scarring. Fibroblasts are attracted to the site of the scar and

causes inflammation (Richeldi et al.,2017). Oxygen exchange is disrupted due to impaired alveolar structure in the fibrotic lungs. They can be idiopathic (Idiopathic Pulmonary Fibrosis, IPF) or secondary to other conditions such as autoimmune diseases, occupational exposures, or drug reactions. (iii) Asthma : A chronic inflammatory disease of the airways that leads to recurrent episodes of wheezing, breathlessness, chest tightness, and coughing. Airway inflammation and hyperreactivity lead to reversible bronchoconstriction and increased mucus production. It can be triggered by allergens, respiratory infections, exercise, smoke, and environmental pollutants (Fireman,2003).

Pulmonary edema is a symptom of acute/chronic lung injury. It refers to the accumulation of extravascular fluid in the parenchyma of the lungs decreasing the gas exchange function. It is a pathologic feature in various diseases. There are two classes of edema 1. Cardiogenic pulmonary edema – It is caused by heart failure and back pressure of lung blood vessels (Weismann ,2005). 2. Noncardiogenic pulmonary edema – It causes leakage of fluid due to lung injury (Ware et al.,2005).

Since my research project focuses on the effects of ventilation on the newborn lung, the following sections will refer to this in particular.

1.4.1 Ventilator-induced lung injury (VILI)

Premature infants are prone to ventilator-induced lung injury (VILI) due to unfavorable factors like insufficient surfactants, non-uniform ventilation and partial presence of amniotic fluid in the lungs (Carvalho et al.,2013). Lung injury caused due to ventilation have been long studied and has been the contributing factor for mortality in patients with various respiratory diseases like acute respiratory distress syndrome (ARDS) (Brower et al.,2000) and bronchopulmonary dysplasia (Jobe et al.,2001). Alveolar structure largely gets compromised due to edema formation as a consequence of VILI (Tomashefski 1990).The major mechanisms causing ventilation mediated lung injury includes high inflation pressure (barotrauma) and overdistension due to high volume (volutrauma) (Beitler et al.,2016). Lung injury also occurs due to cyclic strain occurring during mechanical ventilation. Transpulmonary pressures and end expiration pressures also contribute to damage when they reach their maximum peaks in magnitude. Ventilation induced lung injury also activates proinflammatory cytokines leading to systemic inflammation (Tremblay et al.,1997).

1.5 Models to study lung development

1.5.1 *In vivo* and *in vitro* models in pulmonary research

***In vivo* models** : Laboratory mice, both wildtype and transgenic mice have been widely used in basic pulmonary research, to study gene function and regulation and to find targets using disease models. Wildtype inbred mice or transgenic mice developed using Cre-lox technology have been extensively used to study lung specific sub populations (Rawlins & Perl,2012) (Table 2). Though transgenic mice have been effective in targeting the cellular population of interest in lung, the off-target effects on other organs is a major drawback (Manghwar et al.,2020) (Table 2). There exists early embryonic lethality in homozygous mutants making it difficult to analyze the embryonic and developmental stages of interest (Papaioannou & Behringer,2012).

Table 2 : **List of commonly used mouse lines in pulmonary research to target subpopulation of cells in lungs**

No.	Lung subpopulation	Mouse strain	Reference
1	Endodermal progenitors	Shh-Cre, Nkx2-5-Cre, Gata 5- Cre	Harfe et al.,2004, Moses et al.,2001, Xing et al.,2001
2	Alveolar epithelial type I cells	Aqp5-Cre	Flodby et al.,2010
3	Alveolar epithelial type II cells	Sftpc-CreER^{T2}	Chapman et al.,2011
4	Clara cells	Scgb1a1-rtTA	Perl et al.,2011
5	Ciliated cells	Foxj1-Cre	Rawlins et al.,2007
6	Basal cells	Krt5-Cre	Rock et al.,2009
7	Smooth muscle cells	Sm22-CreER^{T2}	Kühbandner et al.,2000

***In vitro* models** : In recent years, there has been major progress in the development of several *in vitro* models which are designed to mimic *in vivo* conditions (Figure 4). *In vitro* models ranges from the basic monolayer cell culture model to advanced 3D culture models (Conway et al.,2020).**Monolayer cell cultures** are the standard adherent cell cultures. Cells grow attaching to an artificial membrane (Hahon & Zimmerman,2020). The cell culture medium provides all required nutrients for the cells to grow and allows cells to proliferate. It is relatively easier to remove the necrotic cells as they are usually detached and can be removed my changing the medium. **Air liquid interface** (ALI) made a breakthrough in the field by allowing the cells to grow on a porous membrane in an air interface between the growing cells and the cell culture media (Lacroix et al.,2018). ALI plays an important role in studying the respiratory epithelial cells due to physiological relevance of the model to study the air to cell interaction. (Gultom et al.,2020). **Precision Cut Lung Slices** (PCLS) have also been widely used. It involves slicing fresh lung tissue into precise sections which are usually 200-500µm thick. These sections retain the structural and functional properties of the lung tissue. Slices can be maintained in culture for several days to weeks, providing extended observation periods

(Pieretti et al.,2014). Several **3D cell cultures** have been developed for both proximal and distal regions of the lungs like the bronchiolar sphere, bronchoalveolar lung organoids (BALO) to study the junction between the bronchi and the alveoli and the distal alveolospheres comprising alveolar epithelial, mesenchymal and endothelial cell types (Vazquez-Armendariz et al.,2020;da Costa et al.,2021). 3D organoids are self-organizing. Stem cells are grown in matrigel matrix to form organoids and plays critical role in understanding interaction between different cell types (Strikoudix et al.,2019). (4) **Lung-on-a-chip** is a novel *in vitro* technique making use of a microfluidic device that mimics the mechanical, chemical, and biological properties of the lung, including its cellular and structural components. The chip contains microchannels that simulate the airways and blood vessels of the lung. These channels allow for the flow of fluids, mimicking airflow and blood flow. (Shreshtha et al.,2020)

Major advantages of *in vitro* models include reduced usage of experimental animals and minimal cost involved in performing the experiments. Despite its advantages, cells grown *in vitro* models do not fully represent the complex microenvironment that exists in a tissue and hence the need to develop physiologically relevant models emerge (Sakagami,2006).

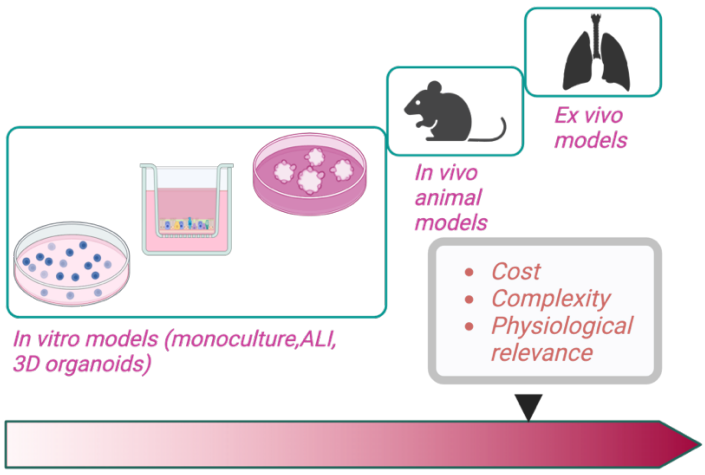

Figure 4: Schematic representation of different models to study lung development and pulmonary diseases. Hierarchy of different models starting from the *in vitro* models to the *in vivo models* and later to the *ex vivo* approaches based on the physiological relevance, cost and complexity of the experimental models. Illustration created with BioRender.com. (Adapted from Lacroix et al.,2018).

1.5.2 *Ex vivo* lung models in pulmonary research:

1.5.2.1 *Ex vivo* ventilated and perfused lung model in small animals

The *ex vivo* ventilated and perfused model involves isolating a lung from a mouse and maintaining it in a functional state where it is mechanically ventilated and perfused with a physiological solution. This setup preserves the lung's structural and functional characteristics, allowing for detailed experimental analysis. Isolated, ventilated and perfused lung models are studied in small animals like mice and rats. The isolated lung is ventilated by an appropriate ventilator and the lungs are connected to a perfusion circuit that delivers a physiological solution through the pulmonary vasculature. This circuit usually includes a perfusion pump which maintains continuous flow of the perfusate through the lung's blood vessels, mimicking normal blood flow. The perfusion solution consists of a balanced mixture of electrolytes, nutrients, and sometimes oxygen to support tissue viability. Albumin or other plasma proteins are often included to maintain oncotic pressure. The perfusate may be oxygenated using an oxygenator to simulate arterial blood oxygen levels. This *ex vivo* experimental setup is used to study lung physiology and pathology allowing researchers to investigate various aspects of lung function, including gas exchange, vascular responses, and the effects of interventions, in a controlled environment. Several studies on hypoxic pulmonary vasoconstriction have employed isolated, ventilated and perfused model to understand the pathophysiology of the disease (Yoo et al.,2013). The main advantage is the low cost to conduct such experiments with small animals. Among the above-mentioned small animals, mice are the most commonly used animal models. It is advantageous to use mice as a model organism for isolated, ventilated and perfused lung model due to the availability of various protein antibodies and genetic probes.

Small animals have their own disadvantage due to their fragile nature and undergo ventilation damage rapidly. The degree of injury is higher and more difficult to repair whereas in large animals, atelectasis can be identified or edema can be removed via bronchoscopy due to their bigger size, which is not easily possible in small animals (Ghadiali. et al.,2009). Isolated, ventilated and perfused lung model in mice have been largely studied to achieve non-injurious ventilation strategies with various tidal volume and PEEP values (Wolthuis et al.,2009) (Table 3)

Table 3: Mechanical ventilation parameters in adult C57Bl/6 mice.

No	Parameter	Mice
1	Tidal Volume	7-8ml /kg
2	PEEP (Positive end expiration pressure)	2-3 cm H_2O
3	Respiration rate	120 breaths/min

1.5.2.2 *Ex vivo* ventilated and perfused lung model in large animals

These models involve isolating the lung from a large animal (such as a pig or sheep) and maintaining it in a functional state with mechanical ventilation and perfusion systems. This setup aims to replicate the lung's physiological environment as closely as possible. The experimental setup components are similar to small animals with the exception of size. A Porcine model of isolated, ventilated and perfused lung acts as closest model to humans. This model has highest gene sequence similarity to humans making it more comparable. This model serves as a direct path for clinical relevance making it a superior model (Critser et al.,2009). Larger animals have a major disadvantage of increased animal cost, large sized equipment and space required add to the cost. The amount of perfusate consumed in performing isolated pig lung model is much higher than small animals making it expensive performing larger experimental replicates. An advantage of large animal models would include an easier preparation of the animal for the procedure due to the larger size when compared to smaller animals. It also provides an opportunity to use the same equipment that can be used in human clinical trials. (Steen et al.,2003).

The physiological parameters used in larger animal models like tidal volume, positive end expiration pressure (PEEP), perfusion flow rate better reflect the physiological parameters of human lung (Table 4) (Nelson et al.,2014).

Table 4: Physiological *ex vivo* lung parameters of a pig compared to the normal human values.

No	Parameter	Pig	Human
1.	Tidal Volume	6-8 ml/kg body weight	6-8 ml/kg body weight
2.	PEEP (Positive end expiration pressure)	5 cm H_2O	3-5cm H_2O
3.	Pulmonary artery pressure	10-15mm Hg	12-20mm Hg

1.5.2.3 *Ex vivo* ventilated and perfused lung model in humans

Animal models for experimental research have been used extensively to study human respiratory physiology. However, these models do not match the basic anatomical and physiological differences between animals and humans, causing major challenges to translate findings to clinical trials. Thereby, human *ex vivo* pulmonary models have been developed. (Matthay et al.,2019). In recent years, *ex vivo* lung ventilation and perfusion model in humans has become more relevant in lung transplantation centers and has become a method for lung preparation and preservation. It has been studied that using this method, human lungs could be evaluated before transplantation into the recipient. Using this model lungs could be rehabilitated if the lungs were atelectatic or edematous. By this method, viability of the lungs could be

improved, and the number of available healthy lungs could be substantially increased in the lung transplantation community **(**Weathington et al.,2018). *Ex vivo* studies were also conducted on human lungs to evaluate the supine position or prone position in which *ex vivo* ventilated and perused lungs worked more effectively. It was found that placement of lungs in prone position during *ex vivo* ventilation and perfusion caused reduced ischemia reperfusion injury (IRI), providing better static compliance and less inflammation (McCurry et al.,2022).

Ex vivo lung ventilation and perfusion are performed at a physiological temperature of 37 ℃ by restoring the ventilation and circulation in the lungs through a specific perfusate. A membrane oxygenator is used in the *ex vivo* model to mimic the oxygen consumption in the body via deoxygenation. The *ex vivo* lung ventilation and perfusion model in humans comprises a ventilator, an endotracheal cannula, a specific perfusate, a membrane oxygenator, a pump and a thermostat. *Ex vivo* lung ventilation and perfusion of donor lungs becomes invalid in case of severe infection like pneumonia or when multiple lobes of the lungs are injured. (Pan et al.,2018). Currently, there are different types of *ex vivo* lung ventilation and perfusion models performed in humans namely (i) Toronto system (ii) Lund system – It is the extended slightly modified version of the *ex vivo* lung protocol (iii) Organ care system (OCS), the portable *ex vivo* lung ventilation and perfusion system (Watanabe et al., 2021). Donor lungs for transplantation are cryopreserved after harvest and lungs are connected to the *ex vivo* lung ventilation and perfusion device along with perfusion and are transported at the ambient temperature to the recipient. Evaluation of the lungs after the *ex vivo* procedure can be performed by bronchoscopy and lungs can be imaged to eliminate other abnormalities like edema, embolism and infection. Parameters of mechanical ventilation are to be maintained throughout the procedure. Blood gas analysis and hemodynamics evaluation are also performed in the lungs and helps in determining the overall quality of the lungs before transplantation (Loor et al.,2021).

The major disadvantage of the human *ex vivo* lung ventilation and perfusion is a very low availability of organs and the huge variability that exists between different donor lungs. (Galasso et al.,2019)

Lungs that undergo acute and chronic lung injury do not survive well on *ex vivo* lung ventilation and perfusion model without any additional interventions. An alternative approach was developed which links human *ex vivo* ventilated and perfused lung connected to porcine providing a cross-circulation to the human lungs. In the study, conducted by (Hozain et al.,2020). Injured human lungs were connected to a living pig whose venous blood was used to perfuse the lungs and gas exchange was provided via mechanical ventilation.

Immunosuppressants were provided to prevent cross-reactions and xenogeneic rejections. Human lungs were maintained in such conditions up to 24 hours and found a profound improvement on lung function and overall health. Thereby this model provides a new approach to repair or recover injured lungs prior to transplantation. This model serves as a great tool to study organ repair and regeneration (Kelly Wu et al.,2022).

1.6 Modes of ventilation

Most commonly studied modes of ventilation include positive and negative pressure modes of ventilation. Positive and negative pressure ventilation refers to two different methods of assisting or controlling breathing through mechanical ventilation. They differ in how they manipulate air into and out of the lungs.

1.6.1 Positive pressure mode of ventilation

In the positive pressure ventilation mode, air is pushed into the airways using a mechanical ventilator. The pressure gradient causes the air to flow into the airways down to the alveoli (Pinsky,1994). The positive pressure ventilation can either be volume controlled or pressure controlled. Tidal volume is the volume of air inhaled or exhaled with each breath. In tidal volume-based ventilation, the ventilator is set to deliver a specific tidal volume with each breath, regardless of the pressure required to achieve that volume. A specific tidal volume is set based on the weight of the mice, whereas in pressure-controlled ventilation, a gradient of inspiratory and expiratory pressures is fixed to enable an appropriate ventilation. The volume of air delivered can vary depending on the lung mechanics. (Gali & Goyal,2003). Atelectasis is a condition where there is a collapse of the lung either partially or completely. To prevent atelectasis, a positive pressure remains at the end of each expiration cycle to avoid collapse of the lung.

Different terminologies used in ventilation:

1. Tidal volume – Tidal volume refers to the amount of air moving into and out of the lungs on each cycle of respiration.
2. Positive end expiration pressure (PEEP) – PEEP is the pressure that exists in the lungs at the end of the expiration. There are two types of PEEP. Intrinsic PEEP : Intrinsic PEEP occurs when expiration is incomplete and lungs are not completely deflated to

reach an equilibrium point. Extrinsic PEEP: Extrinsic PEEP is the pressure applied during mechanical ventilation.

3. Inspiratory pressure – Inspiratory pressure is the pressure delivered to the airways and the alveoli.
4. Respiration rate –Respiration rate refers to the number of breaths/min.

1.6.2 Negative pressure mode of ventilation

Negative pressure ventilation involves the generation of negative pressure on the surface of the thorax thereby causing the lungs to expand and allow air to flow in during inflation. Negative pressure ventilation is known to mimic physiological respiration (Corrado & Gorini, 2002). Sub atmospheric pressures used in this mode of ventilation causes expansion of the thorax. Negative pressure mode of ventilation does not force air into the lungs, thereby a reduced risk of barotrauma (lung injury due to excessive pressure). Negative pressure was introduced in the clinical setting, during the polio pandemic in mid 20th century and named the device employed as iron lung (Corrado et al.,1996) It consisted of a horizontal cylinder inside which the patient is laid. Apart from the head, rest of the body is sealed inside the cylinder. Air is pumped in and out of the cylinder which caused changes in pressure and generation of vacuum inside the cylinder enabling the patient to inhale and exhale.

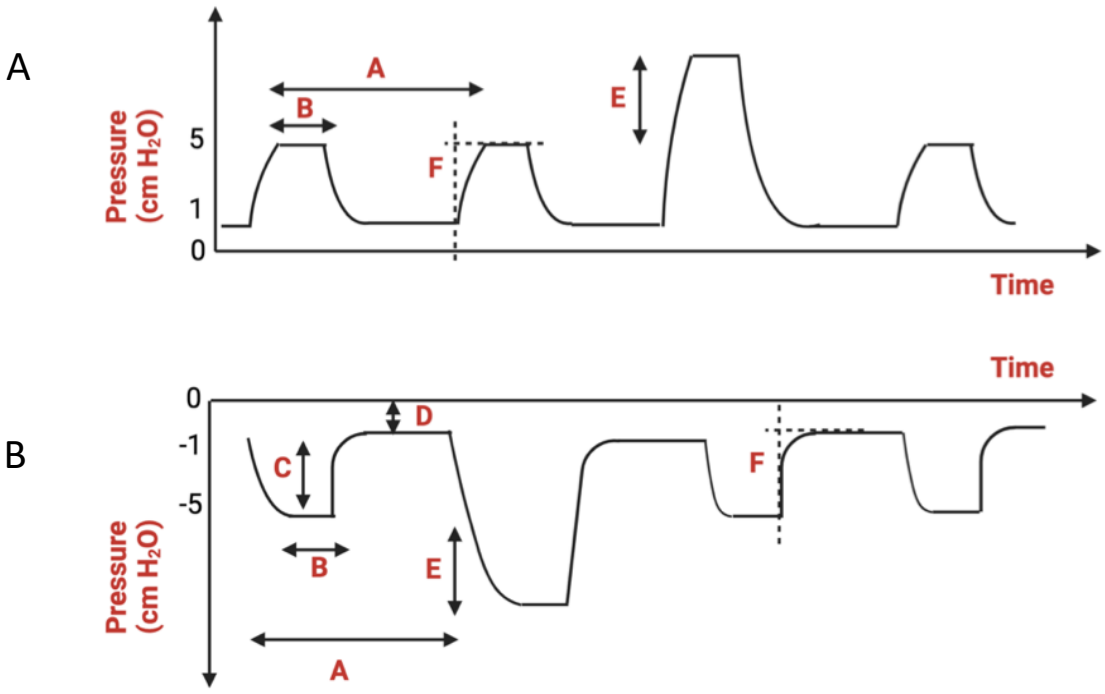

Figure 5: Scheme representing the pressure vs time curves during positive and negative pressure ventilation modes. A) Positive pressure ventilation curve. B) negative pressure ventilation curve. **(**Adapted from Operating instructions of Hugo Sachs PLUGSYS® module VCM type 681). Illustration created with BioRender.com.

- **A.** Duration of one cycle of respiration(Inspiration + Expiration)
- **B.** Inspiration duration
- **C.** Inspiration phase in negative pressure system
- **D.** End expiration in negative pressure system. (PEEP in case of positive pressure)
- **E.** Deep inspiration mode set up to the entire inspiratory reserve volume to prevent atelectasis.
- **F.** Distortion of the pressure curve resulting from the dead volume in the artificial thorax.

1.7 Lung perfusion solutions

Several different perfusate solutions have been used in isolated, ventilated and perfusion lung models. In our present study, we utilized several different formulations of perfusion medium to study alveolarization.

The buffer **Krebs-Henseleit Buffer (KHB)** was used as a perfusate solution to initially optimize the *ex vivo* system with respect to the flow rate of the perfusate. KHB buffer was widely used in the isolated adult mouse lung protocols. The composition of this buffer was designed adapting the physiological levels (Table 5).

Table 5 : Composition of Krebs-Henseleit Buffer (KHB)

NaCl	**125 mmol/liter**
KCl	4.3 mmol/liter
KH_2PO_4	1.1 mmol/liter
$CaCl_2$	2.4 mmol/liter
$MgCl_2$	1.3 mmol/liter
Glucose	275mg/100ml

Sodium bicarbonate was used to adjust the final pH. It was important to bubble this buffer with carbon dioxide to maintain a physiological pH between 7.37- 7.4. Glucose in the medium acts as exogenous carbon source for the metabolism. KHB remained to be a protein-free buffer making the oncotic pressure physiologically lower thereby leading to excessive edema in this model, despite the minimal flowrate of the system.

STEEN Solution™ was developed to enable the perfusion of *ex vivo* human lungs, making them suitable for transplantation (Medeiros et al.,2012).This buffer solution included human serum albumin which helped in maintaining the optimal osmotic pressure. Dextran 40 present in the solution coated the endothelium and aided in protecting it from leukocyte interaction.

Epithelial cell medium consisted of basal medium with essential and non-essential amino acids, vitamins, growth factors supplemented with 4% human serum albumin.

The use of human serum albumin aided to maintain the osmotic pressure. Highly cellular lung structure was observed with Steen solution and methylprednisolone was utilized to suppress immune cell activity. Different combinations of growth medium and growth factors were titrated at several different concentrations to maintain the lungs in desired experimental conditions.

Alveologenesis medium (adapted from Pieretti et al.,2014) consisted of M199 media supplemented with vitamin A, vitamin C and hydrocortisone. The former was known to improve alveolarization and the latter was employed to inhibit inflammation.

2. Aim of the project:

Lung diseases such as bronchopulmonary dysplasia (BPD), chronic obstructive pulmonary disease (COPD), idiopathic pulmonary fibrosis (IPF), and acute respiratory distress syndrome (ARDS) disrupt alveolar structure and integrity in infants and adults leading to compromised lung function. Elucidating the mechanisms underlying alveolar development will provide insights into how alveoli form and mature, which is crucial to studying normal lung function and understanding regeneration processes after lung injury. Several *in vivo* and *ex vivo* models are available to study lung development. The use of transgenic mice is often constrained due to a global lethal phenotype due to on/off-target effects. *In vitro* models such as the 2D cell culture model, 3D organoids model, and precision cut lung sections (PCLS) lacked stretch forces induced by breathing movements. Developing a model mimicking physiologic ventilation and perfusion would provide an opportunity to study and manipulate mechanisms of normal structural lung maturation *ex vivo*. Therefore, this project aims to establish an *ex vivo* model of ventilated and perfused neonatal mouse lungs in order to enhance our understanding of how alveolar structures in the lungs are formed by studying the process of alveolarization in *ex vivo* conditions. The sub-aims of the project (Figure 6) include,

1. **Establishment** of an *ex vivo* lung ventilation and perfusion setup for neonates to mimic alveolarization.

2. **Optimization** of the established *ex vivo* model to reduce ventilation-related lung damage.
3. **Characterization** of the *ex vivo* ventilated and perfused neonatal lungs in terms of alveolar structure and gene expression.

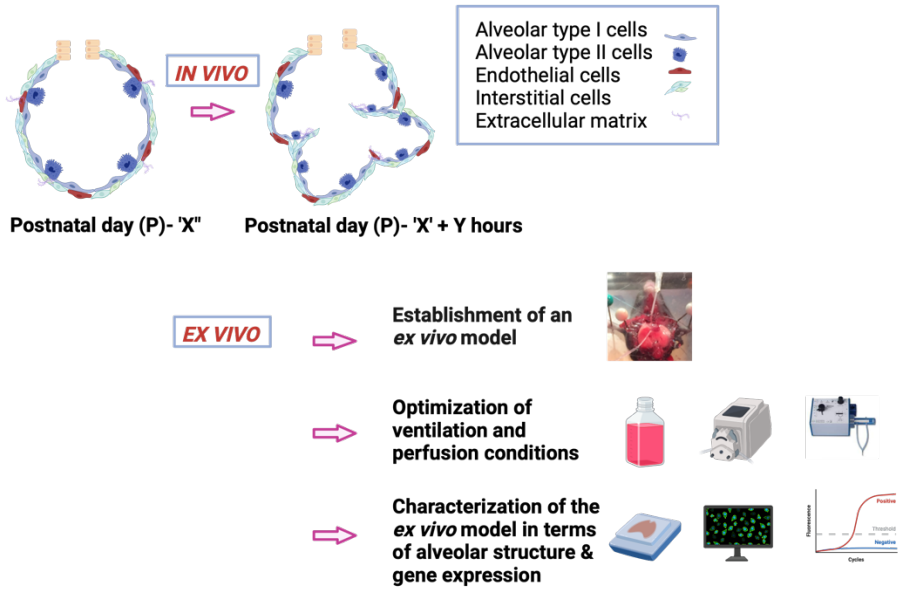

Figure 6: Aims of the study include: (1) Establishment of the *ex vivo* ventilation and perfusion of postnatal mice lung model. (2) Characterization of *ex vivo* ventilated and perfused postnatal lungs. Non-ventilated *in vivo* grown lungs served as control. (3) Optimization of the established *ex vivo* ventilation and perfusion model for postnatal lungs. Postnatal day (P). Created with BioRender.com

3. Materials

3.1 Equipment

Product	Company
3-Stop Tygon® E-Lab Tubing, 0.89 mm ID, 12/pack, Orange/Orange	Hugo Sachs Elektronik, Germany
Airway/Thoracic Pressure Transducer MPX, Range ± 100 cmH_2O, HSE Connector	Hugo Sachs Elektronik, Germany
Automated microtome (Leica RM 2165)	Leica Microsystems, Germany
Base unit for the mouse Isolated Perfused Lung (73-2329)	Hugo Sachs Elektronik, Germany

BD Microlance 3 special cannulas 30 G 1/2 0.3 x 13 mm (yellow)	BD Biosciences, Germany
Block Clamp to Mount Second Transducer	Hugo Sachs Elektronik, Germany
Cidex	Fleischhacker, GmbH&Co.KG, Germany
Coverslips 24x36 mm	Menzel GmbH&Co.KG, Germany
Dako Pen (PAP Pen) – Fat marker	Kisker Biotech GmbH & CoKG
Differential Low-Pressure Transducer DLP2.5, Range ± 2.5 cmH_2O, HSE Connector	Hugo Sachs Elektronik, Germany
Discofix® C three-way valve	B. Braun SE, Germany
Embedding cassettes	Leica Microsystems, Germany
F25 Refrigerated/Heating Circulator	JULABO GmbH, Germany
Filtered tips (10 µl, 100 µl, 1000 µl)	Nirbe plus, Germany
Greiner CLiP® Neo 24 G	Vigmed AB, Sweden
Greiner CLiP® Neo 26 G	Vigmed AB, Sweden
Heating chamber	Memmert, Germany
Histological glass slides 25x75x1 mm (SuperFrost UltraPlus®)	R. Langenbrinck, Germany
Ice machine	Castelmac SPA, Italy
Injekt ® Luer Solo 10ml	B. Braun SE, Germany

Injekt ® Luer Solo 1ml	B. Braun SE, Germany
Injekt ® Luer Solo 5ml	B. Braun SE, Germany
Ismatec Peristaltic pump, REGLO ICC.	Cole-Parmer Instrument Company Ltd, United Kingdom
Ismatec Tygon tubing ID:0.19mm Wall 0.90mm (Orange/Red)	IDEX Health &Science GmbH, Germany
Isopropyl alcohol (99.8%)	Merck KGaA, Germany
Lab Stand with Triangular Base Plate	Hugo Sachs Elektronik, Germany
Micro cannulation system (18000-10)	Fine Science Tools (F.S.T), Germany.
Micro tubes (0.5 ml, 1.5 ml, 2.0 ml)	Saarstedt, Germany
Microtome blades (MX35 Premier)	Thermo Fisher Scientific, USA
MicroVent Ultra-Low Volume Ventilator, Type 848	Harvard Apparatus, USA
Moria MC31 Forceps - curved/serrated Graefe Forceps - straight/serrated Spring Scissors - straight, 8mm Cutting edge.	Fine Science Tools (F.S.T.), Germany Fine Science Tools (F.S.T.), Germany Fine Science Tools (F.S.T.),Germany Fine Science Tools (F.S.T.),Germany
Mounting medium (Pertex®, 41-4012- 00)	Medite GmbH, Germany
Nano drop (ND-1000)	Kisker-Biotech, Germany
Needles (BD Microlance 3®)	Becton Dickinson GmbH, Germany

Nonabsorbable braided silk suture thread, Size 6/0 (18020-60)	Fine Scientific Tools (F.S.T), Germany
Paraffin cooling station Leica EG 1150C	Leica, Germany
Paraffin embedding station Leica EG 1140H	Leica, Germany
PCR Plate sealer PX1	Biorad, Germany
pH meter-766 Calimatic	Knick, Germany
PLUGSYS Case, Type 603	Hugo Sachs Elektronik, Germany
PLUGSYS Time Counter Module (TCM)	Hugo Sachs Elektronik, Germany
PLUGSYS Transducer Amplifier Module (TAM-A)	Hugo Sachs Elektronik, Germany
PLUGSYS Transducer Amplifier Module (TAM-D) – For perfusion pressure measurement	Hugo Sachs Elektronik, Germany
PLUGSYS Ventilation Control Module with Integral Pump (VCM-P)	Hugo Sachs Elektronik, Germany
Precellys® 24 bead beating Tissue Homogenizer	Thermo Fisher Scientific, USA
Real-Time polymerase chain reaction (PCR) Detection System (CFX Connect)	Biorad, Germany
Seraflex® surgical thread USP 5/0, EP1	Serag Wiessner,Naila, Germany.
Silk Suture Thread Size 6/0 (22,5m)	Fine Science Tools (F.S.T.), Germany
Silk Suture Thread Size 7/0 (90m)	Fine Science Tools (F.S.T.), Germany
Superfrost Plus Gold glass slides	Gerhard Menzel B.V. & Co. KG, Germany
Syringes (Injekt®-F) (1 ml, 2 ml, 5 ml, 20 ml)	B.Braun, Germany
Table centrifuge mikro 200R	Hettich, Germany

Thermocycler T3000	Biometra, Germany
Thermomix/Frigomix Circulator	B. Braun SE, Germany
Ultrapure Milli-Q® water	Millipore, Germany
Vortexer MS1 shaker	IKA GmbH, Germany.
Warp red chromogen kit	Biocare Medical, USA
Water bath used during paraffin sectioning	Leica Microsystems, Germany
Weighing balance	Mettler Toledo, Switzerland
Zyto Chem Plus AP Polymer System (Mouse/Rabbit)	Zytomed Systems GmbH, Germany

3.2 Reagents:

Name	Company
1X Insulin/Transferrin/Selenium	Gibco, Thermo Fischer Scientific, USA
Antibody Diluent (ZUC025-100)	Zytomed Systems, Germany
Bovine serum albumin (BSA)	Merck KgaA, Germany
Cell proliferation ELISA BrdU (colorimetric) 1000X conc	Roche, Germany
Complete epithelial cell medium kit	Cell Biologics, USA
Eosin Y, alcoholic (6766007)	Thermo Fisher Scientific, USA
Ethanol 70% Ethanol 96% Ethanol 99.6%	SAV Liquid Production GmbH, Germany Otto Fischar GmbH & Co. KG, Germany Otto Fischar GmbH & Co. KG, Germany
Fluor mount	Serva Electroforesis GmbH, Germany
Formaldehyde (3,5 – 3,7%, stabilized with methanol)	Otto Fischar GmbH & Co. KG, Germany
Heparin- Natrium 5000 I.E	Ratiopharm, Germany

Human – Albumin 20%	CSL Behring GmbH,Germany
Hydrocortisone	Sigma-Aldrich, USA
Isotonic Sodium chloride solution 0.9%	B. Braun SE, Germany
Modified M199 media	Thermo Fisher Scientific, USA
Nuclease Free water	Thermo Fisher Scientific, USA
PBS (Phosphate buffered saline)	Pan Biotech, Germany
Platinum™ SYBR™ Green qPCR Super Mix-UDG	Thermo Fisher Scientific, USA
RNeasy ®Mini Kit (74106)	Qiagen, Germany
Rodent decloaker buffer (10x)	BioCare medical
Rodent M blocking solution	Fisher Scientific, USA
STEEN™ solution	XVIVO Perfusion, Sweden
TRIS (4855.2)	Carl Roth, Germany
Tris wash buffer (TBS, 20%)	Zytomed Systems GmbH
TritonX-100 (X100)	Merck KGaA, Germany
Urostamin®,100mg/ml	Serumwerk, Germany
Vitamin A	Sigma-Aldrich, USA
Vitamin C	Sigma-Aldrich, USA
Warp Red Chromogen Kit (WR 806)	Biocare medical, USA
Xylazine 20mg/ml	Serumwerk, Germany
Xylol	Carl Roth, Germany
β-Mercaptoethanol (4227.3)	Carl Roth, Germany

3.3 Softwares

Name of the software	Company
BioRender.com	BioRender, Canada
GraphPad Prism 9.0	GraphPad software, USA
ImageJ	NIH, USA
Leica LAS	Leica, Germany
Leica Qwin	Leica, Germany
Microsoft Office package	Microsoft, USA

NDP scan	Hamamatsu Photonics, Japan
NDP.view2	Hamamatsu Photonics, Japan

3.4 Cell culture media composition

Epithelial cell culture medium

Epithelial cell culture medium from Cell Biologics, USA, consisted of 500 ml of basal medium. The medium composition included essential and non-essential amino acids, organic and inorganic compounds, vitamins, hormones, growth factors, and trace minerals supplemented with 0.5 ml Insulin-Transferrin-Selenium (ITS), 0.5 ml epithelial growth factor (EGF), 5 ml antibiotic-antimycotic solution, and 4% human albumin.

Alveologenesis medium

Alveologenesis medium composed of modified M199 basic medium from Thermo Fisher Scientific, USA, containing 0.6N NaOH supplemented with 2% FCS, 1% penicillin, streptomycin, fungizone, 2µg/ml vitamin C, 0.1 µg/ml hydrocortisone,0.1µg/ml of retinoic acid and 4% human albumin. BrdU (1X) was also supplemented to the media to study ongoing proliferation in the lungs of the *ex vivo* model.

3.5 Anesthesia mixture:

Injection (I.P)

- Dosage: 20 mg xylazine /kg body weight and 100 mg ketamine hydrochloride /kg body weight.
- Preparations: Ketamine (Ketamine 10%, 100 mg/ml); Xylazine (Rompun® 2%, 20 mg/ml) Additionally, anti-coagulant added.
- Dosage: 50 I.U. heparin/g body weight
- Preparation: Heparin sodium 250,000 IU (10 ml), Ratiopharm GmbH, Ulm
- Dilution: NaCl
- For 1 ml injection preparation - 0.1 ml xylazine + 0.1 ml ketamine + 0.6 ml sterile 0.9% NaCl solution + 0.2ml Heparin.

3.6 Primer sequences used in qRT-PCR:

Table 6: Primer sequences used for assessing gene expression by qRT-PCR

Gene	Forward Primer	Reverse Primer
Podoplanin (*Pdpn*)	ACAGGGCAAGTTGGAAGC	TGGGAGATGGCCAAGACATC
Surfactant protein C (*Sftpc*)	GGTCCTGATGGAGAGTCCAC	GATGAGAAGGCGTTTGAGGT
Smooth muscle alpha-2 actin (*Acta2*)	GTCCCAGACATCAGGGAGTAA	TCGGATACTTCAGCGTCAGGA
Perilipin-2 (*Plin2*)	CCTCAGCTCTCCTGTTAGGC	CACTACTGCTGCTGCCATTT
Proliferation marker protein* Ki-67 *(Mki67)	GTCGCTTTGGACAGTGAACCT	TTCTTGTTCTTAACTTCTTGGTGCAT
Fibroblast growth factor (*Fgf 10*)	GTCAAAGCCATCAACAGCAAC	CCTCTCCTGGGAGCTCCTTT
Wnt family member 5a (*Wnt5a*)	ATGCAGTACATTGGAGAAGGTG	CGTCTCTCGGCTGCCTATTT
Platelet and endothelial cell adhesion molecule 1 (*Pecam1*)	AGCCTCACCAAGAGAACGGA	GCACAGGACTCTCGCAATCC
Vimentin (*Vim*)	CACTAGCCGCAGCCTCTATTC	GTCCACCGAGTCTTGAAGCA
Porphobilinogen deaminase (*Pbgd*)	ATGTCCGGTAACGGCGGC	GGTACAAGGCTTTCAGCATCG

Different alveolar cell type compartments was analyzed by qRT-PCR with the above marker gene expression. PBGD (Porphobilinogen deaminase) served as an internal housekeeping control gene. Primer sequences are listed in Table 6.

4. METHODS

4.1 Experimental mice

In this study, C57BL6/J wild-type mice were employed in experiments. Mice were kept in ventilated cages and provided food and water *ad libitum*. Breeding of these mice was planned accordingly, and pups born were utilized for the experiments. Mice from postnatal day 5 to day 14 were used in the experimental procedures to achieve the aim of the project. Animal protocols in these investigations were approved by the Regierungspräsidium Giessen (G64/2019, G30/2022).

4.2 *Ex vivo* lung model for postnatal mice

4.2.1 *Ex vivo* lung model of ventilation and perfusion using positive pressure mode of ventilation

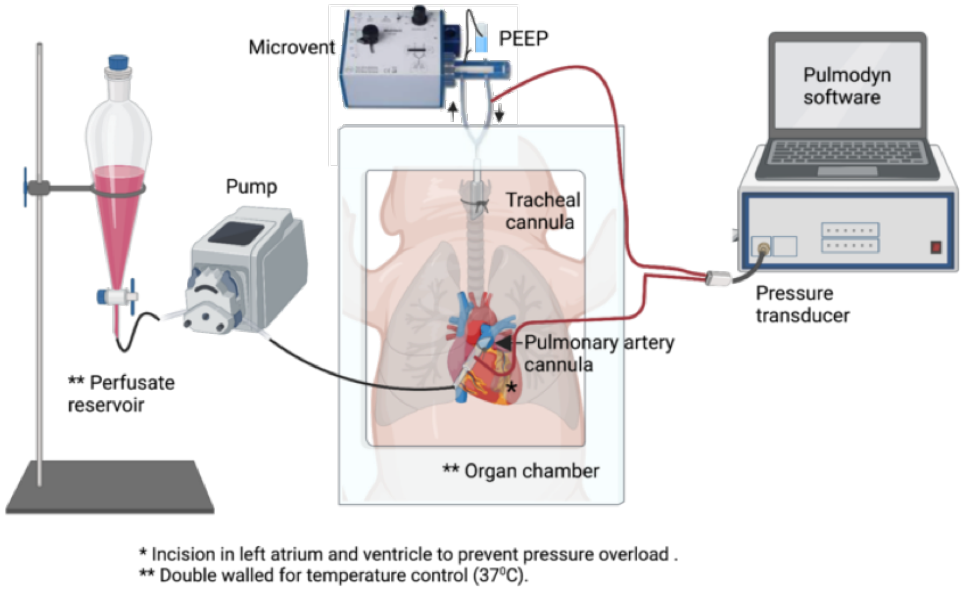

Figure 7: Schematic representation of the *ex vivo* lung model of positive pressure ventilation and perfusion. Ventilation was provided by a micro vent based on tidal volume (volume-controlled). The perfusate reservoir contained the cell culture medium. The medium was pumped into the pulmonary artery through a peristaltic pump using a constant flow of 10µl /min. Positive end expiration pressure (PEEP) was employed through tubing inserted into the water column to prevent the collapse of the lungs . Lungs was placed in a water jacketed temperature-controlled chamber. Ventilation and perfusion pressures were monitored using the Pulmodyn software.

Positive pressure ventilation involved the air being delivered to the lungs by applying a positive pressure (Figure 7). This increased the interalveolar pressure and the pressure gradient caused the air to flow into and out of the lungs. The positive pressure ventilation setup of the neonatal mice consisted of a perfusate reservoir, which carried the cell culture medium by a peristaltic pump at its lowest flow rate into the lungs via the pulmonary artery cannula. This system has no re-circulation, with the left atrium cut off for the media to flow out. The perfusate reservoir was a double-walled chamber that helped to maintain and stabilize the temperature at 37 ºC throughout the experimental procedure. Ventilation of the lungs was deployed using a Microvent ventilator (type 848) from Hugo Sachs Electronik GmbH with a gas mixture (5% CO_2, 21% O_2 and rest nitrogen). The micro vent worked as a constant-volume respiration pump. It included a rotary plunger without any valves. The plunger performed a continuous appropriate forward and rotating movement and provided controlled inspiration and expiration during each stroke. The microvent also consisted of a compartment to support the water column, which helped in setting up the PEEP. The core system of the device included a double-walled chamber where the extracted lungs were placed, to maintain the physiological temperature. The chamber consisted of a provision for attaching the pulmonary artery cannula. Ventilation and pulmonary artery pressure were measured through the transducers, and the values were displayed on the Pulmodyn software. The tracheal cannula for mice younger than P8 was made in-house using the 26G CLiP® neo and 24G CLiP® neo for ventilating mice older than P8 cannula. The pulmonary artery cannula was also made in-house using the delicate fine plastic part of the F.S.T micro cannulation system.

Prior to the experimental procedure, the entire system was flushed with cidex solution followed by flushing with distilled water. The zero calibration of the pressure measuring system was carried out before the start of the experiment. Mice were anesthetized with the anesthesia mix according to their body weight. The toe reflex was checked before starting the experiment. When no reflex was observed, mice were placed on a pad inside the chamber, and the surgical procedure of opening the pup was initiated by cutting the skin below the thorax, continuing up to the trachea. All muscles surrounding the larynx were cleared until the long tracheal tube was clearly visible. A knot was made for the tracheal suture using sera flex thread to fix the trachea. The cannula was inserted into the trachea by making a tiny cut below the larynx. The tracheal cannula's position was adjusted so that it was neither too deep nor too far away from the lung to provide optimal ventilation. Once the ventilation was established, tidal volume, respiration rate, and ventilation pressure were observed to confirm that there were no discrepancies observed.

Pressure-controlled positive pressure ventilation

Fixed airway pressures were titrated and utilized for pressure-controlled positive pressure experiments. Pressure-controlled ventilation was achieved by using a water column to release extra pressure created inside the lungs, thereby preventing over-inflation. Similarly, the positive end-expiratory pressure was created by inserting a tube inside the water column, which creates a pressure based on the principle of hydrostatic pressure thereby keeping the alveoli open after each expiration (Figure 8). The pressure gradient created by the inspiratory and expiratory pressure provides efficient ventilation in a pressure-controlled mode.

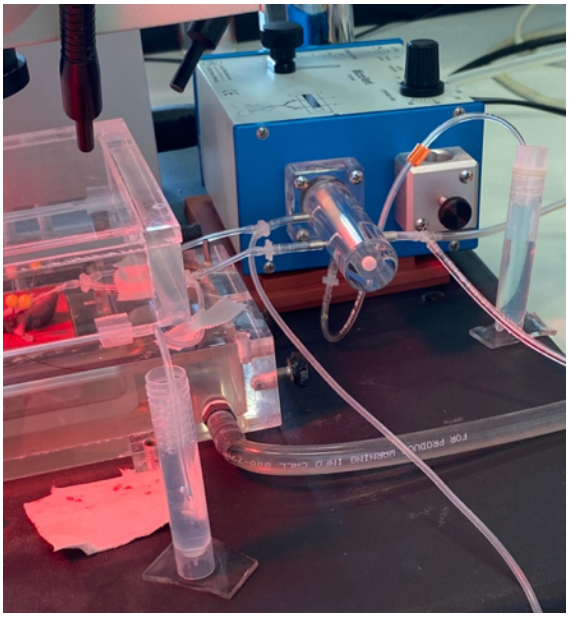

Figure 8: Pressure-controlled positive-pressure ventilation was achieved using tubing inserted into the water column. A pressure gradient was created between inspiratory pressure and the positive end-expiratory pressure (PEEP) by releasing excessive pressure built up inside the lungs through a tube (inspiratory) inserted into the water column.

4.2.2 *Ex vivo* model of negative pressure ventilation and perfusion in postnatal mice lungs

The negative pressure ventilation system in neonatal mice was developed using the ventilation control module with a pressure regulator (VCM-R) type 681 of the PLUGSYS® system from Hugo Sachs GmbH. This module works with both positive and negative pressure. Positive pressure was used during the experimental lung preparation and then was shifted to a negative pressure module during the actual experiment.

The ventilation was generated with the help of nozzles. Positive pressure was generated using a restrictor nozzle and negative pressure was generated rhythmically using a venturi nozzle. The ventilation control module worked by providing a compressed gas supply from a tank in the range of 2-8 bar. During positive pressure ventilation, a gas mixture (5% CO_2, 21% O_2, and rest nitrogen) for ventilation was turned on. The gas mixture was passed on through the restrictor nozzle to provide positive rhythmic pressure at the desired magnitude. The rhythm of the airflow was controlled electronically based on inspiration and expiration pressures, respiration rate, and deep inspiration breath with the help of the corresponding controls in the ventilation control module. After the preparation of the mouse (steps of the preparation similar to the positive pressure ventilation system as described in 4.2.1) with the pulmonary artery cannula, the ventilation mode was shifted to negative pressure. The venturi nozzle created a vacuum providing the required negative pressure. The magnitude of the vacuum was controlled in the ventilation module.

The negative pressure ventilation setup for the neonatal mice is illustrated in Figure 9 and consisted of the perfusate reservoir filled with cell culture medium passing through a peristaltic pump to the pulmonary artery cannula. Mice were placed in a double-walled chamber at a temperature of 37 ºC. This system provided both positive and negative pressure modes of ventilation. Preparation was kept in the positive pressure mode and shifted to negative pressure mode for the experiment through a 3-way stopcock valve. Perfusion through the pulmonary artery was established, similar to the positive pressure mode of ventilation with the help of an in-house cannula. The pulmodyn software recorded the tracheal pressure, the pulmonary artery pressure and the chamber pressure using appropriate transducers.

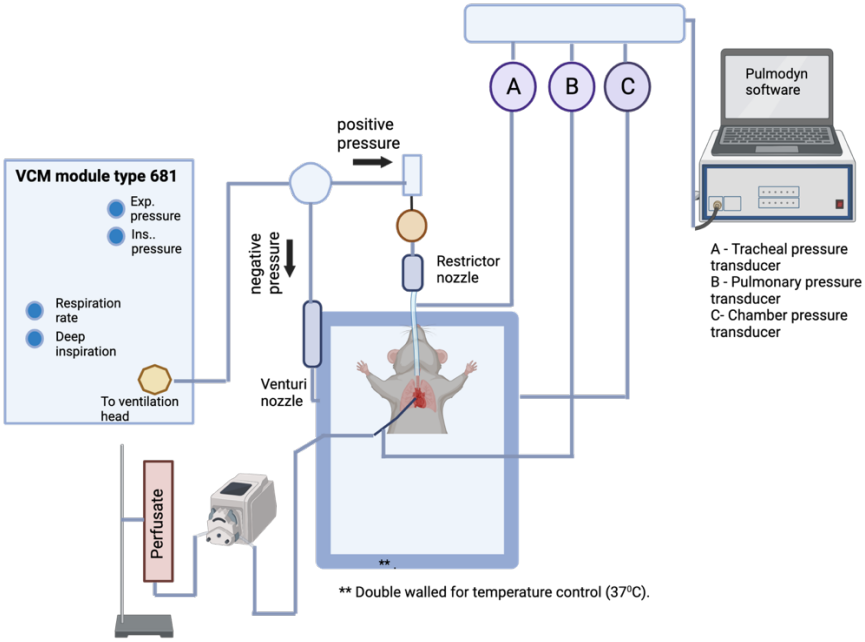

Figure 9: Schematic representation of negative pressure mode of ventilation and perfusion. Lungs were placed in a temperature-controlled chamber. The perfusate reservoir carried the cell culture medium by a peristaltic pump into the lungs via the pulmonary artery cannula. The VCM module type 681 provided the controls for the positive and negative pressure through a 3-way stop-clock valve by their respective nozzles. Pulmodyn software monitored the tracheal, pulmonary artery, and chamber pressures.

4.3 Lung fixation and tissue processing

Lungs were flushed with sterile saline solution by cutting the right ventricle and inserting the cannula into the pulmonary artery. Lungs were flushed until they turned white, confirming they were blood-free. This was followed by fixation of lungs with 4% paraformaldehyde (PFA) through the trachea at a pressure of 20 cm H_2O. Lungs stayed in 4% PFA for 24 hours at room temperature and were then shifted to PBS at 4°C until the tissue was processed for dehydration. Lungs were embedded in paraffin for further sectioning and staining.

4.4 Sectioning of lungs embedded in paraffin blocks

Lungs were embedded in paraffin after fixation. The paraffin blocks were cut into thin sections using a microtome. Sections of 2 µm were cut for hematoxylin and eosin staining. Sections of 5 µm were used for immunofluorescence staining.

4.5 Hematoxylin and eosin staining

Lung section slides were deparaffinized by placing the slides in the incubator at 60 °C for 1 hour. Slides were then washed in xylol (3X) for 10 minutes, followed by 5 minutes washes of reducing concentrations of ethanol (99.6 % (*v*/*v*), 96 % (*v*/*v*),70 % (*v*/*v*) followed by 2 minutes washing step with distilled water. Lung tissues were next stained with Mayer's Hematoxylin solution for 20 minutes followed by 5 minutes tap wash with flowing tap water over the slides. Following it was the immersion of slides in eosin-y-alcoholic solution for 4 minutes and a brief rinse with distilled water. Lung tissues were then dehydrated twice with 96 % (*v*/*v*) ethanol for 2 minutes and then with 99.6 % (*v*/*v*) ethanol for 5 minutes. Slides were submerged for 5 minutes in isopropanol, three times submerged for 5 minutes in Xylol, and mounted with Pertex, which served as mounting medium.

4.6 Alveolar morphometry

Lung sections that were formalin-fixed and embedded in paraffin were cut into 2 µm sections and deparaffinized with triple xylol treatment and rehydrated with decreasing ethanol concentrations and stained with hematoxylin and eosin. Stained sections were used for alveolar morphometry measurements. Total lung scans were performed using a Leica microscope (Leica, Wetzlar, Germany) and analyzed using Leica Q win V3 software to analyze alveolar wall thickness, mean linear intercept, and total airspace. Mean Linear Intercept (MLI) refers to the average distance between the airspaces in the lung. Horizontal lines were placed across each lung and the length of each line that intersects airspace was measured. The ratio of total length of lines (L) to the number of intercept with airspaces (N) provided the mean linear intercept.
MLI = Total length of lines/Number of intercepts with airspaces = L/N.
Airspace percentage represented the proportion of lung's total volume occupied by airspaces. It was calculated as follows :
Airspace percentage = (Area of airspace)/(Total area of tissue section) * 100
The analysis was done on the alveolar compartment of the lungs with the exclusion of bronchi and vessels above 50µm diameter. The air space was determined to be a non-parenchymatous, non-stained area. This software was previously described (Pichl et al., 2019; Seimetz et al., 2011; Seimetz et al., 2015; Weissmann et al., 2014). The parameters measured included mean linear intercept, percentage of air, and septal thickness.

4.7 Gene expression analysis by quantitative reverse transcriptase PCR (qRT-PCR)

RNA isolation and cDNA preparation

Frozen lung tissue was homogenized in a homogenizer with ceramic beads including 300 µl RLT buffer and 3 µl beta mercaptoethanol per sample. RNA isolation was carried out using the Qiagen RNeasy® mini kit. Mini spin columns were filled with 300 µl of 70% ethanol. Columns were centrifuged for 15 seconds at 10,000 rpm at 20 °C. The supernatant was discarded and 700 µl of RL1 wash buffer was added to the tubes and centrifuged for 15 seconds at 10000 rpm. The supernatant was again discarded, and 500 µl of RPE buffer was added, and the sample was centrifuged for 1 minute at 10000 rpm. The supernatant was discarded, and 35 µl of RNAse-free water was added directly to the membrane and centrifuged at 10,000 rpm for 1 minute. Isolated RNA samples were placed on ice to avoid degradation. RNA concentration was determined using a photometric method using a nanodrop.

Complementary DNA (cDNA) was prepared using the iScript-cDNA synthesis kit. A master mix was prepared with 4 µl of iScript ™ reaction mix, 1 µl of reverse transcriptase, the required amount of RNA sample, and RNAse-free water to reach the target concentration of 1µg of RNA. PCR strips were loaded into the thermal cycler, and the program for cDNA preparation was started.

Master mix:

The below master mix (Table 7) was prepared (per sample):

Table 7: Master mix to prepare cDNA for gene expression studies

Component	Volume
iScript™ reaction mix	4 µl
Reverse transcriptase	1 µl
Total	**5 µl**

Components added in PCR tubes (per sample)

Component	Volume
Master mix	5 µl
RNAse-free water and sample	15µl (containing 1µg RNA)
Total	**20 µl**

Target concentration of cDNA – 400 ng/µl

Standard initial concentration – 1000 ng/µl. Dilution with nuclease free water (30 µl) to achieve target concentration. RNA samples are stored at -80 °C.

cDNA PCR program (Biometra personal Combi Thermocycler) is outlined in Table 8:

Table 8 : Cycling conditions used for cDNA preparation

Step	**Temperature**	**Duration**
Lid temperature	99 °C	Preheating on
1 (Priming)	25 °C	5 min 00 s
2 (Reverse transcription)	46 °C	20 min 00 s
3 (Reverse transcriptase inactivation)	95 °C	01 min 00 s
4	4 °C	Pause/Stand by

qRT-PCR using SYBR® green method

To perform the qRT-PCR, a master mix was prepared containing forward and reverse primers of the respective gene to be studied along with 5 µl of SYBR® green and 3.5 µl of RNAse-free water. Samples were pipetted in duplicates on a 96-well plate. A negative template control was also added to the plate for each primer. It contained the master mix but not the cDNA sample. After adding the reaction mixture, respective primers, and controls, the plate was sealed, briefly centrifuged, and placed on the cycler (BioRad CFX Connect RT System). For qRT-PCR analysis, Ct values were used to calculate the delta Ct and delta delta Ct values and the fold change. The housekeeping gene employed here was Porphobilinogen deaminase (PBGD). The following formulas were used:

Delta Ct = Ct value of experimental gene of interest - Ct value of housekeeping gene
Delta Delta Ct = Delta Ct of test experimental gene – Average of (Delta Ct of experimental control)
Fold Change = 2 ^ (-delta delta Ct)

Components added in qRT-PCR plate (Table 9):

Table 9: Components added in qPCR multi well plate to analyze gene expression.

Component	**Volume**
SYBR® green super mix	5 µl

RNAse-free water	3.5 µl
Primer mix (forward 10µM and reverse 10µM)	0.5µl
cDNA diluted in nuclease-free water (200ng/µl)	1 µl
Total	**10 µl /well**

qRT-PCR program (Biorad CFX Connect RT system) (Table 10)

Table 10: Cycling conditions used for assessing gene expression by qPCR

Step	Reaction	Temperature	Duration
1	Preheating	95 °C	5 min 00 s
2	Denaturation	95 °C	00 min 10 s
3	Annealing	60 °C	00 min 10 s
4	Extension	72 °C	00 min 10 s
5	Plate reading	65 °C	
6	Storage	4 °C	

Denaturation, annealing and extension – 41X

4.8 Immunofluorescence staining

Slides with the lung sections were heated at 59 °C for 60 minutes. This step helped in melting the paraffin wax. After this step, slides were immersed in Xylol for 5 minutes for 3 times. Slides were then immersed in decreasing concentrations of ethanol starting from 99.6% Ethanol twice for 5 minutes, followed by 96% and 70% ethanol each for 5 minutes. Slides were washed in distilled water for 1 minute 3 times. Slides were then cooked in an antigen retrieval buffer (Rodent decloaker pH 6) for 30-45 minutes, depending on the antibody. The cuvette containing the slides was cooled down to room temperature after cooking and was washed with distilled water followed by PBS wash (pH 7.4) for 5 minutes. Tissue sections underwent blocking with 10% BSA for 60 minutes. After blocking, slides were washed in PBS pH 7.4 twice for 5 minutes. Primary antibody diluted in 10% BSA at respective dilution was added on the tissue sections and left undisturbed at 4°C overnight. After the completion of primary antibody incubation, slides were washed for four times for 5 minutes with PBS pH 7.4. The secondary antibody was also diluted in 10% BSA in their respective dilutions and incubated for 2 hours at

room temperature, followed by 5 minutes of PBS wash. Nuclear staining was performed using Hoechst at a dilution of 1:5000 for 10 minutes. The next step included washing the slides with PBS for four times for 3 minutes. Slides were dried for 5 minutes before covering the tissue sections with mounting medium. Slides were stored in a dark box at 4 °C until imaging.

List of primary antibodies

Table 11: List of primary antibodies used for immunostaining

Target	Host	Dilution	Company	Cat. No
Podoplanin (PDPN)	Goat	1:200	R & D biosystem	AF3244
Surfactant protein C (SFTPC)	Rabbit	1:200	Millipore	ab3786
Ki67	Rat	1:200	Thermo Fisher	14-5698-82
Perilipin-2 (PLIN2)	Rabbit	1:200	Abcam	ab52356
Smooth muscle alpha-2 actin (αSMA)	Rabbit	1:200	Sigma	SAB5500002

List of secondary antibodies

Table 12: List of secondary antibodies used for immunostaining

Fluorophore	Host/Target	Dilution	Company	Cat No
Alexa Fluor 488	Goat anti-rabbit	1:500	Thermo Fisher	A-11008
Alexa Fluor 555	Goat anti-rat	1:500	Invitrogen	A-21434
Alexa Flour 555	Donkey anti-goat	1:500	Invitrogen	A-21432
Alexa Flour 488	Donkey anti-rabbit	1:500	Invitrogen	A-21206

4.9 Immunohistochemistry – BrdU staining

Lung section slides were deparaffinized by placing in the incubator at 60 □C for 1 hour. Slides were then washed in Xylol 3 times for 5 minutes, followed by 5 minutes washes of reducing concentrations of ethanol (99 % (*v*/*v*), 96 % (*v*/*v*),70 % (*v*/*v*) followed by a 2 minutes washing step with distilled water. Slides were placed in antigen retrieval buffer (1X Rodent decloaker) and were cooked for 45 minutes. The slides were cooled down at room temperature for 30

minutes. Slides were washed with distilled water and immersed in a TBS buffer at pH 7.2 before being blocked with 10% BSA for 60 minutes. Slides were again washed four times with TBS pH 7.2. Anti-BrdU antibody (Invitrogen, B-35128) was diluted in antibody diluent (1:100) in which sections were incubated overnight at 4 □C. Slides were washed four times for 5 minutes with TBS buffer at pH 7.2 and 20 minutes with post-block AP polymer kit followed by TBS wash three times for 5 minutes and then 30 minutes of AP polymer kit (rat/mouse) was added. Slides were then washed with TBS and distilled water. Warp red chromogen kit was added for 4 minutes for color development, followed by a TBS wash and 5 minutes in hematoxylin (1:10). Slides were then washed in tap water for 10 minutes and then dehydrated again with 96 % (*v/v)* ethanol, isopropanol and three times with xylol and covered with a coverslip using a mounting medium, Pertex.

4.10 Image Processing and Analysis

Immunofluorescence-stained slides were imaged on a fluorescence microscope (Leica, Wetzlar, Germany). Leica and Zen software were employed to process the images and to apply the scale bar. Images were also obtained from a whole-slide scan for H and E-stained slides and were processed with NDPI view software. All the graphs were prepared with GraphPad V9 software.

4.11 Statistical Analysis

Statistical analysis was performed using GraphPad V9 software. Data were presented as mean± SD. For comparison between two groups, a student's t-test (unpaired) was employed. A one-way ANOVA test was utilized to determine the differences between more than two groups. $p<0.05$ was flagged with * , $p<0.01$ was flagged with ** and $p<0.001$ was flagged with ***.

5. RESULTS:

5.1. Establishment of a positive pressure *ex vivo* ventilation and perfusion model for postnatal mice lungs.

5.1.1 *Ex vivo* volume-based positive pressure ventilation of neonatal mouse lungs

Volume-based positive pressure ventilation is based on delivering a stable tidal volume during ventilation. To investigate alveolarization *ex vivo*, we exposed the neonatal mouse lungs to a low tidal volume and tested the short and long-term impact of ventilation on alveolar growth.

Lungs of neonatal mice were isolated at postnatal day 7 (P7) or P9, followed by *ex vivo* ventilation using a micro vent with a tidal volume of 7 µl/g body weight of the mice and PEEP of 3.7 cm H_2O. Perfusion with epithelial cell medium was provided through the pulmonary artery, and the lungs were ventilated for four or sixteen hours.

Ex vivo ventilation for 16 hours adversely affected alveolar structural maturation, resembling an emphysema-like histological phenotype (Figure 10 B) compared to the unventilated control lungs (Figure 10A). A clear evidence of edema was observed during the experiment, as the time of ventilation and perfusion was extended . The images from the H and E staining also showed the collapse of the alveolar walls superimposed on each other (Figure 10B). Unventilated *in vivo* control lungs harvested from the same litter showed normal lung development. Exposure of isolated lungs to volume-based positive pressure ventilation and perfusion for a short period of four hours resulted in similar structural damage and emphysema-like phenotype of the alveolar architecture (Figure 11).

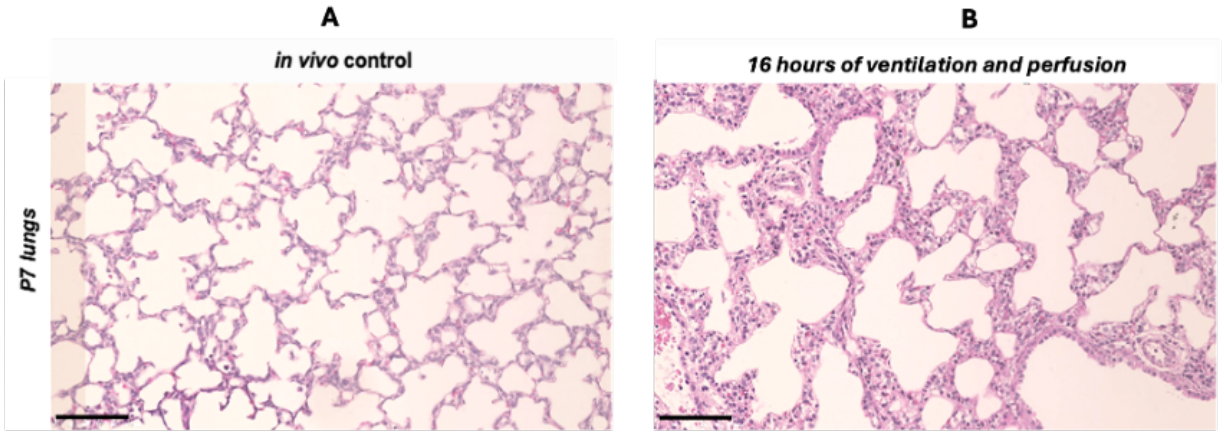

Figure 10 : *Ex vivo* volume-controlled ventilation and perfusion for 16 hours in neonatal mouse lungs Representative images of hematoxylin & eosin (H&E) stained lungs of neonatal mice at postnatal day 7 (P7) after exposure to *ex vivo* ventilation with a tidal volume of 7 µl/g body weight and positive end expiration pressure (PEEP) of 3.7 cm H_2O. The respiration rate was set to 230 breaths/min with a perfusate flow rate of 10 µl/min. A) Unventilated *in vivo* control lungs were flushed with saline before paraffin fixation. B) *Ex vivo* ventilated and perfused lungs after 16 hours of ventilation and perfusion; n=2. Scale bar: 100µm.

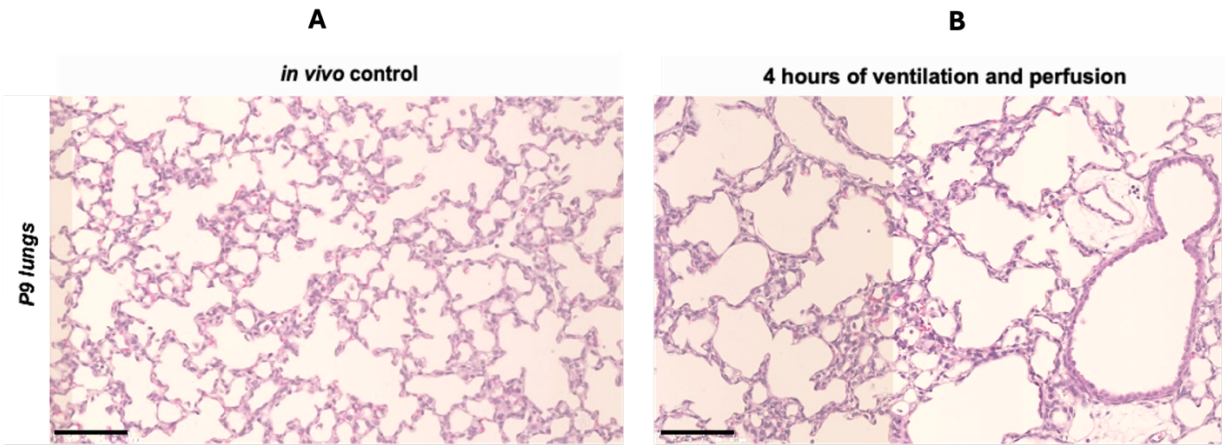

Figure 11: *Ex vivo* volume-controlled ventilation and perfusion for 4 hours in neonatal mouse lungs Representative images of hematoxylin & eosin (H&E) stained lungs of neonatal mice at postnatal day 9 (P9) after exposure to *ex vivo* ventilation with a tidal volume of 7 µl/gm body weight and a positive end expiration pressure (PEEP) of 3.7cm H_2O. The respiration rate was set to 230 breaths/min, the flow rate of the perfusate was set to 10 µl/min. A) Unventilated *in vivo* control lung flushed with saline before paraffin fixation. B) *Ex vivo* ventilated and perfused lungs after 4 hours of ventilation and perfusion. n=3 lungs ;Scalebar:100µm.

5.1.2 *Ex vivo* pressure-based positive pressure ventilation and perfusion of neonatal mouse lungs

Isolated lungs were ventilated using pressure-controlled positive pressure ventilation with a constant inspiratory pressure of 6.5 cm H_2O through the airways and a PEEP of 3.2 cm H_2O. Lungs were perfused with a flow rate of 10 µl/min. After four hours of ventilation and perfusion, the lungs of 6 and 8-day-old mice were formalin-fixed, sectioned, and H&E stained. Interestingly, the lung histological images showed a normal alveolar architecture without disruption of alveolar growth or maturation after four hours compared to *in vivo* unventilated control lungs (Figure 12 A,B). Since lung structure was preserved after four hours of ventilation at P6 and P8, the duration of the ventilation period was extended to 6 hours and 10 hours (Figures 13 A-B and 14 A-D) respectively. While the H&E images displayed a lung morphology which was uninjured after *ex vivo* ventilation compared to unventilated *in vivo* control lungs, nuclei appeared hyperplastic in lungs after 4, 6, and 10 hours of ventilation and perfusion with epithelial cell medium.

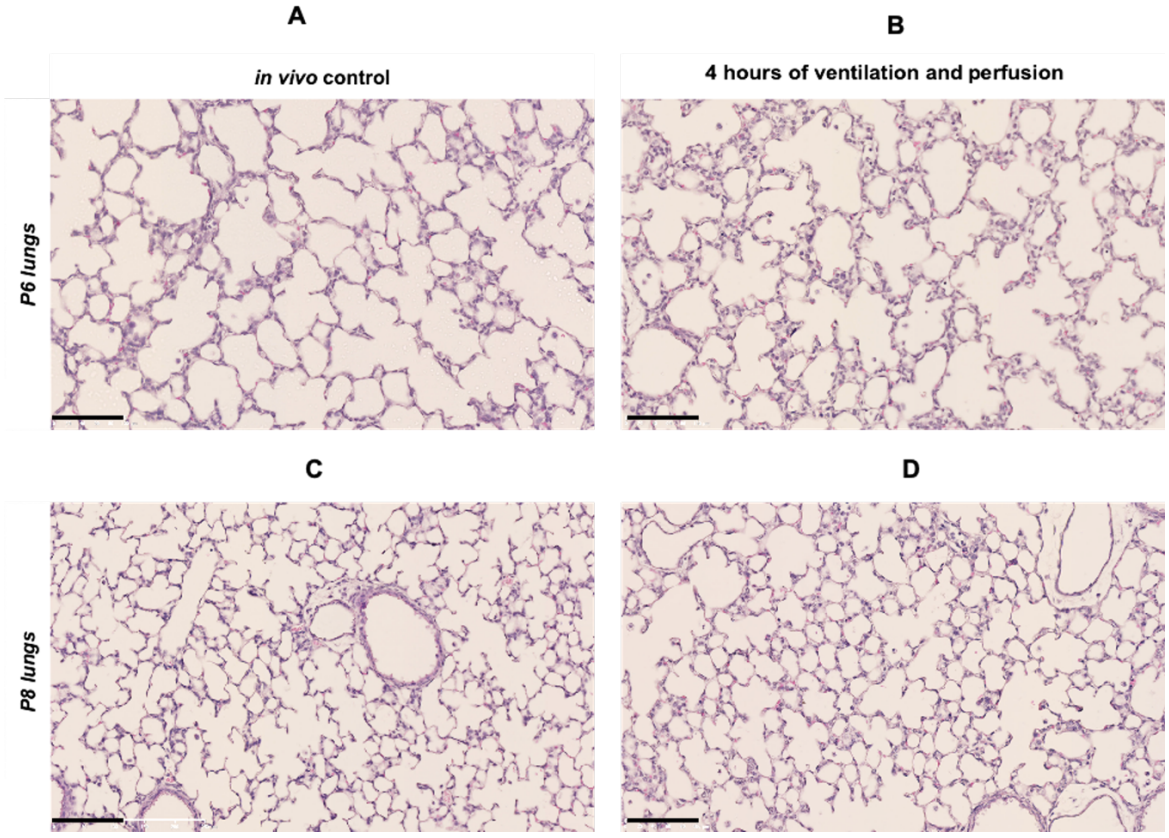

Figure 12: *Ex vivo* pressure controlled positive pressure ventilation and perfusion of neonatal mouse lungs for four hours at postnatal days 6 (P6) and 8 (P8). A, B) Representative images of hematoxylin & eosin (H&E) stained lungs of neonatal mice after ventilation with inspiratory pressure of 6.5 cm H_2O and a positive end expiration pressure (PEEP) of 3.2 cm H_2O for four hours at postnatal day 6 (P6). The respiration rate was set to 230 breaths/min, and the flow rate of the perfusate was 10µl/min. Unventilated control lungs were flushed with saline before paraffin fixation (A). *Ex vivo* lungs after 4 hours of ventilation and perfusion (B). C, D) Representative images of hematoxylin & eosin (H&E) stained neonatal mice lungs ventilated with an inspiratory pressure of 6.5 cm H_2O and a positive end expiration pressure (PEEP) of 3.2 cm H_2O for four hours at postnatal day (P8). The respiration rate was set to 230 breaths/min, and the flow rate of the perfusate was 10 µl/min. Unventilated control lung flushed with saline before paraffin fixation (C). *Ex vivo* lungs after 4 hours of ventilation and perfusion (D);n =3; Scale bar: 100µm.

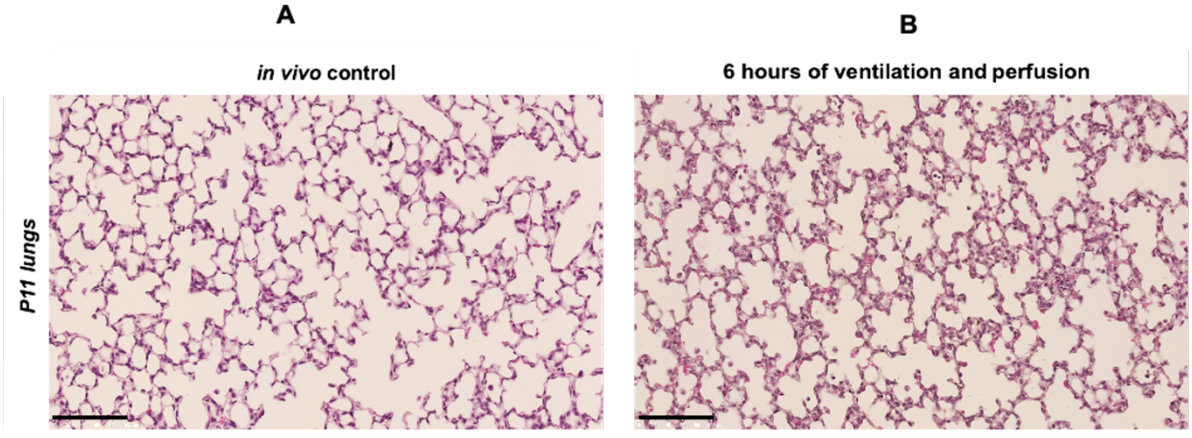

Figure 13: *Ex vivo* pressure controlled positive pressure ventilation and perfusion for 6 hours in neonatal mouse lungs at postnatal day 11 (P11). Representative images of hematoxylin & eosin (H&E) stained lungs of neonatal mice exposed to ventilation with an inspiratory pressure of 6.5 cm H_2O and a positive end expiration pressure of 3.2 cm H_2O at postnatal day 11 (P11). The respiration rate was set to 230 breaths/min, and the flow rate of the perfusate was 10µl/min.(A) Unventilated *in vivo* control lung flushed with saline before paraffin fixation. (B) *Ex vivo* ventilated and perfused lung after 6 hours of ventilation and perfusion; n=3; Scalebar:100µm.

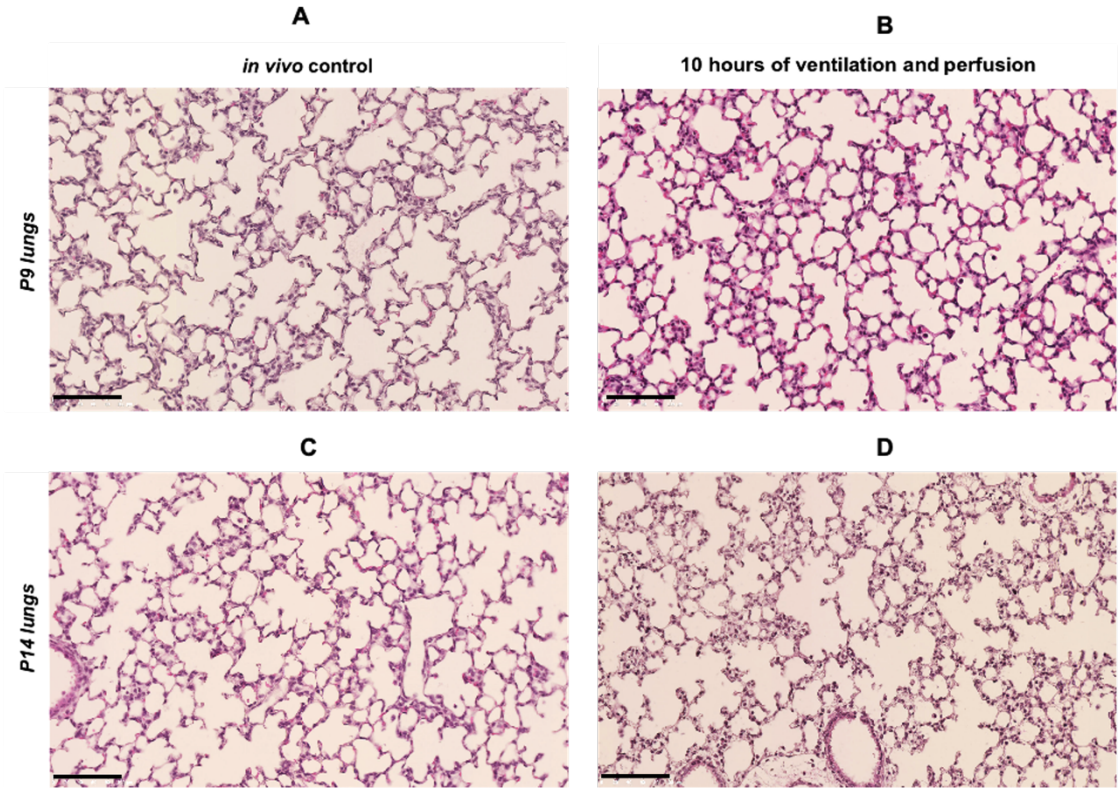

Figure 14: *Ex vivo* pressure controlled positive pressure ventilation and perfusion for 10 hours in postnatal mice lungs at postnatal day 9 (P9) and postnatal day 14 (P14). Representative images of hematoxylin & eosin (H&E) stained lungs of neonatal mice ventilated with an inspiratory pressure of 6.5cm H_2O and a positive end expiration pressure of 3.2 cm H_2O for 10 hours at postnatal day 9 (P9) and postnatal day (P14). The respiration rate was set to 230 breaths/min, and the flow rate of the perfusate was 10µl/min. (A, B) Unventilated *in vivo* control lungs flushed with saline before paraffin fixation, and *ex vivo* ventilated and perfused lungs after 10 hours of ventilation and perfusion respectively. (C, D) Unventilated *in vivo* control lung flushed with saline before paraffin fixation, and *ex vivo* ventilated and perfused lungs after 10 hours of ventilation and perfusion respectively; n=3; Scale bar:100 µm.

5.2 Optimization of the perfusate to study lung development using the *ex vivo* lung ventilation and perfusion model

Optimization of the composition of the medium was essential for a successful *ex vivo* lung model. *Ex vivo* ventilated and perfused lungs of postnatal mice were studied with different

media compositions to optimize the structural architecture of the lungs and to increase the running time of the experiment. Several compositions of the medium were analyzed.

5.2.1 Krebs-Henseleit Buffer (KHB)

Mice at postnatal day 8 (P8) were subjected to ventilation at an inspiratory pressure of 6.5 cm H_2O, PEEP of 3.2 cm H_2O, perfusion cannula was inserted into the pulmonary artery carrying the KHB at a constant pH in a flowrate of 10µl/min with a respiration rate of 230 breaths/min. After 4 hours of ventilation and perfusion, 2 µm lung sections were stained with H&E to observe the lung structure. Figure 15 A (right) Lungs showed an edematic appearance and the alveolar septa were thickened compared to the unventilated *in vivo* control lungs (Figure 15 A (left)).

5.2.2 Steen Solution™

Mice at postnatal day 8 (P8) were subjected to positive pressure ventilation at an inspiratory pressure of 6.5 cm H_2O, PEEP of 3.2 cm H_2O, respiration rate of 230 breaths/min, and steen solution was perfused through the pulmonary artery at a flowrate of 10µl/min. After 4 hours of ventilation and perfusion, lungs were stained with H&E to observe the lung structure. Figure 15 B (right) showed representative H&E images, which appeared highly cellular and edematous due to the thickening of septal walls compared to the unventilated *in vivo* control lungs (Figure 15 B (left)).

5.2.3 Epithelial media with 4% human serum albumin

Epithelial cell medium consisted of basal medium with essential and non-essential amino acids, vitamins, and growth factors supplemented with 4% human serum albumin. At postnatal day 8 (P8), mice were subjected to positive pressure ventilation at an inspiratory pressure of 6.5 cm H_2O, PEEP of 3.2 cm H_2O, and a respiration rate of 230 breaths/min. After 4 hours of positive pressure ventilation and perfusion with epithelial cell medium, H&E images showed undisrupted architecture of the lung (Figure 15 C (right)) similar to the unventilated control lungs without any rupture of septa (Figure 15 C (left)).

5.2.3 Epithelial media with 6 % human serum albumin and methylprednisolone

To further optimize the lung structure, 6% human albumin was added along with an epithelial cell-specific medium. At postnatal day 8 (P8), mice were subjected to positive pressure ventilation at an inspiratory pressure of 6.5 cm H_2O, PEEP of 3.2cm H_2O, respiration rate of 230 breaths/min. After 4 hours of ventilation and perfusion with the medium, the lungs were

stained with H&E to evaluate the lung structure. In Figure 15D (right), the architecture of the lung appeared hypercellular with thickened alveolar septa when compared to unventilated *in vivo* control lungs Figure 15D (left).

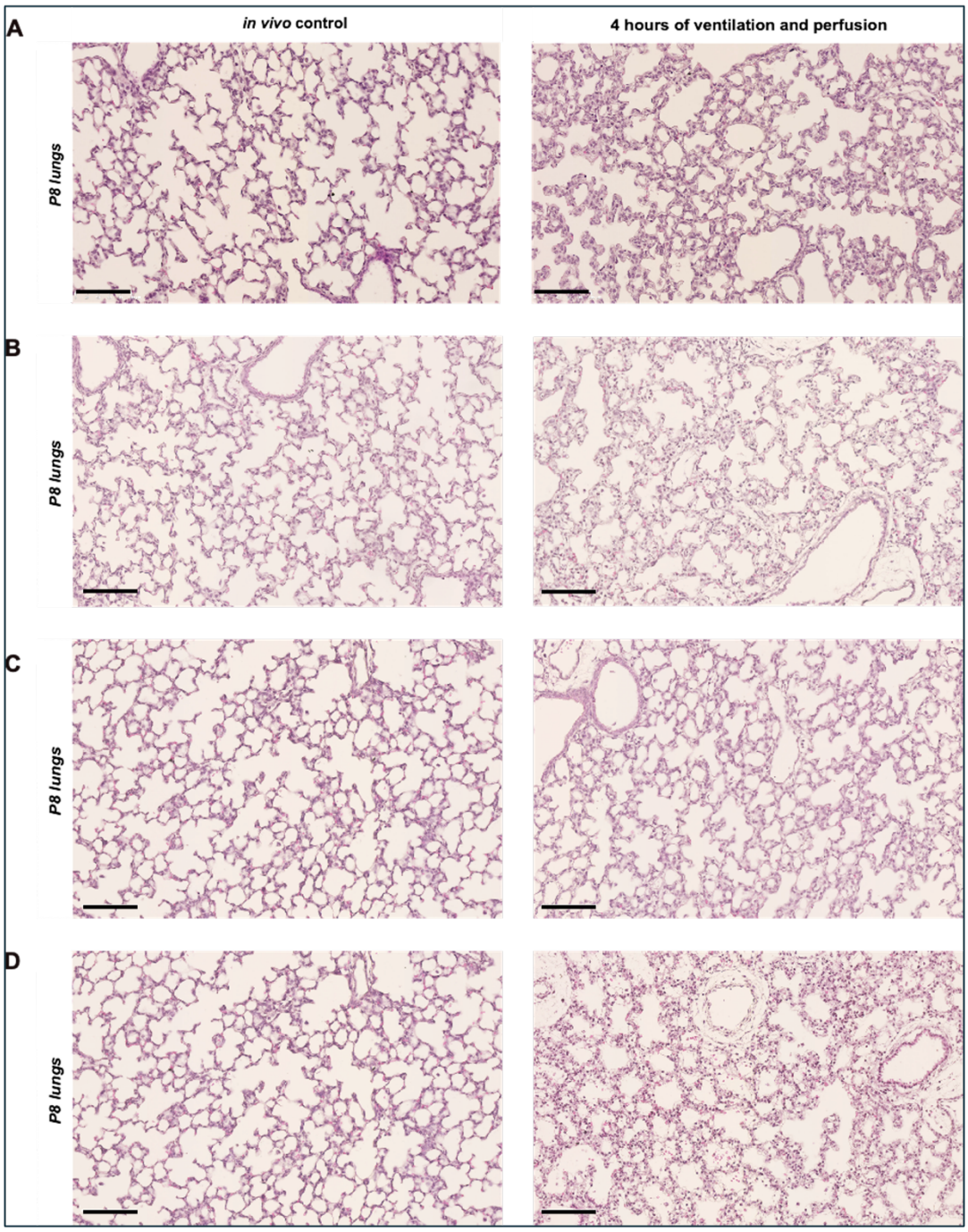

Figure 15: Optimization of the perfusate in the *ex vivo* ventilated and perfused lungs of postnatal mice lungs at postnatal day 8 (P8). Representative images of hematoxylin & eosin (H&E) stained lungs of neonatal mice ventilated with an inspiratory pressure of 6.5 cm H_2O and a positive end expiration pressure of 3.5 cm H_2O for 4 hours at postnatal day (P8). The respiration rate was set to 230 breaths/min. Flow rate of the perfusate was set to 10µl/min. n=4 lungs. Representative H&E images of unventilated *in vivo* control lungs (left) flushed with saline

before paraffin fixation. Images on the right represent lungs ventilated with positive pressure and perfused with respective perfusate medium for 4 hours. (A). KHB (Krebs-Henseleit buffer) + sodium bicarbonate. (B). Steen solution. (C). Epithelial media + 4% human albumin. (D). Epithelial media + 6% human albumin + methylprednisolone. Scale bar:100 µm; n=3.

5.3 *Ex vivo* ventilation and perfusion of early postnatal day 7 (P7) versus late postnatal day 14 (P14) mice

Isolated lungs were ventilated with an inspiratory ventilation pressure of 6.5-7 cm H_2O, PEEP 3.2 cm H_2O, a respiration rate of 230 breaths/min, and perfusion of a flow rate of 10 µl/min with epithelial cell-specific medium and 4% human albumin for 10 hours. H&E images of P14 lungs displayed undisrupted normal alveolar architecture similar to the *in vivo* unventilated control lungs. (Figure 16, A and B). However, P7 lungs were highly disrupted and displayed alveolar wall rupture and larger airspaces (Figure 16, C and D).

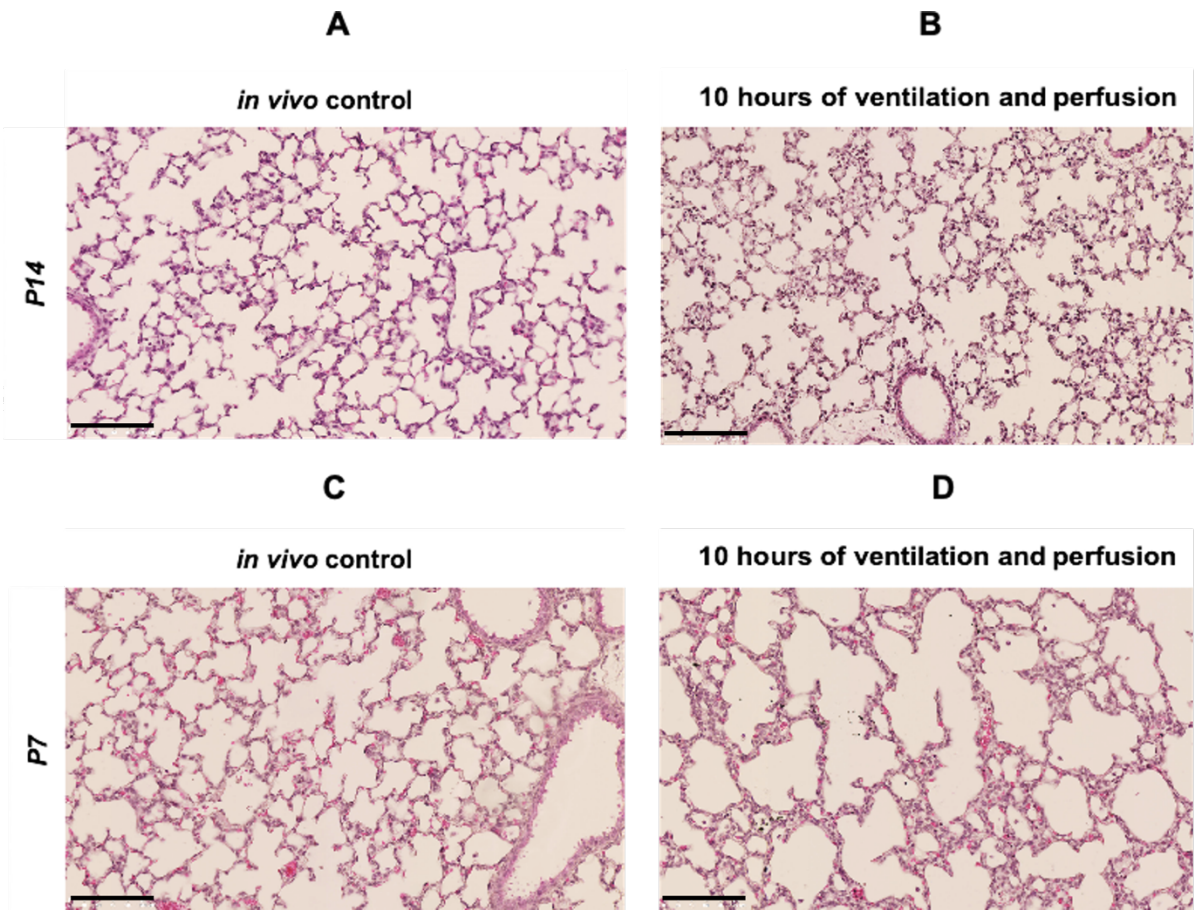

Figure 16: *Ex vivo* ventilation and perfusion using pressure-controlled positive pressure ventilation in early postnatal day 7 (P7) versus late postnatal day 14 (P14) mice for 10 hours. Representative images of hematoxylin & eosin (H&E) stained lungs of neonatal mice lungs ventilated with an inspiratory pressure of 7.1 cm H_2O and positive end expiration pressure of 3.7 cm H_2O. The respiration rate was set to 230 breaths/min, and the flow rate of the perfusate (epithelial cell medium with 4% human albumin) was 10µl/min. A, B) Lungs of

14-day-old mice: unventilated *in vivo* control lungs flushed with saline before formalin fixation and paraffin embedding (A); *ex vivo* lungs ventilated and perfused with epithelial cell medium for 10 hours (B). (C, D) Lungs of 7-day-old mice: unventilated *in vivo* control lung flushed with saline before formalin fixation (C); *ex vivo* lungs ventilated and perfused with epithelial cell medium for 10 hours (D). n=3 ; Scale bar :100 µm.

5.4 *Ex vivo* negative pressure ventilation and perfusion of postnatal mice lungs at postnatal day 8 (P8)

Since prolonged positive pressure ventilation and perfusion resulted in edema and lung damage, negative pressure ventilation and perfusion was established.

Isolated lungs were ventilated with negative inspiratory ventilation pressure of -6.5 cm H_2O, end expiration pressure of -3.2 cm H_2O, a respiration rate of 100 breaths/min, and perfusion flow rate of 10µl/min with epithelial cell-specific medium and 4% human albumin for 10 hours. On postnatal day (P8), the lungs displayed undisrupted normal alveolar architecture without edema formation after 6 hours of ventilation and perfusion compared to the *in vivo* unventilated control lungs (Figure 17 A,B).

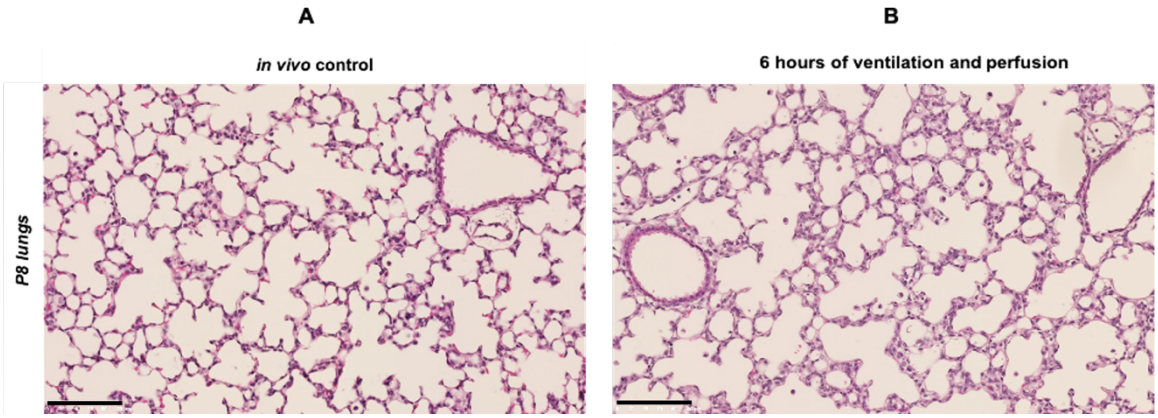

Figure 17: *Ex vivo* negative pressure ventilation and perfusion of neonatal mice for 6 hours at postnatal day 8 (P8). Representative images of hematoxylin & eosin (H&E) stained lungs of neonatal mice lungs ventilated with inspiratory pressure of -6.5 cm H_2O and the end expiration pressure of -3.2 cm H_2O. The respiration rate was set to 100 breaths/min on postnatal day 8 (P8). The flow rate of the perfusate was set to 10 µl/min. (A) Unventilated *in vivo* control lungs flushed with saline before paraffin fixation. (B) Lungs ventilated with negative pressure perfused with epithelial cell medium for 6 hours; n=3 lungs; Scale bar:100 µm.

5.4.1 Alveolar morphometry in *ex vivo* negative pressure ventilated and perfused postnatal lungs at postnatal day 8 (P8)

We next assessed quantitative histomorphometry of the lungs of 8-day-old mice that were ventilated with negative pressure and perfused *ex vivo*. P8 lungs were ventilated and perfused

with epithelial cell culture medium and 4% human albumin with an inspiratory pressure of -6.5 cm H_2O, end expiration pressure of -3.2 cm H_2O, and a respiration rate of 100 breaths/minute, and a perfusate flow rate of 10 µl/minute for 4 hours and 6 hours respectively. Figure 18 represents H&E images of unventilated *in vivo* control lungs (Figure 18 A) and lungs after ventilation and perfusion for 4 hours (Figure 18 B) or 6 hours (Figure 18 C) with 20X magnification and 40X magnification. The alveolar structure was intact without disruption. However, interstitial edema was observed, contributing to septal wall thickness. Morphometric measurements of the lungs were performed (Figure 18 D, E, F) and showed an inclination towards reduction of the mean linear intercept (MLI; surrogate parameter for alveolar size) after 4 and 6 hours of ventilation and perfusion when compared to unventilated *in vivo* control lungs (Figure 18 D). The percentage of air in the lungs was decreased and varied across the two different time points of 4 and 6 hours of the experiments (Figure 18 E). Septal wall thickness was increased after 4 and 6 hours of negative pressure ventilation and perfusion in mouse lungs at P8 (Figure 18 F).

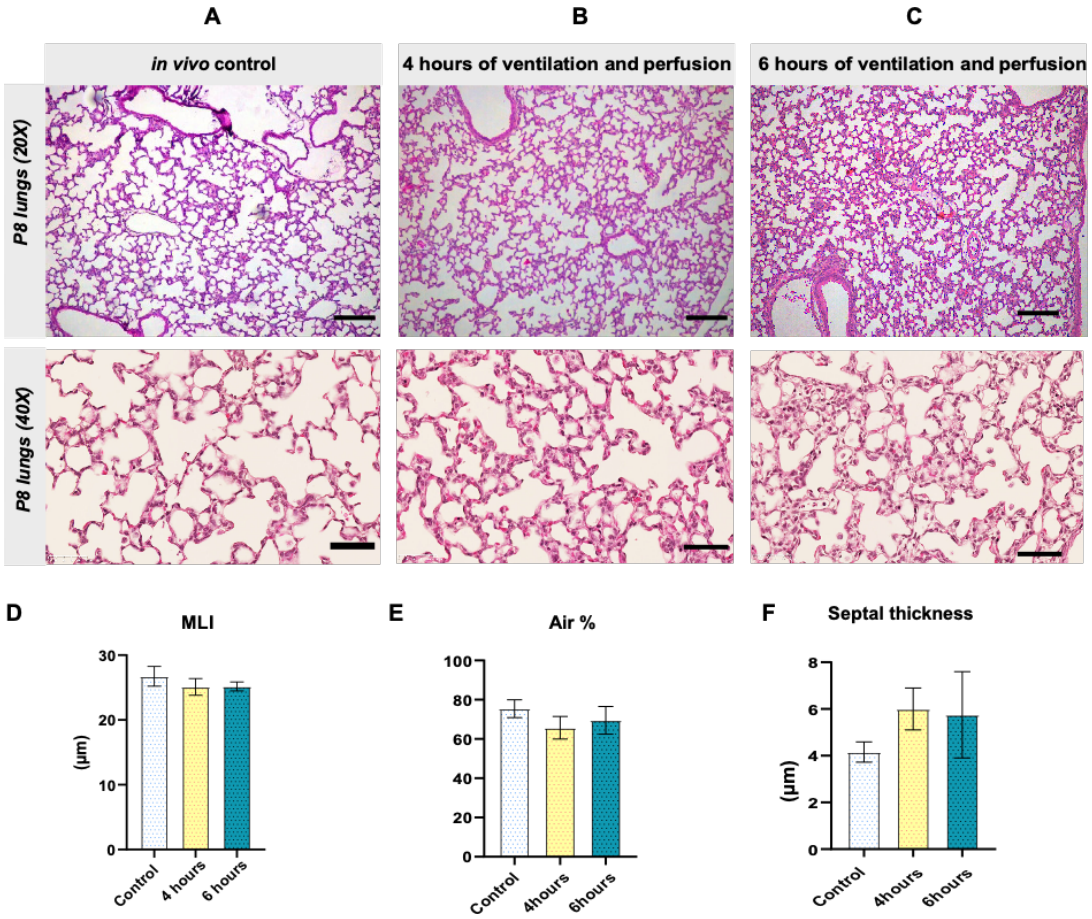

Figure 18: *Ex vivo* negative pressure ventilated and epithelial cell medium perfused lungs at postnatal day 8 (P8).(A-C) Representative images of hematoxylin & eosin (H&E) stained lungs at postnatal day 8 (P8)

representing *in vivo* unventilated control lungs (A), *ex vivo* lungs after 4 hours of ventilation and perfusion (B), and *ex vivo* ventilated and perfused lungs after 6 hours of ventilation and perfusion (C). The upper panel represented lungs imaged at 20X magnification, scale bar:100µm and lower panel represented lungs imaged at 40X magnification, scale bar:50µm. (D-F) Alveolar morphometry of 8-day-old mouse lungs ventilated at negative pressure: mean linear intercept (MLI) in µm (D), percentage of air (E), and septal wall thickness (F) in µm after 4 and 6 hours of ventilation and perfusion compared to unventilated *in vivo* control lungs. Data represented as mean +/- SD ; one-way ANOVA test was performed; n=3.

5.4.2 Characterization of alveolar cell types in *ex vivo* negative pressure ventilated postnatal mouse lungs

5.4.2.1 Alveolar epithelial type II cells (ATII) in *ex vivo* negative pressure ventilation and perfusion of mouse lungs at postnatal day 8 (P8)

Isolated lungs, after *ex vivo* ventilation and perfusion with epithelial cell medium, were stained for markers of different alveolar epithelial cell types. In Figure 19 A, alveolar epithelial type I cells (ATI) were marked as thin, long cells extending over the air sacs and stained against anti-T1 alpha (1:200; podoplanin, PDPN) and was labeled as red by Alexa flour 555 (1:500). The immunofluorescent staining demonstrates a well preserved alveolar lining by the ATI cells that was not disrupted after 4 (Figure 19 B) and 6 hours (Figure 19 C) of ventilation and perfusion and was similar to unventilated *in vivo* control lungs (Figure 19 A). In parallel, the cuboidal ATII cells were stained against surfactant protein C (SFTPC), and the cells were labeled green by Alexa flour 488 (1:500) in Figures 19 A, B, and C. While the alveolar lining by ATI cells were undisrupted after 4 and 6 hours of ventilation and perfusion compared to unventilated *in vivo* control lungs, the ATII cells showed an increase in their cell numbers. In Figure 19 D, quantification of the ATII cells was performed by counting the number of cells labeled green and the total number of nuclei labeled blue by Hoechst. A ratio of the percentage of SFTPC-positive cells to the total number of nuclei was represented as a bar graph. A significant increase in ATII cells was observed after 6 hours of ventilation and perfusion.

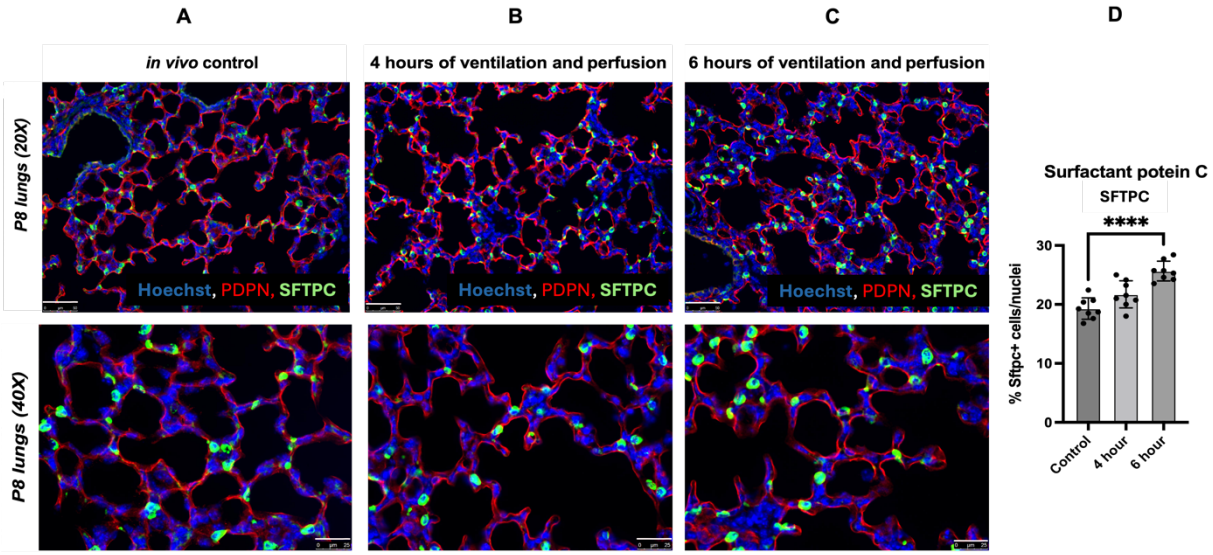

Figure 19: Alveolar epithelial type II (ATII) cells in neonatal lungs after *ex vivo* negative pressure ventilation and perfusion at postnatal day 8 (P8). Immunofluorescence staining of 5 µm sections was performed on mouse lungs of postnatal day 8 (P8) mice after ventilation with negative pressure and perfused with epithelial cell medium for 4 hours and 6 hours along with unventilated *in vivo* control lungs. Alveolar epithelial type I (ATI) cells were stained against T1alpha (podoplanin (PDPN); Alexa Flour 555, red), alveolar epithelial type II (ATII) cells were stained against surfactant protein C (SFTPC; Alexa Flour 488, green) and nucleus was stained with Hoechst (blue). The upper panel represents lung images at 20X magnification; scale bar:50 µm. The lower panel represents lung images at 40X magnification; scale bar:25 µm. Quantification of ATII cells was performed and is represented as the ratio of the percentage of SFTPC-positive cells to the total number of nuclei (D).Data represented as mean +/- SD ; unpaired t-test was performed. **** $p<0.0001$.

5.4.2.2 Cell proliferation after 4 and 6 hours of *ex vivo* negative pressure ventilation and perfusion with epithelial cell medium in neonatal mouse lungs at postnatal day 8 (P8)

It was essential to study the impact of *ex vivo* negative pressure mode of ventilation and perfusion on the proliferation of cells in neonatal mouse lungs at P8. To investigate this, immunofluorescence staining of proliferating cells was performed by staining against Ki67; proliferating cells were marked in red (Alexa Fluor 555). No significant changes in the number of Ki67 positive cells after 4 and 6 hours (Figure 20 B and C) of negative pressure ventilation and perfusion with epithelial cell medium were observed compared to the unventilated *in vivo* control lungs (Figure 20 A). Quantification was performed by counting the number of Ki67 positive cells and the total number of nuclei. This was represented in bar graphs as the ratio of percentage of number of Ki67 positive cells to the total number of nuclei (Figure 20 D).

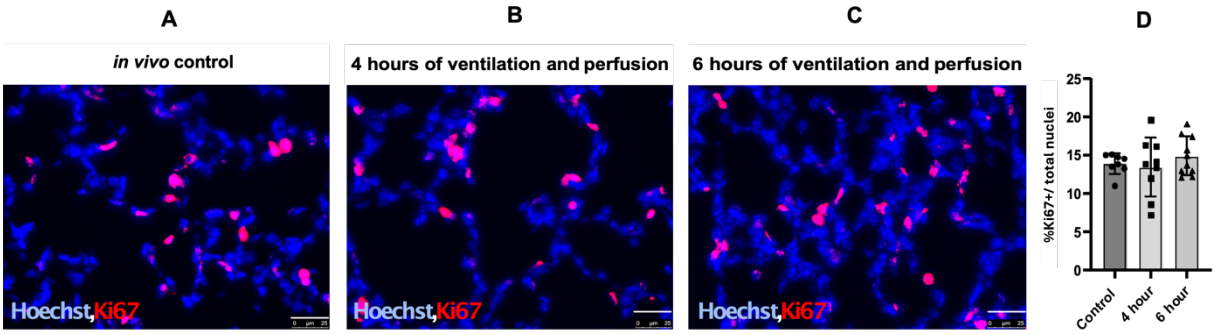

Figure 20: Ki67 positive cells after 4 and 6 hours of *ex vivo* negative pressure ventilation and perfusion of neonatal mouse lungs at postnatal day 8 (P8). (A-C) Representative images of immunofluorescence staining of 5 µm sections of unventilated *in vivo* control lungs (A) and of lungs after ventilation with negative pressure and perfused with epithelial cell medium for 4 hours (B) and 6 hours (C). Proliferation was assessed by staining against Ki67 (Alexa Fluor 555, red) and nuclear staining by Hoechst (blue). (D) Quantification of proliferating cells is represented as the percentage of Ki67 positive cells to the total number of nuclei. Scale bar:25 µm; Data represented as mean +/-SD; one-way ANOVA was performed; n=3.

5.4.2.3 Alpha smooth muscle actin (αSMA) positive cells in lungs after *ex vivo* negative pressure ventilation and perfusion with epithelial cell medium of neonatal mice for 4 and 6 hours at postnatal day 8 (P8)

Alpha smooth muscle actin (αSMA) is a contractile filament that serves as a marker for myofibroblasts. The presence of αSMA-positive cells was analyzed in the *ex vivo* lungs of 8-day-old mice after negative pressure ventilation and perfusion with epithelial cell medium for 4 and 6 hours. Immunofluorescence staining against αSMA was performed. It was noticed that every secondary septum showed αSMA protein at the septal tips with no significant change in the number of αSMA-positive cells after 4 and 6 hours of ventilation and perfusion when compared to the unventilated *in vivo* control lungs as represented in Figure 21.

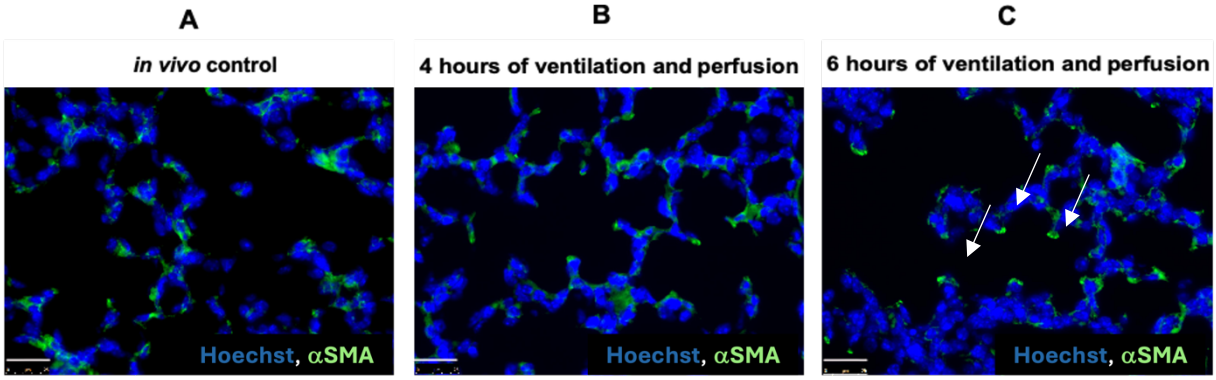

Figure 21: Alpha smooth muscle actin (αSMA) positive cells in lungs of 8-day-old mice after *ex vivo* negative pressure ventilation and perfusion for 4 and 6 hours. (A-C) Lungs from 8-day-old mice were ventilated *ex vivo* with negative pressure at an inspiratory pressure of -6.5 cm H_2O, end-expiratory pressure of -3.2 cm H_2O, a respiration rate of 100 breaths/min, and perfusion at a rate of 10µl/min with epithelial cell medium. Immunofluorescence staining against alpha-smooth muscle actin (αSMA; 1:200) was performed on the unventilated *in vivo* control lungs (A), lungs after 4 hours of ventilation and perfusion with epithelial cell medium (B), and lungs after 6 hours of ventilation and perfusion with epithelial cell medium (C). Myofibroblasts were labeled in green (Alexa flour 488,1:500), nuclear staining Hoechst (blue). White arrows indicate the secondary tips with αSMA. Representative images were represented in 40X magnification. Scale bar:25µm; n=3.

5.4.3 Assessment of gene expression in *ex vivo* lungs after ventilation with negative pressure and perfusion with epithelial cell medium at postnatal day (P8)

Next, we assessed the expression of genes encoding for markers of ATI and ATII cells. No significant change was observed in the gene expression of podoplanin (*Pdpn*) and surfactant protein C (*Sftpc*), markers of ATI and ATII cells, respectively (Figures 22 A, B). Moreover, the analysis of the proliferation marker Ki67 (*MKI67)* and the lipofibroblast marker perilipin 2 (*Plin2)* showed a tendency to increase after 4 hours of negative pressure ventilation and perfusion with epithelial cell medium (Figure 22 C, D). In addition, the expression of the myofibroblast marker, alpha-smooth muscle actin (*Acta2*) showed a tendency to be downregulated after 4 hours of negative pressure ventilation and perfusion (Figure 22 E).

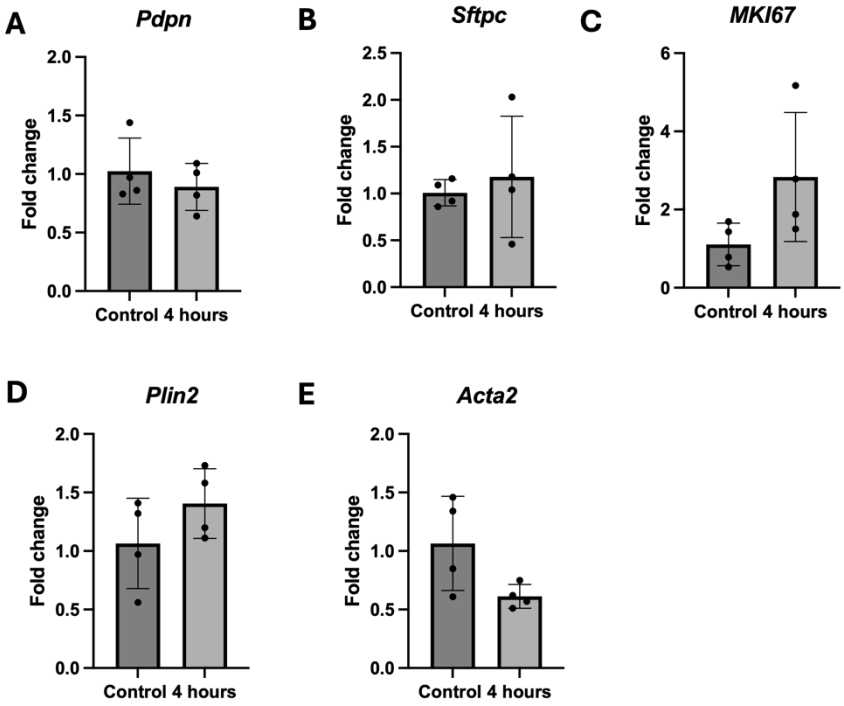

Figure 22: Gene expression in *ex vivo* lungs of postnatal day 8 (P8) old mice after 4 hours of negative pressure ventilation and perfusion.(A-E) Relative gene expression of podoplanin (*Pdpn*; ATI marker, A), surfactant protein C (*Sftpc*; ATII marker, B), *MKI67* (proliferation marker, C), perilipin 2 (*Plin2*; lipofibroblast marker, D), and alpha-smooth muscle actin (*Acta2*; myofibroblast marker, E) was assessed by qRT-PCR from the frozen *ex vivo* lungs after ventilation with negative pressure at an inspiratory pressure of -7.5 cm H_2O, end-expiratory pressure of -3.2 cm H_2O, a respiration rate of 100 breaths/min, a flow rate of 10 µl/min and a perfusion with epithelial cell medium for 4 hours compared to the unventilated *in vivo* control lungs. PBGD (Porphobilinogen deaminase) served as the housekeeping gene. Data represented as mean+/-SD; n=4; Student's t-test was performed.

In Figure 23, the gene expression profile of lungs ventilated with negative pressure and perfused with epithelial cell medium was investigated by qRT-PCR. In this study, we observed a differentially regulated gene expression between ATI and ATII cells. Podoplanin (*Pdpn*) was significantly upregulated in the lungs after 6 hours of ventilation and perfusion with epithelial cell medium (Figure 23 A). However, surfactant protein C (*Sftpc*) expression remained unchanged when compared to the unventilated control lungs (Figure 23 B). The expression of the proliferation (*MKI67*) and lipofibroblast marker (*Plin2*) displayed a tendency to increase after 6 hours of ventilation and perfusion with epithelial cell medium (Figure 23 C, D). *Acta2* expression was strongly upregulated after 6 hours of negative pressure ventilation and perfusion (Figure 23 E).

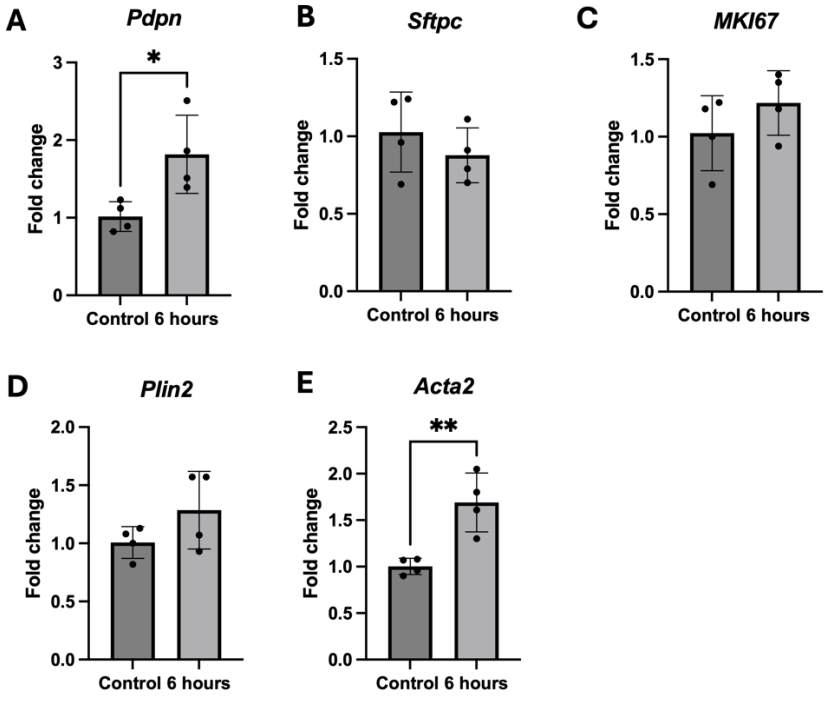

Figure 23: Gene expression in *ex vivo* lungs of postnatal day 8 (P8) mice after 6 hours of negative pressure ventilation and perfusion.(A-E) Relative gene expression of podoplanin (*Pdpn*;ATI marker, A) surfactant protein C (*Sftpc*;ATII marker, B) marker of proliferation of *Ki-67* (*MKI67*, C), perilipin 2 (*Plin2*;lipofibroblast marker, D), and alpha-smooth muscle actin (*Acta2*; myofibroblast marker, E) was assessed by qRT-PCR from the *ex vivo* lungs of postnatal day 8 (P8) mice after ventilation with negative pressure at an inspiratory pressure of -7.5 cm H_2O, end-expiratory pressure of -3.2 cm H_2O, a respiration rate of 100 breaths/min, a flow rate of 10 µl/min, and perfusion with epithelial cell medium for 6 hours and compared to the respective unventilated *in vivo* control lungs. Data represented as mean+/-SD; n=4; statistical significance performed by student´s t-test. $p<0.05$ was flagged with * and $p<0.01$ was flagged with **.

5.5 *Ex vivo* negative pressure ventilation and perfusion with alveologenesis medium in mouse lungs at postnatal day 9 (P9) and postnatal day 5 (P5)

5.5.1 Alveolar morphometry of lungs from postnatal day 9 (P9) and postnatal day 5 (P5) mice after *ex vivo* negative pressure ventilation and perfusion

Mice were ventilated with negative pressure with an inspiratory pressure of -6.5 cm H_2O and an expiration pressure of -3.2 cm H_2O. The respiration rate was set to 100 breaths/min, and the flow rate of the perfusate was 10µl/min with alveologenesis medium. The experiments were performed with mouse lungs at P9 for 4 and 6 hours to study the early mechanisms and structural changes observed in these *ex vivo* ventilated and perfused lungs. Lung morphology was analyzed using H&E-stained lung sections. Unventilated *in vivo* control lungs are represented in Figure 24 A; however, Figures 24 B and C show lungs after ventilation and perfusion with alveologenesis medium for 4 hours or 6 hours, respectively. No major edema was observed and lung structure was maintained after 4 and 6 hours of negative pressure ventilation and perfusion compared to the unventilated *in vivo* control lungs. For quantitative histomorphometry, mean linear intercept, air percentage, and septal wall thickness were assessed (Figures 24 D,E,F). Mean linear intercept (MLI) was found to be reduced in the lungs of 9-day-old mice after 4 and 6 hours of ventilation and perfusion when compared to the unventilated *in vivo* control lungs (Figure 24 D). Air percentage was similar in unventilated *in vivo* control lungs and lungs of 4 and 6 hours of ventilation and perfusion (Figure 24 E). Additionally, alveolar septal thickness was reduced after 4 and 6 hours of ventilation and perfusion, implying no major interstitial edema (Figure 24 F).

.

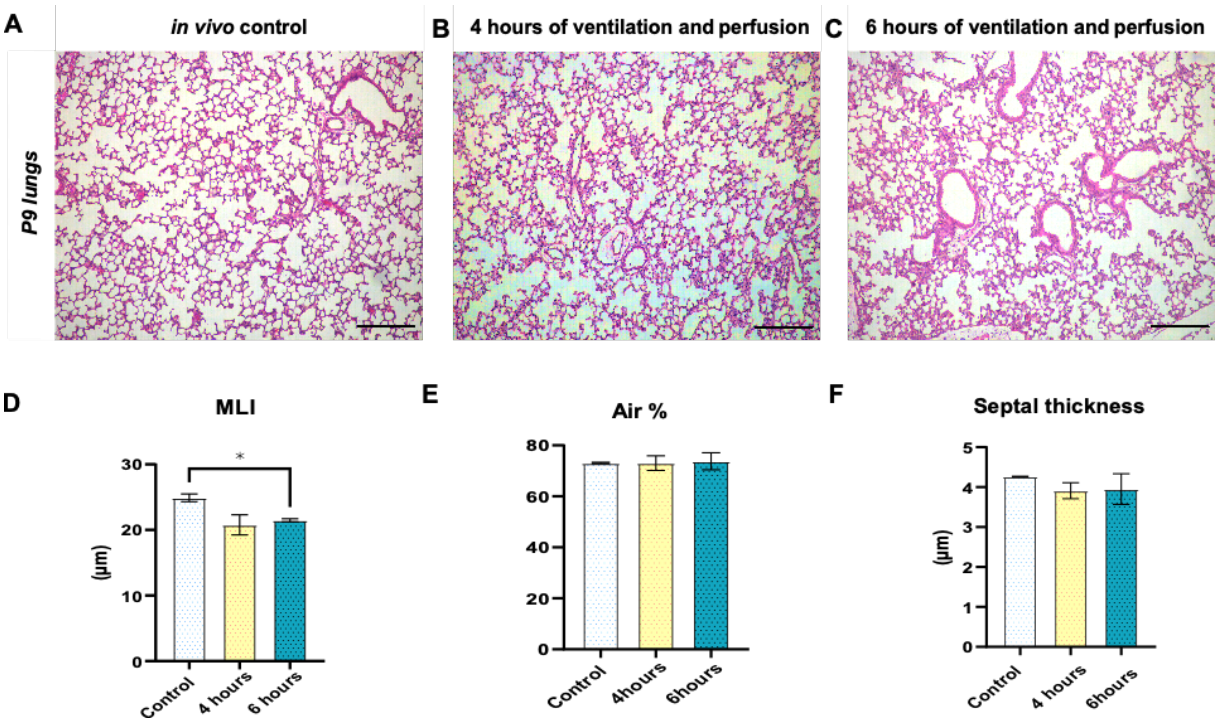

Figure 24: *Ex vivo* negative pressure ventilation and perfusion with alveologenesis medium in neonatal mouse lungs at postnatal day 9 (P9). (A-C) Representative images of hematoxylin and eosin (H&E) stained mouse lungs at postnatal day 9 (P9): unventilated *in vivo* control lungs (A); lungs after *ex vivo* ventilation at negative pressure with an inspiratory pressure of -6.5 cm H_2O, end expiration pressure of -3.2 cm H_2O, a respiration rate of 100 breaths/min, and a flow rate of the perfusate (alveologenesis medium) of 10µl/min for 4 hours (B) and 6 hours (C). (D-F) Assessment of alveolar morphometry parameters: Mean Linear Intercept (MLI, D), percentage of air (E), and septal thickness (F). Scale bar:100 µm; Data represented as mean+/-SD; n=3; Significance was provided by one-way ANOVA test, $p<0.05$ was flagged with *.

Mouse lungs of 5-day-old mice ventilated and perfused with alveologenesis medium preserved lung morphology after 4 and 6 hours of ventilation and perfusion (Figure 25 A-C). The alveolar morphometry showed a mild and significant reduction in the MLI after 4 hours and 6 hours of ventilation and perfusion, respectively (Figure 25 D). The percentage of air was similar in unventilated controls and lungs after 4 hours of ventilation and perfusion. On the contrary, the percentage of air was reduced after 6 hours of ventilation and perfusion compared to the unventilated *in vivo* control lungs (Figure 25 E). Septal wall thickness was decreased in the lungs after 4 hours of ventilation and perfusion compared to the unventilated *in vivo* control lungs. However, septal walls were thickened after 6 hours of ventilation and perfusion compared to *in vivo* control lungs represented in Figure 25 F.

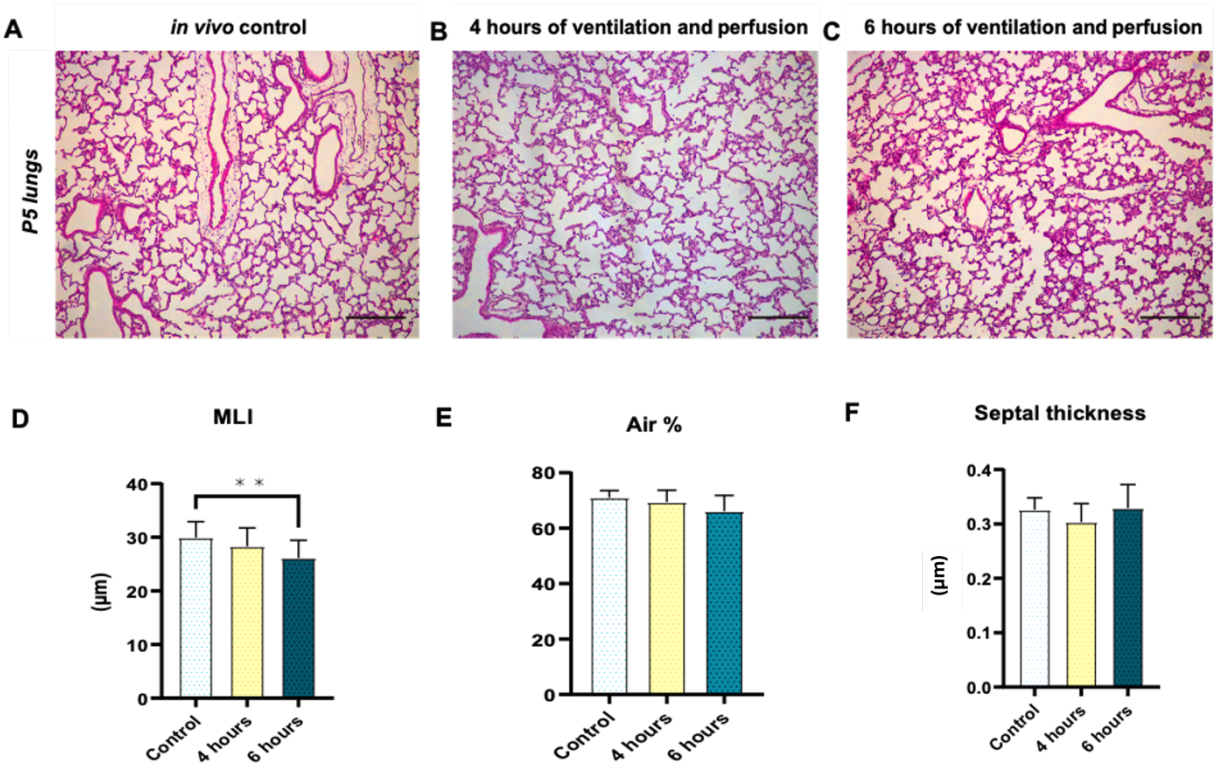

Figure 25: *Ex vivo* negative pressure ventilation and perfusion with alveologenesis medium in neonatal mouse lungs at postnatal day 5 (P5). (A-C) Representative images of hematoxylin and eosin (H&E) stained mouse lungs at postnatal day 5 (P5): unventilated *in vivo* control lungs; lungs after *ex vivo* ventilation at negative pressure with an inspiratory pressure of -6.5 cm H_2O, end expiration pressure of -3.2 cm H_2O, a respiration rate of 100 breaths/min, and a flow rate of the perfusate (alveologenesis medium) of 10 µl/min for 4 hours (B) and 6 hours (C). Alveolar morphometry parameters such as Mean Linear Intercept (MLI), air percentage and septal thickness were represented in bar graphs for unventilated *in vivo* control lungs and lungs ventilated with negative pressure for 4 hours and 6 hours, respectively. (D-F) Scale bar: 100 µm; n=3; Data represented as mean+/-SD; Significance was provided by one-way ANOVA test, $p<0.05$ was flagged with * and $p<0.01$ was flagged with **.

5.5.2 Characterization of alveolar cell types in *ex vivo* negative pressure ventilated lungs of neonatal mice

5.5.2.1 Cell proliferation in *ex vivo* lungs ventilated with negative pressure and perfusion with alveologenesis medium in lungs of neonatal mice.

To investigate the effect of proliferation on mouse lungs at P5 and P9, lungs were ventilated with negative pressure and perfused with alveologenesis medium, followed by immunofluorescence staining against Ki67. Proliferating cells were labeled red by Alexa flour 555 (Figure 26 (I) A-C). The quantification of proliferating cells was performed by counting the number of Ki67 positive cells and counting the total number of nuclei and represented as the ratio of the percentage of Ki67 positive cells to total nuclei. At P9, no difference was

observed in the rate of proliferating cells in lungs after 4 hours, whereas there was tendency to decrease after 6 hours of negative pressure ventilation and perfusion with alveologenesis medium (Figure 26 (I) D). On the other hand, we observed an increased ratio of proliferating cells after 4 hours and 6 hours of negative pressure ventilation and perfusion in the lungs at P5 (Figure 26 (I) E) .

Additionally, proliferation of cells in the lungs ventilated with negative pressure and perfused with alveologenesis medium was confirmed by adding BrdU to the media. Proliferating cells were quantified by counting number of BrdU positive cells per field (Figure (II) A-C). At P9, no change in the number of cells after 4 and 6 hours of ventilation and perfusion was observed, as represented in Figure 26 (II) D. On the other hand, P5 lungs showed an increase in number of proliferating cells from 4 to 6 hours of ventilation and perfusion in comparison to the unventilated *in vivo* control as shown in Figure 26 (II) E.

.

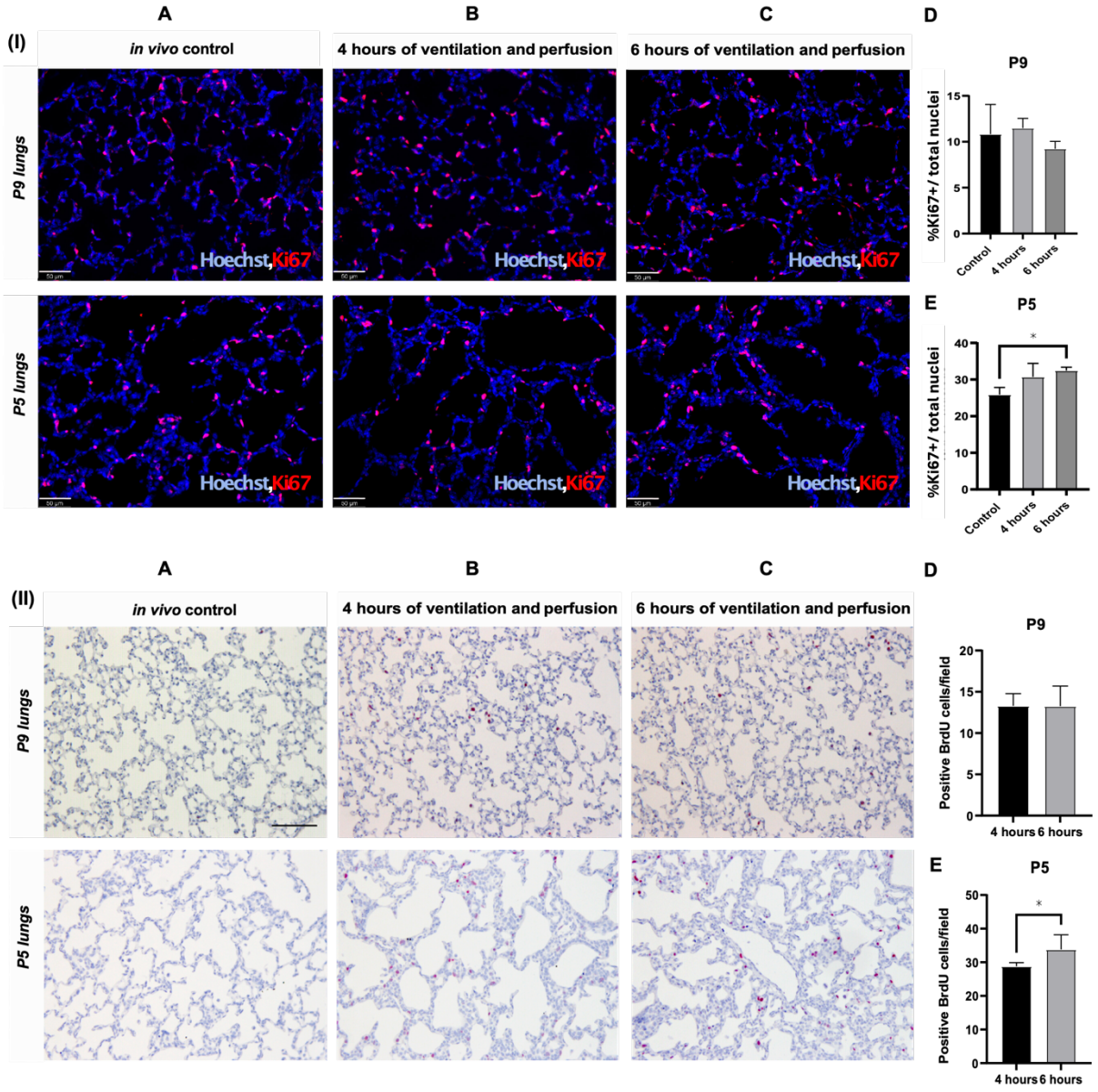

Figure 26: Cell proliferation after 4 and 6 hours of *ex vivo* negative pressure ventilation and perfusion with alveologenesis medium in neonatal mouse lungs. Lungs from P9 and P5 mice were ventilated *ex vivo* with negative pressure at an inspiratory pressure of -6.5cm H_2O, end-expiratory pressure of -3.2cm H_2O, the respiration rate of 100 breaths/min and perfused at a rate of 10 µl/min with alveologenesis medium. (i) Representative images of immunofluorescence staining of 5 µm sections in P9 and P5 mice lungs ventilated with negative pressure and perfused with alveologenesis medium for 4 and 6 hours, respectively. Proliferation was assessed by staining against **Ki67** (Alexa Fluor 555, red) and nuclear staining by Hoechst (blue). The quantification of proliferating cells was represented by a percentage of Ki67 positive cells in total number of nuclei. Scale 50µm, n=4; Student's t-test was performed, $p<0.05$ was flagged with *. (ii) Representative images of immunohistochemistry staining of 3µm sections in P9 and P5 mice lungs ventilated with negative pressure and perfused with alveologenesis medium for 4 hours and 6 hours respectively. Unventilated *in vivo* control lungs were not perfused and thus, did not have **BrdU** in the lungs. However, anti-BrdU was included in these lung sections during the staining procedure and served as a negative control. Proliferating cells were labeled red in both P9 and P5 lungs, ventilated, and perfused

for 4 and 6 hours. These cells were quantified by the number of positive cells/field. Scale bar:75µm , n=4. Student's t-test was performed, $p<0.05$ was flagged with *.

5.5.2.2 Impact of *ex vivo* negative pressure ventilation and perfusion with alveologenesis medium on alveolar epithelial cells in neonatal mouse lungs

Lung sections of 5-day and 9-day-old mice were assessed to analyze alveolar epithelial cells after 4 and 6 hours of negative pressure ventilation and perfusion with alveologenesis medium. Double immunofluorescence staining was performed against T1α (podoplanin, PDPN, ATI marker) and *Sftpc* (ATII marker) along with Hoechst for nuclear staining after 4 hours (Figure 27 B) and 6 hours (Figure 27 C) of ventilation and perfusion. The findings were compared to unventilated *in vivo* control (Figure 27 A). The alveolar lining by ATI was well preserved and the number of ATII cells was increased in the lungs after negative pressure ventilation and perfusion with alveologenesis medium. The quantification of ATII cells was carried out by counting number of SFTPC-positive cells. The result was represented as a ratio of the percentage of a number of SFTPC-positive cells to a total number of nuclei. We observed an increasing trend of ATII cells after 4 and 6 hours of negative pressure ventilation and perfusion lungs of mice at P9 (Figure 27 D, upper panel) when compared to the unventilated control lungs. Similarly, there was a strong upregulation of ATII cells in the lungs at P5 after 6 hours (** P value 0.0013), similar to the increase after ventilation and perfusion for 4 hours (Figure 27 E, lower panel).

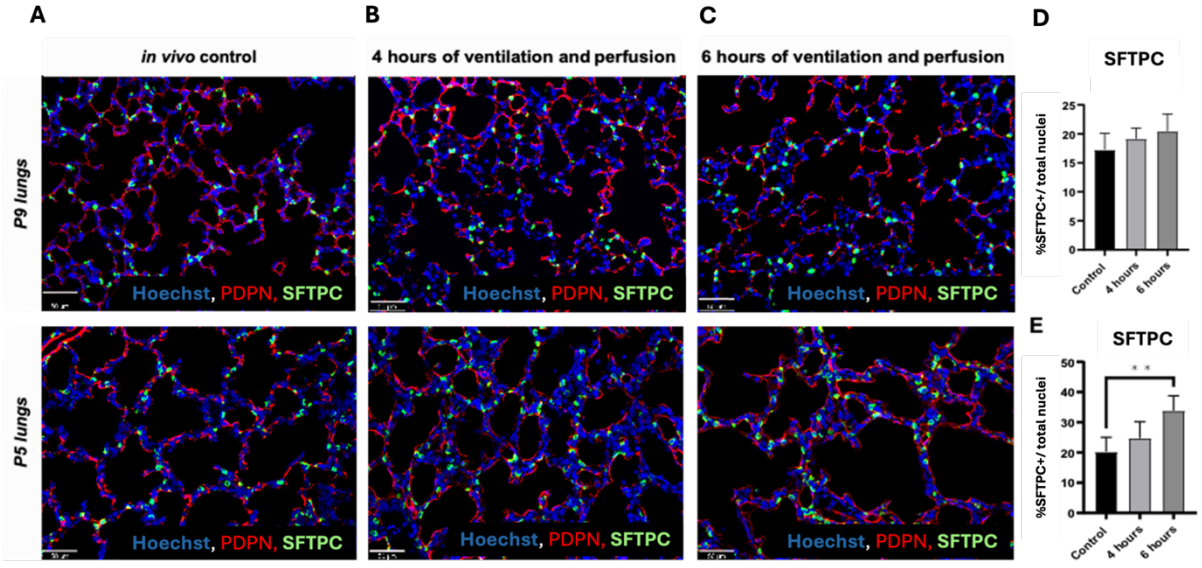

Figure 27: Alveolar epithelial cells type I (ATI) and type II (ATII) in lungs of neonatal mice at postnatal day 5 (P5) and postnatal day 9 (P9) after *ex vivo* negative pressure ventilation and perfusion with alveologenesis medium for 4 and 6 hours. Lungs from 5-day and 9-day-old mice were ventilated *ex vivo* with negative pressure at an inspiratory pressure of -6.5 cm H_2O, end-expiratory pressure of -3.2 cm H_2O, a respiration rate of 100 breaths/min, and a perfusion rate of 10 µl/min alveologenesis medium. (A-C) Representative immunofluorescence staining of T1alpha (podoplanin, PDPN) (alveolar epithelial type I (ATI) cell marker; Alexa Flour 555, red), surfactant protein C (SFTPC) (ATII cell marker; Alexa Flour 488, green), and nuclear staining with Hoechst (blue) in unventilated *in vivo* control lungs (A) as well as in lungs after 4 hours (B) and 6 hours (C) of ventilation; the upper and lower panels show lungs at postnatal day 9 (P9) and P5, respectively. (D, E) The quantification of ATII cells (SFTPC positive cells) is represented as a percentage of SFTPC positive cells to a total number of nuclei for P9 (D) and P5 (E). Scale bar: 50 µm; Data represented as mean+/-SD; n=4; Significance was provided by one-way ANOVA test, $p<0.01$ was flagged with **.

5.5.2.3 Proliferating ATII cells in mouse lungs after *ex vivo* negative pressure ventilation and perfusion with alveologenesis medium for 4 and 6 hours at P9 and P5

To confirm the proliferation of ATII cells, double immunofluorescence staining was performed against Ki67 and anti-surfactant protein C (SFTPC) in lungs after 4 hours and 6 hours of *ex vivo* negative pressure ventilation and perfusion with alveologenesis medium. The analysis revealed proliferating lung ATII cells at both time points, P9 and P5 (Figure 28).Quantification of proliferating ATII cells was carried out by counting number of SFTPC-positive cells. The results was represented as a ratio of percentage of number of SFTPC-positive cells to the total number of nuclei. At P9, an increasing trend of the number of ATII cells after 4 and 6 hours of ventilation and perfusion was observed compared to the unventilated *in vivo* control lungs. There was also strong upregulation of proliferating ATII positive cells in lungs at P5 after 6 hours of *ex vivo* negative pressure ventilation and perfusion (** P value 0.0013), similar to an increase in number of proliferating ATII cells after 4 hours of *ex vivo* negative pressure ventilation and perfusion with alveologenesis medium.

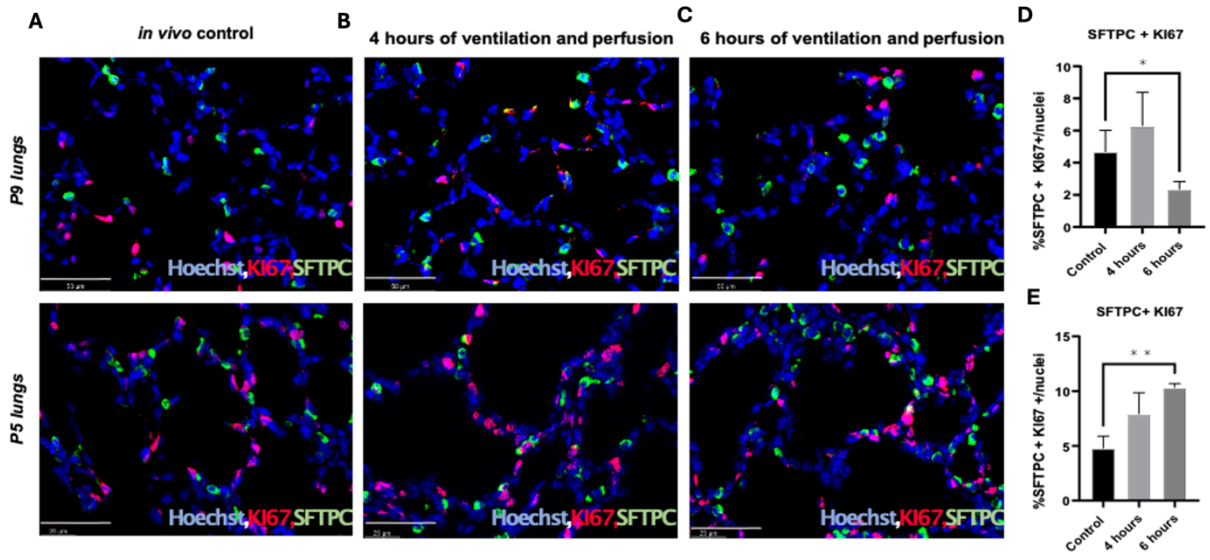

Figure 28: Proliferating alveolar epithelial type II cells after 4 and 6 hours of *ex vivo* negative pressure ventilation and perfusion with alveologenesis medium in P9 and P5 lungs. Lungs from 5-day and 9-day-old mice were ventilated *ex vivo* with negative pressure at an inspiratory pressure of -6.5 cm H_2O, end-expiratory pressure of -3.2 cm H_2O, a respiration rate of 100 breaths/min, and a perfusion rate of 10µl/min alveologenesis medium. (A-C) Immunofluorescence staining against *Ki67* (proliferation marker; Alexa Flour 555, red), surfactant protein C *(*SFTPC; alveolar epithelial type II (ATII) cell marker; Alexa Flour 488, green), and nuclear staining by hoechst (blue) in unventilated *in vivo* control lungs (A) as well as in lungs after 4 hours (B) and 6 hours (C) in mice at P9 (upper panel) and P5 (lower panel). (D, E) The proliferating ATII cells were quantified and represented as the percentage of SFTPC-positive cells to the total number of nuclei at P9 (D) and P5 (E). Scale bar: 50 µm; Data represented as mean+/-SD; n=4; Significance was provided by one-way ANOVA test; $p < 0.05$ was flagged with *, and $p < 0.01$ was flagged with **.

5.5.2.4 αSMA positive cells after 4 and 6 hours of *ex vivo* negative pressure ventilation and perfusion with alveologenesis medium.

Alpha smooth muscle actin (αSMA, ACTA2) positive cells were visualized by performing immunofluorescence staining of the lungs of neonatal mice exposed to ventilation with *ex vivo* negative pressure and perfusion with alveologenesis medium at P9 and P5.5µm lung sections were stained against αSMA in P9 and P5 lungs (Figure 29). No major changes in the expression of alpha smooth muscle actin positive cells was detected in both P9 and P5 mice lungs when compared to their respective unventilated *in vivo* control. Since myofibroblasts exhibit an elongated cell morphology, the quantification of αSMA-positive cells relative to nuclei was not performed.

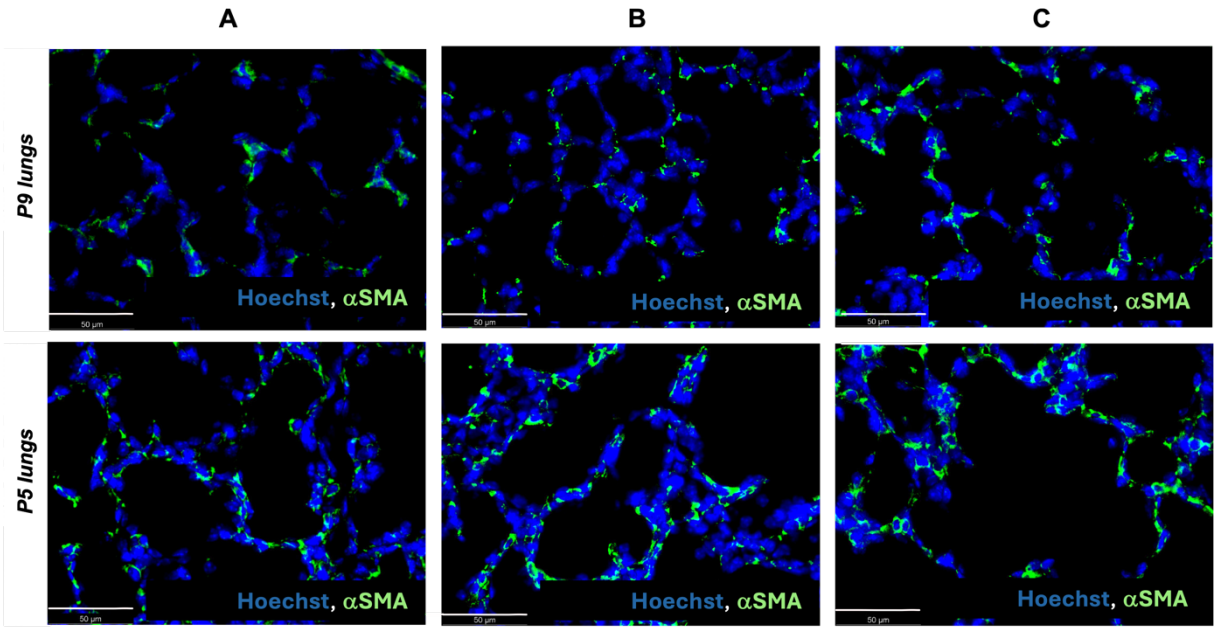

Figure 29: Alpha smooth muscle actin (αSMA) positive cells in lungs after 4 and 6 hours of *ex vivo* negative pressure ventilation and perfusion with alveologenesis medium of neonatal mice at postnatal day 5 (P5) and P9. Lungs from 5-day and 9-day-old mice were ventilated *ex vivo* with negative pressure at an inspiratory pressure of -6.5 cm H_2O, end-expiratory pressure of -3.2 cm H_2O, a respiration rate of 100 breaths/min, and a perfusion rate of 10µl/min alveologenesis medium. (A-C) Immunofluorescence staining against alpha-smooth muscle actin (αSMA; 1:200) was performed on unventilated *in vivo* control lungs (A) as well as lungs after *ex vivo* negative pressure ventilation and perfusion for 4 hours (B) and 6 hours (C) from mice at P9 (upper panel) and P5 lungs (lower panel). αSMA positive cells (myofibroblasts) were labeled in green (Alexa flour 488,1:500) and nuclear staining with Hoechst (blue).Scale bar:50µm; n=4.

5.5.3 Assessment of gene expression in the *ex vivo* model of negative pressure ventilation and perfusion with alveologenesis medium

5.5.3.1 Assessment of gene expression in lungs of mice exposed to the *ex vivo* model of negative pressure ventilation and perfusion with alveologenesis medium at P9

The relative gene expression was assessed by qRT-PCR from total lung homogenates of mice exposed to *ex vivo* ventilation with negative pressure at an inspiratory pressure of -6.5 cm H_2O, end-expiratory pressure of -3.2 cm H_2O, a respiration rate of 100 breaths/min, a perfusion rate of 10µl/min alveologenesis medium for 4 hours. The *ex vivo* ventilated lungs were compared to the unventilated *in vivo* control lungs.

To investigate the distal lung cell types ,the expression of genes encoding for different alveolar cell markers was analyzed. The expression of podoplanin (*Pdpn*), a marker of ATI cells, was significantly increased after 4 hours (Figure 30 A), whereas there was no difference in

expression between the control and 6 hours of *ex vivo* ventilation with negative pressure (Figure 31 A) in lungs at P9. Surfactant protein C (*Sftpc*) showed no significant change in mRNA expression after 4 and 6 hours of ventilation and perfusion when compared to the unventilated *in vivo* control lungs (Figure 30 B and 31 B). The gene expression of the proliferation marker Ki67 was unchanged after 4 and 6 hours of negative pressure ventilation and perfusion (Figures 30 C, 31 C). The expression of *Plin2* (Perilipin2; a marker of lipofibroblasts) showed an increasing trend after 4 hours and 6 hours of ventilation and perfusion (Figures 30 D, 31 D), whereas *Acta2* (a marker of myofibroblasts) expression was unchanged after 4 hours (Figure 30 E), and strongly downregulated after 6 hours of *ex vivo* ventilation and perfusion when compared to the unventilated *in vivo* control lungs (Figure 31 E).

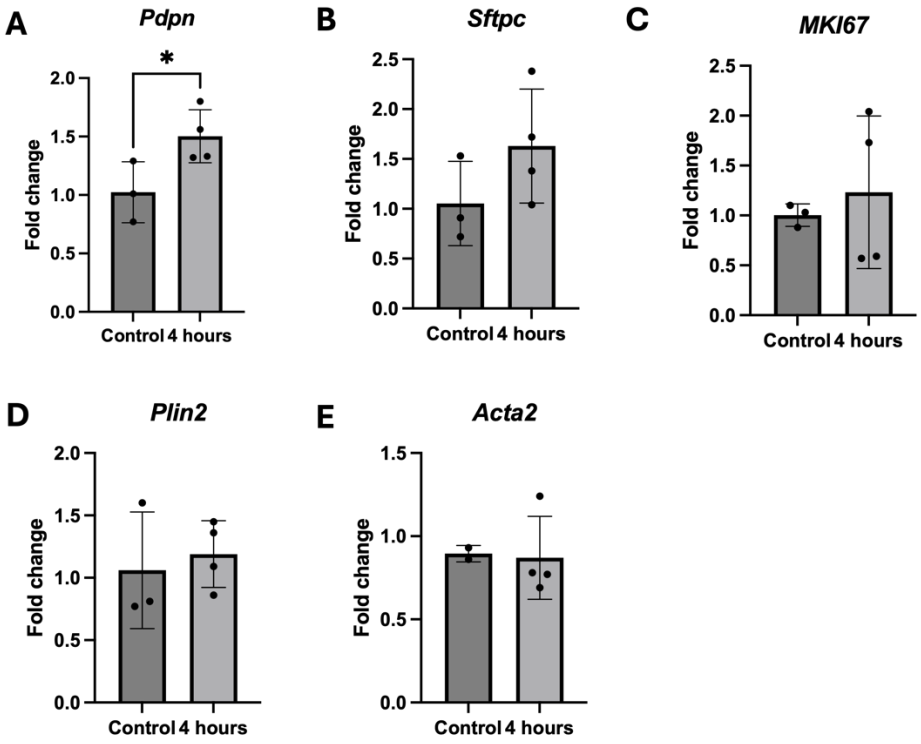

Figure 30: **Assessment of gene expression in lungs of neonatal mice after 4 hours of *ex vivo* negative pressure ventilation and perfusion with alveologenesis medium at postnatal day 9 (P9).** Lungs from 9-day-old mice were ventilated *ex vivo* with negative pressure at an inspiratory pressure of -6.5 cm H_2O, end-expiratory pressure of -3.2 cm H_2O, a respiration rate of 100 breaths/min, and a perfusion rate of 10 µl/min alveologenesis medium. (A-E) Assessment of gene expression in mouse lungs after 4 hours of negative pressure ventilation and perfusion using qRT-PCR: Podoplanin (*Pdpn*, alveolar epithelial type I cell marker, ATI; A), surfactant protein C (*Sftpc*; ATII marker; B), Ki-67 (proliferation marker, C), Perilipin 2 (*Plin2*, lipofibroblast marker; D), and alpha-smooth muscle actin (*Acta2*; myofibroblast marker, E). Fold changes were expressed in mean ± standard deviation in comparison to the unventilated *in vivo* control lungs; Student's t-test was performed; n=3-4. Student's t-test was performed , $p<0.05$ was flagged with *

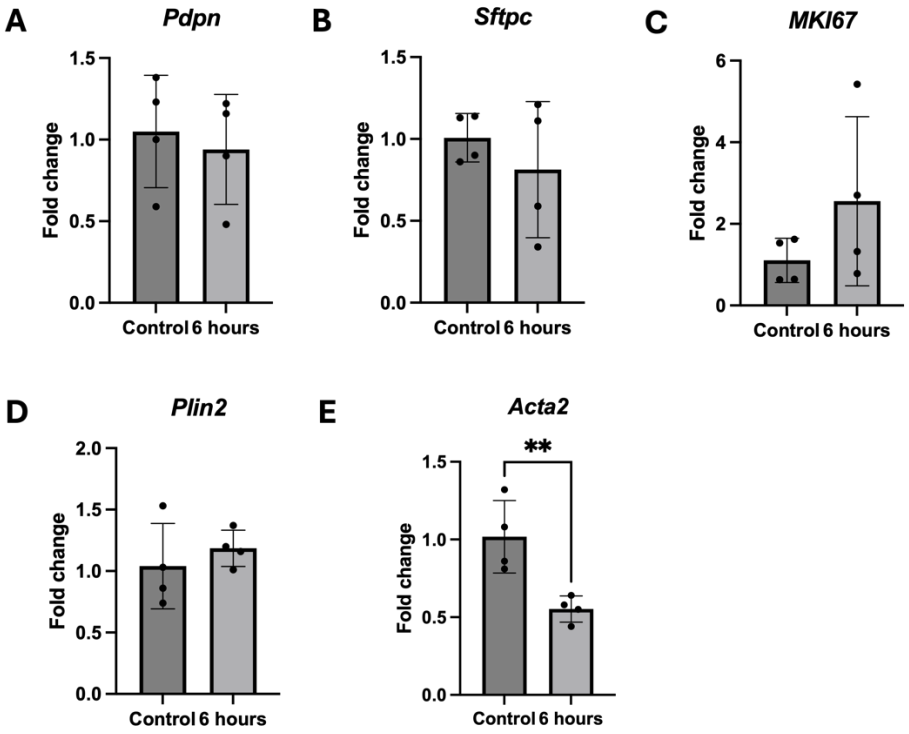

Figure 31: Assessment of gene expression in lungs of neonatal mice after 6 hours of *ex vivo* negative pressure ventilation and perfusion with alveologenesis medium at postnatal day 9 (P9). Lungs from 5-day and 9-day-old mice were ventilated *ex vivo* with negative pressure at an inspiratory pressure of -6.5 cm H_2O, end-expiratory pressure of -3.2 cm H_2O, a respiration rate of 100 breaths/min, and a perfusion rate of 10 µl/min alveologenesis medium. (A-E) Assessment of gene expression in mouse lungs after 6 hours of negative pressure ventilation and perfusion using qRT-PCR: Podoplanin (*Pdpn*, alveolar epithelial type I cell marker, ATI; A), surfactant protein C (*Sftpc*; ATII marker; B), Ki-67 (proliferation marker, C), Perilipin 2 (*Plin2*, lipofibroblast marker; D), and alpha-smooth muscle actin (*Acta2*; myofibroblast marker, E). Fold changes were expressed in mean ± standard deviation in comparison to the unventilated *in vivo* control lungs; n=4; Student's t-test was performed , $p<0.05$ was flagged with *, and $p<0.01$ was flagged with **.

5.5.3.2 Assessment of gene expression of alveolar cell types in lungs of mice exposed to the *ex vivo* model of negative pressure ventilation and perfusion at P5

The relative gene expression of different alveolar cell types was analyzed in the lungs at P5 by qRT-PCR. No change was observed in the expression of podoplanin (*Pdpn*, ATI marker) after 4 hours (Figure 32 A), whereas an inclination to increase after 6 hours in the lungs a P5 was detected (Figure 33 A). Significant upregulation of surfactant protein C (*Sftpc*, ATII marker) after 4 hours and 6 hours of negative pressure ventilation and perfusion with alveologenesis medium was observed (Figures 32 and 33 B). Expression of *Ki67* (proliferation marker), *Plin2* (lipofibroblast marker), and *Acta2* (myofibroblast marker) showed a tendency to increase after

4 hours and 6 hours (Figures 32 and 33 C, D, E) of ventilation and perfusion when compared to the unventilated *in vivo* control lungs.

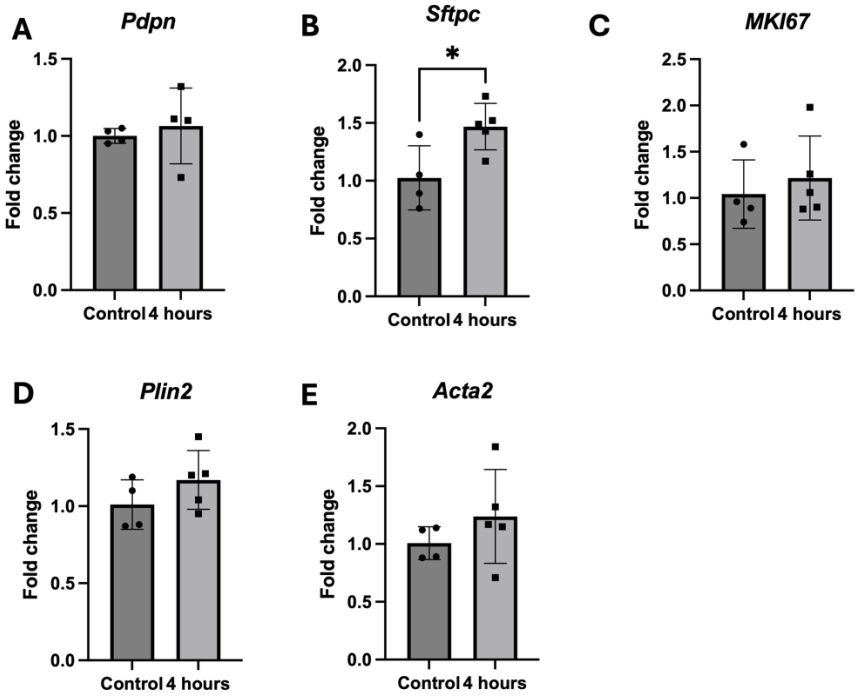

Figure 32: **Assessment of gene expression in lungs of neonatal mice after 4 hours of *ex vivo* negative pressure ventilation and perfusion with alveologenesis medium at postnatal day 5 (P5).** Lungs from 5-day-old mice were ventilated *ex vivo* with negative pressure at an inspiratory pressure of -6.5 cm H_2O, end-expiratory pressure of -3.2 cm H_2O, a respiration rate of 100 breaths/min, and a perfusion rate of 10 µl/min alveologenesis medium. (A-E) Assessment of gene expression in mouse lungs after 4 hours of negative pressure ventilation and perfusion using qRT-PCR: Podoplanin (*Pdpn*, alveolar epithelial type I cell marker, ATI; A), surfactant protein C (*Sftpc*; ATII marker; B), Ki67 (*MKI67*, C), Perilipin 2 (*Plin2*, lipofibroblast marker; D), and alpha-smooth muscle actin (*Acta2*; myofibroblast marker, E). PBGD (Porphobilinogen deaminase) served as the housekeeping gene. Fold changes were expressed in mean ± standard deviation in comparison to the unventilated *in vivo* control lungs; n=4-5. Student's t-test was performed, and $p<0.05$ was flagged with *.

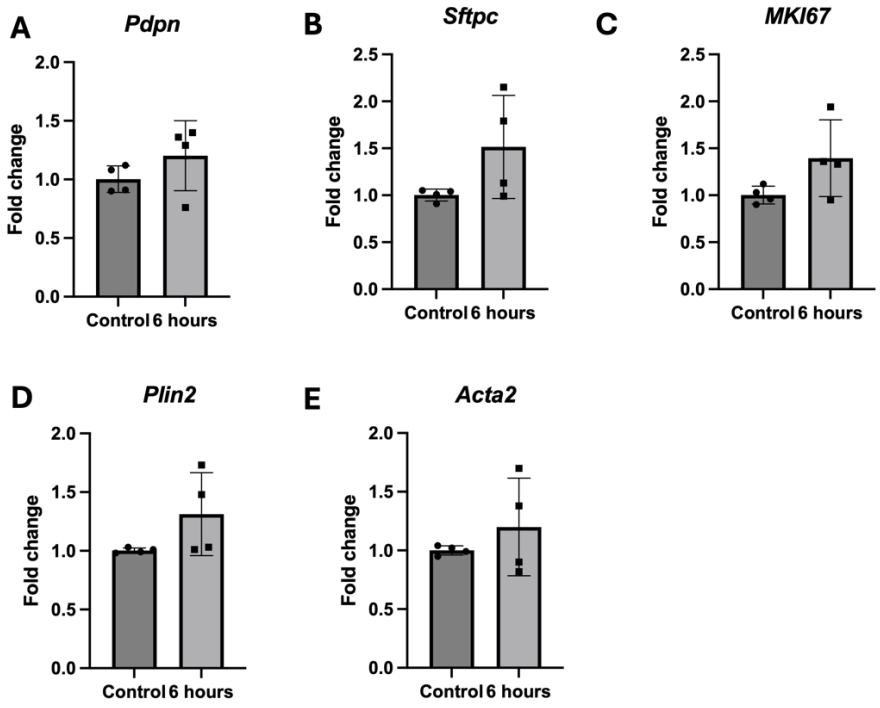

Figure 33: **Assessment of gene expression in lungs of neonatal mice after 6 hours of *ex vivo* negative pressure ventilation and perfusion with alveologenesis medium at postnatal day 5 (P5).** Lungs from 5-day-old mice were ventilated *ex vivo* with negative pressure at an inspiratory pressure of -6.5 cm H_2O, end-expiratory pressure of -3.2 cm H_2O, a respiration rate of 100 breaths/min, and a perfusion rate of 10µl/min alveologenesis medium. (A-E) Assessment of gene expression in mouse lungs after 6 hours of negative pressure ventilation and perfusion using qRT-PCR: Podoplanin (*Pdpn*, alveolar epithelial type I cell marker, ATI; A), surfactant protein C (*Sftpc*; ATII marker; B), Ki-67 (proliferation marker, C), Perilipin 2 (*Plin2*, lipofibroblast marker; D), and alpha-smooth muscle actin (*Acta2*; myofibroblast marker, E). PBGD (Porphobilinogen deaminase) served as the housekeeping gene. Fold changes were expressed in mean ± standard deviation in comparison to the unventilated *in vivo* control lungs; n=4.

5.5.3.3 Assessment of gene expression of stemness markers, mesenchymal and endothelial markers in lungs of mice exposed to the *ex vivo* model of negative pressure ventilation and perfusion at postnatal day 9 (P9) and day 5 (P5)

The relative expression of genes involved in various signaling events in different cell compartments of the lung was analyzed in lung homogenates of mice at P5 and P9 by qRT-PCR. First, we assessed two markers important in the regulation of stemness (e.g., ATII cells): Fibroblast growth factor 10 (*Fgf10*) showed an inclination to upregulate after 4 hours (Figure 34, A upper panel) but no change after 6 hours (Figure 34, A; lower panel) in lungs of mice at P9, whereas *Fgf10* was significantly upregulated in lungs of mice at P5 after 4 and 6 hours (Figure 35, A; upper and lower panel) of *ex vivo* negative pressure ventilation and perfusion. The expression of *Wnt5a* was downregulated after 4 and 6 hours in the lungs of mice at P9

(Figure 34, B). On the other hand, there was no regulation of *Wnt5a* in the lungs of mice at P5 after 4 hours, but it was strongly downregulated after 6 hours (Figure 35, B) of *ex vivo* negative pressure ventilation and perfusion with alveologenesis medium. Platelet and endothelial cell adhesion molecule (*Pecam1*), expressed by endothelial cells showed no gene expression changes after 4 and 6 hours of *ex vivo* negative pressure ventilation and perfusion in mouse lungs at P9 and P5. (Figure 34 C, 35 C upper and lower panel). Vimentin (*Vim*), a mesenchymal cell marker, was downregulated after 4 and 6 hours of negative pressure ventilation and perfusion in mouse lungs at P9 (Figure 34, D upper and lower panel). At P5, mouse lungs showed a significant upregulation of *Vim* after 4 and 6 hours of *ex vivo* negative pressure ventilation and perfusion with alveologenesis medium (Figure 35, D upper and lower panel).

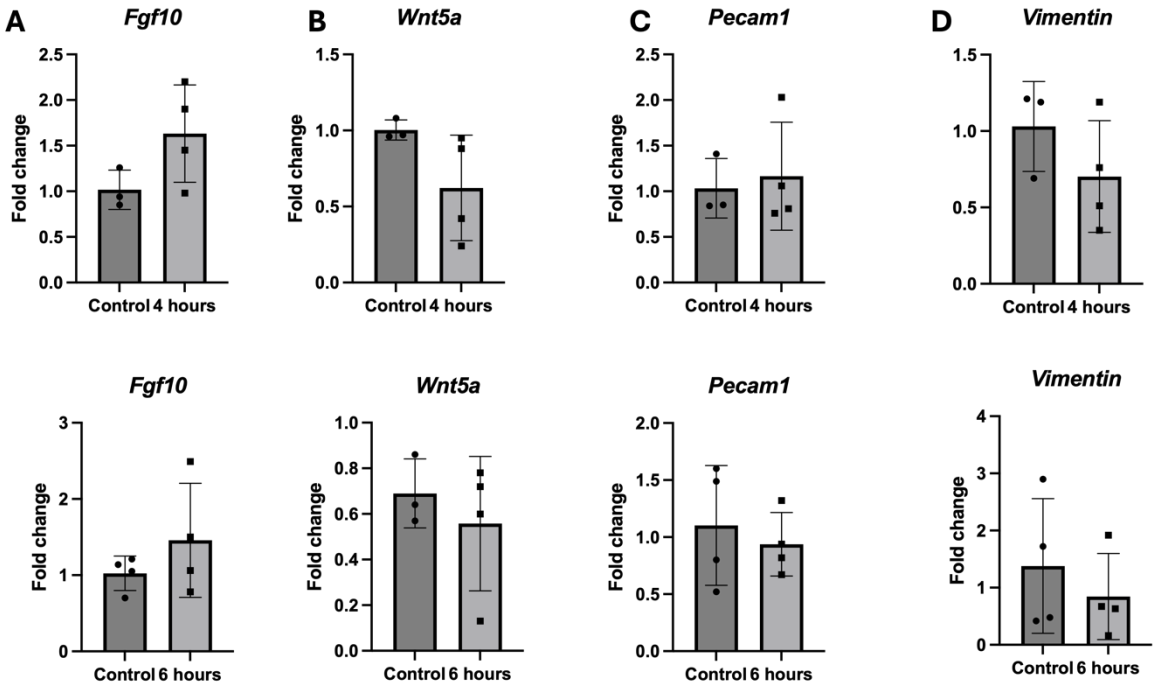

Figure 34: **Assessment of gene expression in lungs of neonatal mice after 4 and 6 hours of *ex vivo* negative pressure ventilation and perfusion with alveologenesis medium at postnatal day 9 (P9).** Lungs from 9-day-old mice were ventilated *ex vivo* with negative pressure at an inspiratory pressure of -6.5 cm H_2O, end-expiratory pressure of -3.2 cm H_2O, a respiration rate of 100 breaths/min, and a perfusion rate of 10 µl/min alveologenesis medium. (A, B) Assessment of gene expression of stemness-regulating ligands in mouse lungs after 4 (upper panel) and 6 hours (lower panel) of negative pressure ventilation and perfusion using qRT-PCR: fibroblast growth factor 10 (*Fgf10*, A) and *Wnt5a* (B). (C, D) Gene expression of endothelial cell marker (*Pecam1*, C) and mesenchymal marker (vimentin, *Vim*) in mouse lungs after 4 (upper panel) and 6 hours (lower panel) of negative pressure ventilation and perfusion using qRT-PCR. Fold changes were expressed in mean ± standard deviation in comparison to the unventilated *in vivo* control lungs; n=3-4; Student's t-test was performed , $p<0.05$ was flagged with *, and $p<0.01$ was flagged with **.

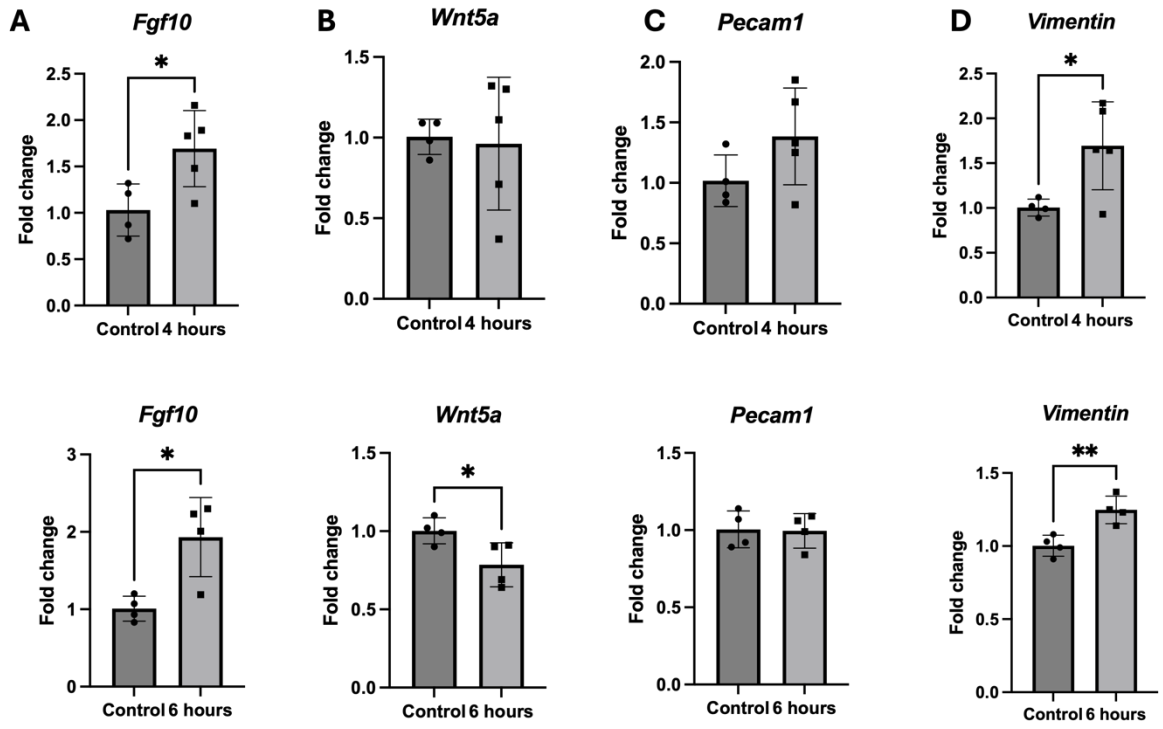

Figure 35: **Assessment of gene expression in lungs of neonatal mice after 4 and 6 hours of *ex vivo* negative pressure ventilation and perfusion with alveologenesis medium at postnatal day 5 (P5).** Lungs from 5-day-old mice were ventilated *ex vivo* with negative pressure at an inspiratory pressure of -6.5 cm H_2O, end-expiratory pressure of -3.2 cm H_2O, a respiration rate of 100 breaths/min, and a perfusion rate of 10µl/min alveologenesis medium. (A, B) Assessment of gene expression of stemness-regulating ligands in mouse lungs after 4 (upper panel) and 6 hours (lower panel) of negative pressure ventilation and perfusion using qRT-PCR: fibroblast growth factor 10 (*Fgf10*, A) and *Wnt5a* (B). (C, D) Gene expression of endothelial cell marker (*Pecam1*, C) and mesenchymal marker (vimentin, *Vim*) in mouse lungs after 4 (upper panel) and 6 hours (lower panel) of negative pressure ventilation and perfusion using qRT-PCR. Fold changes were expressed in mean ± standard deviation in comparison to the unventilated *in vivo* control lungs; n=4; Student's t-test was performed , $p<0.05$ was flagged with *, and $p<0.01$ was flagged with **.

6. Discussion:

Efficient gas exchange constitutes the principal function of the lungs. This is determined by the proper formation of alveoli and secondary septation during the initial stages of development. Abnormalities occurring during the early stages of lung development are the root cause of several diseases occurring in the lung like bronchopulmonary dysplasia (BPD) in infants (Shennan et al.,1988) and chronic obstructive pulmonary disease (COPD), emphysema and fibrosis in adults (Barker et al.,1991). High morbidity and mortality linked to impaired alveoli formation and regeneration have drastically increased the incidence of lung diseases and,

thereby, death worldwide. Understanding alveolarization more deeply at both physiological and molecular levels have become a critical need in paving the way to develop drugs and therapies.

The current study provides insights on

(i) Positive *vs* negative pressure modes of *ex vivo* ventilation and perfusion.
(ii) Time-dependent effects of *ex vivo* ventilation and perfusion on lung structure, alveolar niche, cellular landscape, and gene expression profile.
(iii) Early molecular changes in lungs by *ex vivo* ventilation and perfusion despite normal alveolar structure.

Alveologenesis serves as the ultimate stage of lung development, involving the formation of smaller gas exchange units by a process of secondary septation. In mice, bulk alveolarization occurs between postnatal day 4 to 14 (P4 to P14). (Amy et al.,1977). Several studies have been conducted to study the process of alveolarization. In the study from Pieretti et al. in 2014, alveologenesis was investigated by using an *in vitro* model of precision-cut lung slices in which P4 mice lungs were inflated with agarose, sectioned and cultured on a specific collagen matrix. In this study, several culture media formulations were tested and finalized on a working medium. This was called as alveologenesis medium in the present study, consisted of M199 medium supplemented with hydrocortisone, vitamin A and vitamin C. Retinoic acid (vitamin A) was crucial in the production of elastin and for formation of new septa by expressing elastin genes (Massaro et al.,2010). P4 lung sections were allowed to stay in culture and grow for four days. After four days, the lung sections were assessed for alveolar morphometry and proliferation and observed thinning of septa and a decrease in mean linear intercept similar to P8 lungs. Though this study showed changes in the septation, no further characterization and gene expression analysis of these lung sections was performed.

In vivo models to study alveolarization included the use of transgenic mice to study specific genes. Embryonic lethality is a phenotype prevalent in homozygous mice for genetic mutations. (Papaioannou et al.,2012). The process of generation of the mice was complicated and involved a lot of time (Choi et al.,2012). This paved way to the development of an *ex vivo* model of ventilation and perfusion to mimic physiological alveolarization processes. Previously, studies have been conducted on isolated lung systems on larger animals like rabbits (Baltazar et al., 2021) and small animals like rats (Bobba et al.,2015) and adult mice (Yoo et al.,2013). Isolated perfused lung has been widely used to study lung injury (Haywood et al.,2020), interstitial fluid pressure (Wiig et al., 1985), pulmonary hypertension (Weissmann et al.,1995) and ROS

detection (Weissmann et al., 2005). Isolated perfused lung system included its own advantages (mimicking the mechanics of breathing, control over perfusate and perfusion pressure) and disadvantages (missing neural control, effect of mechanical pumping) (Herget & Chovanec,2010).

Due to technical difficulties in preparation, frequent edema formation, and limited hours of ventilation and perfusion, fewer studies have used this model on small animals. In the present study, we aimed to understand alveolarization by establishing the *ex vivo* model of ventilation and perfusion in postnatal mice.

6.1 Effect of *ex vivo* positive pressure ventilation and perfusion in postnatal mice lungs

Tidal volume-based *ex vivo* positive pressure ventilation was employed to ventilate the lungs. Low tidal volume ventilation was known to reduce ventilation-induced lung injury (Yaroshenko et al., 2016). Tidal volume of 7µl/g body weight was used to ventilate P7 lungs in positive pressure. Lungs that were ventilated and perfused for 16 hours led to excessive edema and showed complete destruction of the alveolar structure, resembling emphysema. Lungs that were ventilated and perfused for 4 hours at a similar low tidal volume also showed destruction of alveoli by loss of alveolar septal walls (alveolar simplification) resembling lungs affected by bronchopulmonary dysplasia. (Thébaud & Abman, 2007). Experiments conducted with pressure-controlled mode of positive pressure ventilation preserved the alveolar architecture after 4, 6, and 10 hours of ventilation and perfusion, unlike the former volume-based mode of ventilation (Ashworth et al.,2018). Lungs ventilated with pressure-based mode and perfused beyond 10 hours resulted in edema formation, leading to fluid accumulation resulting in the end of the running experiment. Previous studies have shown the importance of the air-blood barrier to control edema formation in the lungs (Beretta et al.,2021), which could serve as one of the reasons for the inability of the lungs to survive ventilation beyond 10 hours. Different perfusate solutions were utilized to perfuse the *ex vivo* ventilated lungs to enable them to survive longer hours , mimicking the physiological composition. The use of Krebs-Henseleit buffer (Seeger et al.,1986), Steen solution (dos Santos et al.,2014), and epithelial cell culture medium with 6% albumin to maintain the oncotic pressures (Li et al.,2015) resulted in thickening of alveolar septa due to interstitial edema after 4 hours of ventilation and perfusion. Epithelial cell culture medium with 4% human albumin preserved the lung structure with minimal edema formation after ventilation and perfusion for 4 hours.

Mice ventilated in a pressure-controlled manner and perfused with epithelial cell culture medium maintained lung structure similar to the *in vivo* unventilated control but was limited to

a maximum 10 hours in older mice (P14), but not in younger mice (P7), causing loss of alveolar structure and interstitial edema. Optimization of pressure conditions for ventilation was performed by altering PEEP conditions in gradients, and data suggested a strong inflammation signature with upregulation of TNF alpha signaling (Wilson., 2005; Mukhopadhyay et al.,2006).

6.2 Effect of *ex vivo* negative pressure ventilation and perfusion in postnatal mice lungs

Negative pressure mode of ventilation and perfusion helped in maintaining the lungs without overdistension. Lungs from P8 mice ventilated for 4 and 6 hours preserved lung structure comparable to the *in vivo* unventilated control. However, there was an increase in septal thickness and percentage of air due to interstitial edema after 4 and 6 hours of ventilation and perfusion with epithelial cell culture medium. Decrease in mean linear intercept (MLI) of lungs after 4 hours and 6 hours of ventilation and perfusion indicated possibility of formation of new septa. MLI has been used as a measure to understand morphological changes of alveoli. Increase in MLI corresponded to alveolar simplification, and a decrease in MLI corresponded to new alveoli formation (Dylag et al.,2020). Alveolar epithelial type I and type II cells were analyzed after 4 hours and 6 hours of negative pressure ventilation and perfusion. Alveolar epithelial type I cells were intact, and there was a steady increase in the number of positive alveolar epithelial type II cells after 4 and 6 hours. Alveolar epithelial type II cells are major stress sensors and react to environmental changes. Cell proliferation was analyzed by counting the number of Ki67-positive cells in the lungs of P8 mice after 4 and 6 hours, which did not significantly change compared to the *in vivo* control. Classical alveologenesis is marked majorly by the proliferation of epithelial and mesenchymal cell populations (Rippa et al.,2021). Alpha-smooth muscle actin-positive myofibroblasts played an important role in the secondary septa formation (Rippa et al.,2021). Accumulation of PDGFRα myofibroblasts starts occurring after birth and is accompanied later by elastin. Lungs from 4 and 6 hours of ventilation and perfusion from P8 mice perfused with epithelial cell-specific medium showed the presence of alpha smooth muscle actin positive cells at the tips of the septa, indicating new septa and alveoli formation. Alveolar epithelial cells and mesenchymal cells expression did not alter after 4 hours. However, there was an increase in alveolar epithelial type I cell expression and myofibroblasts expression significantly after 6 hours of negative pressure ventilation and perfusion with epithelial cell medium from the data acquired by qPCR. Alveolar epithelial type II cells showed an inclination to decrease in expression, which could be attributed to the stem

cell properties of differentiating into alveolar type I cells due to external stimuli (Barkauskas et al.,2017).

P9 and P5 lungs were ventilated with negative pressure and perfused with alveologenesis medium. Data from alveolar morphometry indicated decreased mean linear intercept after 4 and 6 hours of ventilation and perfusion. The percentage of air was maintained, and no major edema formation was visible after 4 hours of ventilation, whereas interstitial edema was observed after 6 hours of ventilation and perfusion which resulted in septal wall thickness, suggesting that the negative pressure ventilation and perfusion with alveologenesis medium required fine-tuning and optimization to increase the running time of experiment while maintaining the lung structure without edema and injury. Similar to the epithelial cell medium, alveolar epithelial type I cells and alveolar myofibroblasts were significantly expressed after 6 hours of ventilation and perfusion in P9 mice lungs. In P5 mice lungs, alveolar epithelial type II cells marked by surfactant protein C were significantly upregulated after 4 hours. Alveolar epithelial type I cells, proliferation marker and myofibroblasts marker gene expression did not change compared to the unventilated control lungs. After 6 hours of negative pressure ventilation and perfusion with alveologenesis medium, alveolar epithelial cells and mesenchymal cells indicated an increase in their gene expression when compared to the unventilated control. Cell proliferation in P9 and P5 mice lungs was analyzed by Ki67 and BrdU staining. In both cases, P5 mice lungs showed significant proliferation after 6 hours of ventilation and perfusion. This indicated that younger mice lungs were strongly reactive to the conditions of negative pressure ventilation and perfusion with alveologenesis medium. A similar trend of significant increase in alveolar epithelial type II cells was observed in P5 mice lungs after 6 hours of ventilation and perfusion. To understand the cell type which was undergoing proliferation, alveolar epithelial type II cells and proliferation marker were co-stained, indicating a decrease in proliferative alveolar epithelial type II positive cells after 6 hours in P9 mice lungs. However, an increase in proliferative alveolar epithelial type II cells after 6 hours was observed in P5 mice lungs. Pecam1 is a widely used marker for endothelial cells. Loss of Pecam1 disrupted alveolarization (DeLisser et al.,2016). No significant change in Pecam1 expression was found in P9 and P5 lungs after 4 and 6 hours of negative pressure ventilation and perfusion with alveologenesis medium revealing no significant changes in endothelial cells. Vimentin, an intermediate filament protein, acts as one of the major markers for epithelial-mesenchymal transition (Mendez et al.,2010). P5 mice lungs showed strong upregulation of vimentin expression after 4 and 6 hours of ventilation, whereas P9 mice lungs showed downregulation of vimentin expression when compared to unventilated control.

6.3 Effect on lung stem cell markers in *ex vivo* ventilated and perfused postnatal mice lungs

Studies indicate Fgf10 playing a vital role in lung repair after injury. Fgf10 prevents lung injury and stimulates epithelial regeneration (Gupte et al.,2009). Fgf10 also plays an important role in alveologenesis with respect to mesenchymal cell population and branching morphogenesis (Bellusci et al.,1997). Postnatal day 9 (P9) and postnatal day 5 (P5) mice lungs showed an increased expression of Fgf10 after four and six hours of ventilation and perfusion.

Wnt5a is a critical regulator and ligand for the PCP signaling pathway, which promotes differentiation and polarity during the process of alveologenesis (Pandit et al.,2019). Loss of Wnt5a caused defects in myofibroblasts and decreased proliferation of endothelial and alveolar epithelial type I cells leading to arrest in alveolarization. Dysregulated Wnt5a was observed in various disease conditions like fibrosis and COPD (Li et al.,2020). P9 mouse lungs, after 4 and 6 hours of ventilation and perfusion, showed decreased gene expression of Wnt5a. P5 mice lungs after 6 hours of ventilation and perfusion showed decreased expression of Wnt5a.

7. Limitations of the current study

It is critical to optimize the respiratory pressures and establish ventilation protocol that cuts down the ventilation-induced lung injury and allows the *ex vivo* model of ventilation and perfusion to run for longer hours, which would pave the way for a larger time frame to study the processed alveolarization. Current limitations of the model include edema formation that prevent lung ventilation (Hereero et al.,2018). The age and weight of the postnatal mice makes it difficult to further characterize the pulmonary physiology due to the lack of tools. It is also essential to further investigate positive and negative ventilation modes, characterize the molecular pathways affected by *ex vivo* ventilation and their outcomes in postnatal lung development. A long-running experiment (12-24 hours) of *ex vivo* ventilation and perfusion in postnatal mice could pave the way to a plethora of applications like modulating the process of alveologenesis by adding stem cells to the perfusate, improving alveolarization by adding certain drugs to the perfusate thereby effects on the lung can be studied. Gene editing could also be one of the long-term goals by introducing transgenic mutations through the perfusate, allowing to circulate in the lungs and understand the function of specific genes.

8. Conclusion

Alveolarization has been majorly investigated in recent times paving way to understand different respiratory cell types and molecular mechanisms involved in this well-controlled process. The present study aimed to investigate this critical process of lung development by establishing an *ex vivo* model of lung ventilation and perfusion. This model was first developed for neonates in the current study. Positive pressure ventilation incurred extreme damage to the fragile lung tissue, destroying the lung architecture and increased edema formation. However, morphometry data from negative pressure ventilation of lungs indicated that the negative pressure mode was protective and did not lead to overinflation of the lungs. Gene expression changes in different alveolar cell types provided insights on the processes occurring during the ventilation and perfusion of the lungs in *ex vivo* model. Alveolarization could not be studied over a long period of time as the maximum time of ventilation and perfusion in P5 and P9 lungs were 6 hours. Further ventilation parameter modifications and optimization of perfusates will be required to achieve our aim to study alveolarization using the current *ex vivo* model of lung ventilation and perfusion in neonatal mice.

9. Summary

Lung development has been studied extensively in recent years, generating new cognizance into the origins of different cell types that exist in the lungs as well as molecular pathways that regulate structural changes. Using transgenic mice is often limited due to a global lethal phenotype. This led to the development of tools such as organoid formation or precision-cut lung sections. However, such tools described had a major missing component, such as breathing movement inducing stretch forces. Including these forces to mimic an *in vivo* situation requested to develop an *ex vivo* ventilated and perfused lung model.

This project involved the establishment and validation an of *ex vivo* ventilated and perfused lung model using both positive and negative pressure ventilation. Neonatal mouse lungs were ventilated and perfused *ex vivo* for periods of 4 until 10 hours starting from postnatal day 5 until postnatal day 14 in positive pressure ventilation mode. Structural changes of the *ex vivo* ventilated lungs were compared with structural features of *in vivo* grown respective neonatal mouse lungs. Lungs ventilated using a positive pressure mode of ventilation showed major edema formation and morphological destruction. Alternatively, a negative pressure *ex vivo* ventilation and perfusion model were established for neonates. Optimizing ventilation and perfusion parameters to reach conditions of neonatal mouse physiology represented the first milestone of the project which was achieved by using different ventilation parameter values such as tidal volume, inspiratory pressure, expiratory pressure, respiration rate and perfusion with two different cell culture media along with the flow rate of perfusion. Thereby, ventilation-induced lung structural damage and analyses of possible structural and cellular changes of *ex vivo* ventilated and perfused lungs versus *in vivo* grown neonatal mouse lungs were analyzed.

Establishing an *ex vivo* model for neonates would pave way to a variety of applications like characterizing and modulating alveolarization using lineage tracing, cell depletion, pharmacological interventions, and gene editing thereby, studying cellular and molecular targets in lung development.

10.Zusammenfassung

Die Entwicklung der Lunge wurde in den letzten Jahren umfangreich erforscht, was zu neuen Erkenntnissen über den Ursprung der verschiedenen Zelltypen in der Lunge sowie über die molekularen Wege der Lungenreifung führte. Die Verwendung von transgenen Mäusen ist aufgrund eines letalen Phänotyps oft begrenzt. Dies führte zur Entwicklung von *ex vivo* Techniken wie der Bildung von Organoiden oder präzisionsgeschnittenen Lungenabschnitten. Bei diesen Methoden fehlten jedoch eine wichtige Komponenten, wie z. B. die durch die Atembewegung hervorgerufenen Dehnungskräfte. Die Einbeziehung dieser Kräfte zur Nachahmung einer *in vivo* Situation erforderte die Entwicklung eines *ex vivo* belüfteten und perfundierten Lungenmodells.

Im Rahmen dieses Projekts wurde ein *ex vivo* belüftetes und durchblutetes Lungenmodell mit Über- und Unterdruckbeatmung entwickelt und validiert. Die Lungen neonataler Mäuse wurden vom 5. bis zum 14. postnatalen Tag über einen Zeitraum von 4 bis 10 Stunden im Modus der Überdruckbeatmung *ex vivo* ventiliert und perfundiert. Strukturelle Veränderungen der *ex vivo* beatmeten Lungen wurden mit strukturellen Merkmalen von *in vivo* gereiften neonatalen Mäuselungen verglichen. Lungen, die im Überdruckmodus beatmet wurden, zeigten eine starke Ödembildung und morphologische Veränderungen. Alternativ wurde ein *ex vivo* Ventilations- und Perfusionsmodell mit Unterdruck für neugeborene entwickelt. Die Optimierung von Beatmungs- und Perfusionsparametern, um die Bedingungen der neonatalen Mausphysiologie zu erreichen, stellte den ersten Meilenstein des Projekts dar, der durch die Verwendung verschiedener Beatmungsparameter wie Tidalvolumen, Inspirationsdruck, Exspirationsdruck, Beatmungsrate und Perfusion mit zwei verschiedenen Zellkulturmedien zusammen mit der Flussrate der Perfusion erreicht wurde. Dabei wurden beatmungsinduzierte strukturelle Lungenschäden und Analysen möglicher zellulärer Veränderungen von *ex vivo* beatmeten und perfundierten Lungen im Vergleich zu *in vivo* gereiften neonatalen Mauslungen analysiert.

Die Etablierung eines *ex vivo* Modells für Neugeborene würde den Weg für eine Vielzahl von Anwendungen ebnen, wie z.B. die Charakterisierung und Modulation der Alveolarisierung mit Hilfe von *Lineage Tracing*, Zelldepletion, pharmakologischen Eingriffen und *Gene Editing*, um so zelluläre und molekulare Ziele in der Lungenreifung zu untersuchen.

11. References

1) A., O'Neill, J. D., Hozain, A. E., Tipograf, Y., Ukita, R., Stokes, J. W., Patel, Y. J., Pinezich, M., Talackine, J. R., Cardwell, N. L., Fung, K., Vunjak-Novakovic, G., & Bacchetta, M. (2022). **Technique for xenogeneic cross-circulation to support human donor lungs ex vivo.** *The Journal of Heart and Lung Transplantation : the official publication of the International Society for Heart Transplantation*, S1053-2498(22)02212-4.Advanceonlinepublication https://doi.org/10.1016/j.healun.2022.11.002
2) Acute Respiratory Distress Syndrome Network, Brower, R. G., Matthay, M. A., Morris, A., Schoenfeld, D., Thompson, B. T., & Wheeler, A. (2000). **Ventilation with lower tidal volumes as compared with traditional tidal volumes for acute lung injury and the acute respiratory distress syndrome.** *The New England Journal of Medicine*, *342*(18), 1301–1308. https://doi.org/10.1056/NEJM200005043421801
3) Adams, P. F., Hendershot, G. E., Marano, M. A., & Centers for Disease Control and Prevention/National Center for Health Statistics (1999). Current estimates from the National Health Interview Survey, 1996. *Vital and health statistics. Series 10, Data from the National Health Survey*, (200), 1–203.
4) Agassandian, M., & Mallampalli, R. K. (2013). **Surfactant phospholipid metabolism.** *Biochimica et Biophysica Acta*, *1831*(3), 612–625. https://doi.org/10.1016/j.bbalip.2012.09.010
5) Al Alam, D., El Agha, E., Sakurai, R., Kheirollahi, V., Moiseenko, A., Danopoulos, S., Shrestha, A., Schmoldt, C., Quantius, J., Herold, S., Chao, C. M., Tiozzo, C., De Langhe, S., Plikus, M. V., Thornton, M., Grubbs, B., Minoo, P., Rehan, V. K., & Bellusci, S. (2015). **Evidence for the involvement of fibroblast growth factor 10 in lipofibroblast formation during embryonic lung development**. *Development (Cambridge, England)*, *142*(23), 4139–4150. https://doi.org/10.1242/dev.109173
6) Amy, R. W., Bowes, D., Burri, P. H., Haines, J., & Thurlbeck, W. M. (1977). **Postnatal growth of the mouse lung.** *Journal of Anatomy*, *124*(Pt 1), 131–151.
7) Ashworth, L., Norisue, Y., Koster, M., Anderson, J., Takada, J., & Ebisu, H. (2018). **Clinical management of pressure control ventilation: An algorithmic method of patient ventilatory management to address "forgotten but important variables"**. *Journal of Critical Care*, *43*, 169–182. https://doi.org/10.1016/j.jcrc.2017.08.046

8) Bailey, Regina. **"The Lungs and Respiration."** ThoughtCo, Aug. 12, 2021, thoughtco.com/anatomy-of-the-lungs-373249

9) Barkauskas, C. E., Cronce, M. J., Rackley, C. R., Bowie, E. J., Keene, D. R., Stripp, B. R., Randell, S. H., Noble, P. W., & Hogan, B. L. (2013). **Type 2 alveolar cells are stem cells in adult lung.** *The Journal of Clinical Investigation*, *123*(7), 3025–3036. https://doi.org/10.1172/JCI68782

10) Barker, D. J., Godfrey, K. M., Fall, C., Osmond, C., Winter, P. D., & Shaheen, S. O. (1991). **Relation of birth weight and childhood respiratory infection to adult lung function and death from chronic obstructive airways disease**. *BMJ (Clinical Research Ed.)*, *303*(6804), 671–675. https://doi.org/10.1136/bmj.303.6804.671

11) Beitler, J. R., Malhotra, A., & Thompson, B. T. (2016). **Ventilator-induced Lung Injury**. *Clinics in Chest Medicine*, *37*(4), 633–646. https://doi.org/10.1016/j.ccm.2016.07.004

12) Bellusci, S., Grindley, J., Emoto, H., Itoh, N., & Hogan, B. L. (1997). **Fibroblast growth factor 10 (FGF10) and branching morphogenesis in the embryonic mouse lung.** *Development (Cambridge, England)*, *124*(23), 4867–4878. https://doi.org/10.1242/dev.124.23.4867

13) Beretta, E., Romanò, F., Sancini, G., Grotberg, J. B., Nieman, G. F., & Miserocchi, G. (2021). **Pulmonary Interstitial Matrix and Lung Fluid Balance From Normal to the Acutely Injured Lung.** *Frontiers in Physiology*, *12*, 781874. https://doi.org/10.3389/fphys.2021.781874

14) Bobba, C. M., Nelson, K., Dumond, C., Eren, E., Black, S. M., Englert, J. A., Ghadiali, S. N., & Whitson, B. A. (2021). **A Novel Negative Pressure-Flow Waveform to Ventilate Lungs for Normothermic Ex Vivo Lung Perfusion**. *ASAIO journal (American Society for Artificial Internal Organs : 1992)*, *67*(1), 96–103. https://doi.org/10.1097/MAT.0000000000001168

15) Boyden, E. A., & Tompsett, D. H. (1965). **The changing patterns in the developing lungs of infants.** *Acta Anatomica*, *61*(2), 164–192. https://doi.org/10.1159/000142692

16) Burri P. H. (1974). **The postnatal growth of the rat lung**. Morphology. *The Anatomical Record*, *180*(1), 77–98. https://doi.org/10.1002/ar.1091800109

17) Burri PH**. Lung development and pulmonary angiogenesis.** In: Gaultier C, Bourbon J, Post M, editors. *Lung Disease.* New York: Oxford University Press; 1999. pp. 122–151

18) Caduff, J. H., Fischer, L. C., & Burri, P. H. (1986). **Scanning electron microscope study of the developing microvasculature in the postnatal rat lung**. *The Anatomical Record, 216*(2), 154-164.

19) Carvalho CG, Silveira RC, Procianoy RS. **Ventilator-induced lung injury in preterm infants.** Rev Bras Ter Intensiva. 2013 Oct-Dec;25(4):319-26. doi: 10.5935/0103-507X.20130054. PMID: 24553514; PMCID: PMC4031878.

20) Chapman, H. A., Li, X., Alexander, J. P., Brumwell, A., Lorizio, W., Tan, K., Sonnenberg, A., Wei, Y., & Vu, T. H. (2011). **Integrin α6β4 identifies an adult distal lung epithelial population with regenerative potential in mice**. *The Journal of Clinical Investigation*, *121*(7), 2855–2862. https://doi.org/10.1172/JCI57673

21) Conway, R. F., Frum, T., Conchola, A. S., & Spence, J. R. (2020). **Understanding Human Lung Development through In Vitro Model Systems**. *BioEssays : news and reviews in molecular, cellular and developmental biology*, *42*(6), e2000006. https://doi.org/10.1002/bies.202000006

22) Corrado, A., & Gorini, M. (2002). **Negative-pressure ventilation: is there still a role?.** *The European Respiratory Journal*, *20*(1), 187–197. https://doi.org/10.1183/09031936.02.00302602

23) Corrado, A., Gorini, M., Villella, G., & De Paola, E. (1996). **Negative pressure ventilation in the treatment of acute respiratory failure: an old noninvasive technique reconsidered.** *The European Respiratory Journal*, *9*(7), 1531–1544. https://doi.org/10.1183/09031936.96.09071531

24) Critser, J. K., Laughlin, M. H., Prather, R. S., & Riley, L. K. (2009). **Proceedings of the Conference on Swine in Biomedical Research**. *ILAR journal*, *50*(1), 89–94. https://doi.org/10.1093/ilar.50.1.89.

25) da Silva da Costa, F. A., Soares, M. R., Malagutti-Ferreira, M. J., da Silva, G. R., Lívero, F. A. D. R., & Ribeiro-Paes, J. T. (2021). **Three-Dimensional Cell Cultures as a Research Platform in Lung Diseases and COVID-19.** *Tissue Engineering and Regenerative Medicine*, *18*(5), 735–745. https://doi.org/10.1007/s13770-021-00348-x

26) DeLisser, H. M., Helmke, B. P., Cao, G., Egan, P. M., Taichman, D., Fehrenbach, M., Zaman, A., Cui, Z., Mohan, G. S., Baldwin, H. S., Davies, P. F., & Savani, R. C. (2006). **Loss of PECAM-1 function impairs alveolarization**. *The Journal of Biological Chemistry*, *281*(13), 8724–8731. https://doi.org/10.1074/jbc.M511798200

27) Dickie, R., Wang, Y. T., Butler, J. P., Schulz, H., & Tsuda, A. (2008). **Distribution and quantity of contractile tissue in postnatal development of rat alveolar**

interstitium. *Anatomical Record (Hoboken, N.J. : 2007)*, *291*(1), 83–93. https://doi.org/10.1002/ar.20622

28) dos Santos, P. R., Iskender, I., Machuca, T., Hwang, D., dePerrot, M., Liu, M., Keshavjee, S., Waddell, T. K., & Cypel, M. (2014). **Modified in vivo lung perfusion allows for prolonged perfusion without acute lung injury.** *The Journal of Thoracic and Cardiovascular Surgery*, *147*(2), . https://doi.org/10.1016/j.jtcvs.2013.10.009

29) Eldridge, L., & Wagner, E. M. (2019). **Angiogenesis in the lung.** *The Journal of Physiology*, *597*(4), 1023–1032. https://doi.org/10.1113/JP275860

30) Faffe, D. S., & Zin, W. A. (2009). **Lung parenchymal mechanics in health and disease.** *Physiological Reviews*, *89*(3), 759–775. https://doi.org/10.1152/physrev.00019.2007

31) Fireman P. (2003). Understanding asthma pathophysiology. *Allergy and asthma proceedings*, *24*(2), 79–83.

32) Flodby, P., Borok, Z., Banfalvi, A., Zhou, B., Gao,D., Minoo, P., Ann, D. K., Morrisey, E. E., & Crandall, E. D. (2010). **Directed expression of Cre in alveolar epithelial type 1 cells.** *American Journal of Respiratory Cell and Molecular Biology*, *43*(2), 173–178. https://doi.org/10.1165/rcmb.2009-0226OC

33) Gaitonde, D. Y., Moore, F. C., & Morgan, M. K. (2019). **Influenza: Diagnosis and Treatment.** *American Family Physician*, *100*(12), 751–758.

34) Galasso, M., Feld, J. J., Watanabe, Y., Pipkin, M., Summers, C., Ali, A., Qaqish, R., Chen, M., Ribeiro, R. V. P., Ramadan, K., Pires, L., Bagnato, V. S., Kurachi, C., Cherepanov, V., Moonen, G., Gazzalle, A., Waddell, T. K., Liu, M., Keshavjee, S., Wilson, B. C., … Cypel, M. (2019). **Inactivating hepatitis C virus in donor lungs using light therapies during normothermic ex vivo lung perfusion**. *Nature Communications*, *10*(1), 481. https://doi.org/10.1038/s41467-018-08261-z

35) Gallacher DJ, Hart K, Kotecha S. **Common respiratory conditions of the newborn.** Breathe (Sheff). 2016 Mar;12(1):30-42. doi: 10.1183/20734735.000716. PMID: 27064402; PMCID: PMC4818233.

36) Ghafoor, T., Mahmud, S., Ali, S., & Dogar, S. A. (2003). **Incidence of respiratory distress syndrome.** *Journal of the College of Physicians and Surgeons--Pakistan : JCPSP*, *13*(5), 271–273.

37) Gilroy, A. M., et al. (2008). Atlas of Anatomy, Thieme.

38) Gultom, M., Laloli, L., & Dijkman, R. (2020). **Well-Differentiated Primary Mammalian Airway Epithelial Cell Cultures.** *Methods in Molecular Biology (Clifton, N.J.)*, *2203*, 119–134. https://doi.org/10.1007/978-1-0716-0900-2_10

39) Gupte, V. V., Ramasamy, S. K., Reddy, R., Lee, J., Weinreb, P. H., Violette, S. M., Guenther, A., Warburton, D., Driscoll, B., Minoo, P., & Bellusci, S. (2009). **Overexpression of fibroblast growth factor-10 during both inflammatory and fibrotic phases attenuates bleomycin-induced pulmonary fibrosis in mice.** *American Journal of Respiratory and Critical Care Medicine*, *180*(5), 424–436. https://doi.org/10.1164/rccm.200811-1794OC

40) Hahon, N., & Zimmerman, W. D. (1970). **Chikungunya virus infection of cell monolayers by cell-to-cell and extracellular transmission**. *Applied Microbiology*, *19*(2), 389–391. https://doi.org/10.1128/am.19.2.389-391.1970

41) Harfe, B. D., Scherz, P. J., Nissim, S., Tian, H., McMahon, A. P., & Tabin, C. J. (2004). **Evidence for an expansion-based temporal Shh gradient in specifying vertebrate digit identities**. *Cell*, *118*(4), 517–528. https://doi.org/10.1016/j.cell.2004.07.024

42) Haywood, N., Byler, M. R., Zhang, A., Roeser, M. E., Kron, I. L., & Laubach, V. E. (2020). **Isolated Lung Perfusion in the Management of Acute Respiratory Distress Syndrome.** *International Journal of Molecular Sciences*, *21*(18), 6820. https://doi.org/10.3390/ijms21186820

43) Herget, Jan & Chovanec, Milan. (2010). **Isolated perfused murine lung**. Drug Discovery Today: Disease Models. 7. 131–135. 10.1016/j.ddmod.2011.03.008.

44) Herrero, R., Sanchez, G., & Lorente, J. A. (2018). **New insights into the mechanisms of pulmonary edema in acute lung injury.** *Annals of Translational Medicine*, *6*(2), 32. https://doi.org/10.21037/atm.2017.12.18

45) Herriges, M., & Morrisey, E. E. (2014). **Lung development: orchestrating the generation and regeneration of a complex organ.** *Development (Cambridge, England)*, *141*(3), 502–513. https://doi.org/10.1242/dev.098186

46) Howatt, W. F., Avery, M. E., Humphreys, P. W., Normand, I. C., Reid, L., & Strang, L. B. (1965). **Factors affecting pulmonary surface properties in the foetal lamb.** *Clinical Science*, *29*(2), 239–248.

47) Hozain, A. E., O'Neill, J. D., Pinezich, M. R., Tipograf, Y., Donocoff, R., Cunningham, K. M., Tumen, A., Fung, K., Ukita, R., Simpson, M. T., Reimer, J. A., Ruiz, E. C., Queen, D., Stokes, J. W., Cardwell, N. L., Talackine, J., Kim, J., Snoeck, H. W., Chen, Y. W., Romanov, A., Vunjak-Novakovic, G. (2020). **Xenogeneic cross-circulation for**

extracorporeal recovery of injured human lungs. *Nature Medicine*, *26*(7), 1102–1113. https://doi.org/10.1038/s41591-020-0971-8

48) Iliodromiti, Z., Zygouris, D., Sifakis, S., Pappa, K. I., Tsikouras, P., Salakos, N., Daniilidis, A., Siristatidis, C., & Vrachnis, N. (2013). **Acute lung injury in preterm fetuses and neonates: mechanisms and molecular pathways**. *The Journal of Maternal-Fetal & Neonatal medicine : the official journal of the European Association of Perinatal Medicine, the Federation of Asia and Oceania Perinatal Societies, the International Society of Perinatal Obstetricians*, *26*(17), 1696–1704. https://doi.org/10.3109/14767058.2013.798284

49) Irvin, C. G., & Bates, J. H. (2003). **Measuring the lung function in the mouse: the challenge of size.** *Respiratory Research*, *4*(1), 4. https://doi.org/10.1186/rr199

50) Janssen, R., Piscaer, I., Franssen, F. M. E., & Wouters, E. F. M. (2019). **Emphysema: looking beyond alpha-1 antitrypsin deficiency**. *Expert Review of Respiratory Medicine*, *13*(4), 381–397. https://doi.org/10.1080/17476348.2019.1580575

51) Jobe, A. H., & Bancalari, E. (2001). **Bronchopulmonary dysplasia**. *American Journal of Respiratory and Critical Care Medicine*, *163*(7), 1723–1729. https://doi.org/10.1164/ajrccm.163.7.2011060

52) K.L. Moore, T.V.N. Persaud & M.G. Torchia: **The Developing Human: Clinically Oriented** Embryology, 10th edition, Elsevier (2016), p. 355-378

53) Kelly Wu, W. Kasper, M., & Barth, K. (2017). **Potential contribution of alveolar epithelial type I cells to pulmonary fibrosis.** *Bioscience Reports*, *37*(6), BSR20171301. https://doi.org/10.1042/BSR20171301

54) Knudsen, L., & Ochs, M. (2018). **The micromechanics of lung alveoli: structure and function of surfactant and tissue components**. *Histochemistry and cell biology*, *150*(6), 661–676. https://doi.org/10.1007/s00418-018-1747-9

55) Knust, J., Ochs, M., Gundersen, H. J., & Nyengaard, J. R. (2009). **Stereological estimates of alveolar number and size and capillary length and surface area in mice lungs.** *AnatomicalRecord(Hoboken,N.J.:2007)*, *292*(1),113–122. https://doi.org/10.1002/ar.20747

56) Kühbandner, S., Brummer, S., Metzger, D., Chambon, P., Hofmann, F., & Feil, R. (2000). **Temporally controlled somatic mutagenesis in smooth muscle.** *Genesis (New York,N.Y.:2000)*, *28*(1),15–22.https://doi.org/10.1002/1526-968x(200009)28:1<15::aid-gene20>3.0.co;2-c

57) Lacroix, G., Koch, W., Ritter, D., Gutleb, A. C., Larsen, S. T., Loret, T., Zanetti, F., Constant, S., Chortarea, S., Rothen-Rutishauser, B., Hiemstra, P. S., Frejafon, E., Hubert, P., Gribaldo, L., Kearns, P., Aublant, J. M., Diabaté, S., Weiss, C., de Groot, A., & Kooter, I. (2018). **Air-Liquid Interface *In Vitro* Models for Respiratory Toxicology Research: Consensus Workshop and Recommendations**. *Applied in vitro toxicology*, *4*(2), 91–106. https://doi.org/10.1089/aivt.2017.0034

58) Li, C., Smith, S. M., Peinado, N., Gao, F., Li, W., Lee, M. K., Zhou, B., Bellusci, S., Pryhuber, G. S., Ho, H. H., Borok, Z., & Minoo, P. (2020). **WNT5a-ROR Signaling Is Essential for Alveologenesis.** *Cells*, *9*(2), 384. https://doi.org/10.3390/cells9020384

59) Li, J., Zhou, J., Zhang, D., Song, Y., She, J., & Bai, C. (2015). **Bone marrow-derived mesenchymal stem cells enhance autophagy via PI3K/AKT signaling to reduce the severity of ischaemia/reperfusion-induced lung injury.** *Journal of Cellular and Molecular Medicine*, *19*(10), 2341–2351. https://doi.org/10.1111/jcmm.12638

60) Lindahl, P., Karlsson, L., Hellström, M., Gebre-Medhin, S., Willetts, K., Heath, J. K., & Betsholtz, C. (1997). **Alveologenesis failure in PDGF-A-deficient mice is coupled to lack of distal spreading of alveolar smooth muscle cell progenitors during lung development**. *Development (Cambridge, England)*, *124*(20), 3943–3953. https://doi.org/10.1242/dev.124.20.3943

61) Loor, G., Howard, B. T., Spratt, J. R., Mattison, L. M., Panoskaltsis-Mortari, A., Brown, R. Z., Iles, T. L., Meyer, C. M., Helms, H. R., Price, A., & Iaizzo, P. A. (2017). **Prolonged EVLP Using OCS Lung: Cellular and Acellular Perfusates.** *Transplantation*, *101*(10),2303–2311. https://doi.org/10.1097/TP.0000000000001616

62) Madurga, A., Mizíková, I., Ruiz-Camp, J., & Morty, R. E. (2013). **Recent advances in late lung development and the pathogenesis of bronchopulmonary dysplasia**. *American journal of physiology. Lung Cellular and Molecular Physiology*, *305*(12), L893–L905. https://doi.org/10.1152/ajplung.00267.2013

63) Manghwar, H., Li, B., Ding, X., Hussain, A., Lindsey, K., Zhang, X., & Jin, S. (2020). **CRISPR/Cas Systems in Genome Editing: Methodologies and Tools for sgRNA Design, Off-Target Evaluation, and Strategies to Mitigate Off-Target Effects**. *Advanced Science (Weinheim, Baden-Wurttemberg, Germany)*, *7*(6), 1902312. https://doi.org/10.1002/advs.201902312

64) Mason, R. *Murray & Nadel's Textbook of Respiratory Medicine 5th Edition*, Elsevier Saunders, 2010.

65) Massaro, D., & Massaro, G. D. (2010). **Lung development, lung function, and retinoids.** *The New England Journal of Medicine*, *362*(19), 1829–1831. https://doi.org/10.1056/NEJMe1002366

66) Medeiros, I. L., Pêgo-Fernandes, P. M., Mariani, A. W., Fernandes, F. G., do Vale Unterpertinger, F., Canzian, M., & Jatene, F. B. (2012). **Histologic and functional evaluation of lungs reconditioned by *ex vivo* lung perfusion.** *The Journal of Heart and Lung Transplantation : the official publication of the International Society for Heart Transplantation*, *31*(3), 305–309. https://doi.org/10.1016/j.healun.2011.10.005

67) Mendez, M. G., Kojima, S., & Goldman, R. D. (2010). **Vimentin induces changes in cell shape, motility, and adhesion during the epithelial to mesenchymal transition**. *FASEB journal : official publication of the Federation of American Societies for Experimental Biology*, *24*(6), 1838–1851. https://doi.org/10.1096/fj.09-151639

68) Moses, K. A., DeMayo, F., Braun, R. M., Reecy, J. L., & Schwartz, R. J. (2001). **Embryonic expression of an Nkx2-5/Cre gene using ROSA26 reporter mice**. *Genesis(NewYork,N.Y.:2000)*, *31*(4),176–180. https://doi.org/10.1002/gene.10022

69) Mukhopadhyay, S., Hoidal, J. R., & Mukherjee, T. K. (2006). **Role of TNF alpha in pulmonary pathophysiology.** *Respiratory Research*, *7*(1), 125. https://doi.org/10.1186/1465-9921-7-125

70) Naeem, A., Rai, S. N., & Pierre, L. (2022). **Histology, Alveolar Macrophages**. In *Stat Pearls*. StatPearls Publishing

71) Nelson K, Bobba C, Ghadiali S, Hayes D Jr, Black SM, Whitson BA. **Animal models of ex vivo lung perfusion as a platform for transplantation research.** World J Exp Med. 2014 May 20;4(2):7-15. Doi: 10.5493/wjem.v4.i2.7. PMID: 24977117; PMCID: PMC4073219.)

72) Pacheco-Baltazar, A., Arreola-Ramírez, J. L., Alquicira-Mireles, J., & Segura-Medina, P. (2021). **Isolated Lung Perfusion System in the Rabbit Model**. *Journal of Visualized Experiments : JoVE*, (173), 10.3791/62734. https://doi.org/10.3791/62734

73) Pan, H., Deutsch, G. H., Wert, S. E., Ontology Subcommittee, & NHLBI Molecular Atlas of Lung Development Program Consortium (2019). **Comprehensive anatomic ontologies for lung development: A comparison of alveolar formation and maturation within mouse and human lung.** *Journal of Biomedical Semantics*, *10*(1), 18. https://doi.org/10.1186/s13326-019-0209-1

74) Pan, X., Yang, J., Fu, S., & Zhao, H. (2018). **Application of *ex vivo* lung perfusion (EVLP) in lung .transplantation.** *Journal of Thoracic Disease*, *10*(7), 4637–4642. https://doi.org/10.21037/jtd.2018.07.95

75) Pandit, A. A., Gandham, R. K., Mukhopadhyay, C. S., Verma, R., & Sethi, R. S. (2019). **Transcriptome analysis reveals the role of the PCP pathway in fipronil and endotoxin-induced lung damage**. *Respiratory Research*, *20*(1), 24. https://doi.org/10.1186/s12931-019-0986-1

76) Papaioannou, V. E., & Behringer, R. R. (2012). **Early embryonic lethality in genetically engineered mice: diagnosis and phenotypic analysis**. *Veterinary Pathology*, *49*(1), 64–70. https://doi.org/10.1177/0300985810395725

77) Perl, A. K., Riethmacher, D., & Whitsett, J. A. (2011). **Conditional depletion of airway progenitor cells induces peribronchiolar fibrosis.** *American Journal of Respiratory and Critical Care Medicine*, *183*(4), 511–521. https://doi.org/10.1164/rccm.201005-0744OC

78) Petersson, J., & Glenny, R. W. (2014). **Gas exchange and ventilation-perfusion relationships in the lung.** *The European Respiratory Journal*, *44*(4), 1023–1041. https://doi.org/10.1183/09031936.00037014

79) Pichl, A., Sommer, N., Bednorz, M., Seimetz, M., Hadzic, S., Kuhnert, S., Kraut, S., Roxlau, E. T., Kojonazarov, B., Wilhelm, J., Gredic, M., Gall, H., Tello, K., Richter, M. J., Pak, O., Petrovic, A., Hecker, M., Schermuly, R. T., Grimminger, F., Seeger, W., … Weissmann, N. (2019). **Riociguat for treatment of pulmonary hypertension in COPD: a translational study.** *The European Respiratory Journal*, *53*(6), 1802445. https://doi.org/10.1183/13993003.02445-2018

80) Pieretti, A. C., Ahmed, A. M., Roberts, J. D., Jr, & Kelleher, C. M. (2014). **A novel in vitro model to study alveologenesis.** *American Journal of Respiratory Cell and Molecular Biology*, *50*(2), 459–469. https://doi.org/10.1165/rcmb.2013-0056OC

81) Rawlins, E. L., & Perl, A. K. (2012**). The a"MAZE"ing world of lung-specific transgenic mice.** *American Journal of Respiratory Cell and Molecular Biology*, *46*(3), 269–282. https://doi.org/10.1165/rcmb.2011-0372PS

82) Rawlins, E. L., Ostrowski, L. E., Randell, S. H., & Hogan, B. L. (2007). **Lung development and repair: contribution of the ciliated lineage.** *Proceedings of the National Academy of Sciences of the United States of America*, *104*(2), 410–417. https://doi.org/10.1073/pnas.0610770104

83) Richeldi, L., Collard, H. R., & Jones, M. G. (2017). **Idiopathic pulmonary fibrosis.** *Lancet(London,England)*, *389*(10082),1941–1952. https://doi.org/10.1016/S0140-6736(17)30866-8

84) Rippa, A. L., Alpeeva, E. V., Vasiliev, A. V., & Vorotelyak, E. A. (2021). Alveologenesis: **What Governs Secondary Septa Formatio**n. *International Journal of Molecular Sciences*, *22*(22), 12107. https://doi.org/10.3390/ijms222212107

85) Rock, J. R., Onaitis, M. W., Rawlins, E. L., Lu, Y., Clark, C. P., Xue, Y., Randell, S. H., & Hogan, B. L. (2009). **Basal cells as stem cells of the mouse trachea and human airway epithelium.** *Proceedings of the National Academy of Sciences of the United States of America*, *106*(31), 12771–12775. https://doi.org/10.1073/pnas.0906850106

86) Rydell-Törmänen, K., & Johnson, J. R. (2019). **The Applicability of Mouse Models to the Study of Human Disease.** *Methods in Molecular Biology (Clifton, N.J.)*, *1940*, 3–22. https://doi.org/10.1007/978-1-4939-9086-3_1

87) Sakagami M. (2006). **In vivo, in vitro and ex vivo models to assess pulmonary absorption and disposition of inhaled therapeutics for systemic delivery**. *Advanced DrugDeliveryReviews*, *58*(9-10),1030–1060. https://doi.org/10.1016/j.addr.2006.07.012

88) Schittny J. C. (2017). **Development of the lung**. *Cell and Tissue Research*, *367*(3), 427–444. https://doi.org/10.1007/s00441-016-2545-0

89) Schittny JC, Burri PH. **Development and growth of the lung**. In: Fishman AP, Elias JA, Fishman JA, Grippi MA, Kaiser LR, Senior RM, editors. *Fishman's Pulmonary Diseases and Disorders.* New-York: McGraw-Hill; 2008. pp. 91–114

90) Schittny JC, Mund SI. **A re-examination of the maturation of the alveolar septa revealed that microvascular maturation takes place in parallel to alveolarization**. *Am J Respir Crit Care Med.* 2008;177:A317.

91) Schittny, J. C., Djonov, V., Fine, A., & Burri, P. H. (1998). **Programmed cell death contributes to postnatal lung development.** *American Journal of Respiratory Cell and Molecular Biology*, *18*(6), 786–793. https://doi.org/10.1165/ajrcmb.18.6.3031

92) Schuessler, T. F., & Bates, J. H. (1995). A computer-controlled research ventilator for small animals: design and evaluation. *IEEE Transactions on Bio-medical Engineering*, *42*(9), 860–866. https://doi.org/10.1109/10.412653

93) Seeger, W., Walmrath, D., Heimburger, N., & Neuhof, H. (1986**). Fibronectin decreases pulmonary vascular permeability under baseline conditions and after administration of arachidonic acid in rabbit lungs.** *Thrombosis Research*, *44*(2), 135–146. https://doi.org/10.1016/0049-3848(86)90129-5

94) Seimetz, M., Parajuli, N., Pichl, A., Bednorz, M., Ghofrani, H. A., Schermuly, R. T., Seeger, W., Grimminger, F., & Weissmann, N. (2015). **Cigarette Smoke-Induced Emphysema and Pulmonary Hypertension Can Be Prevented by Phosphodiesterase 4 and 5 Inhibition in Mice.** *PloS one*, *10*(6), e0129327. https://doi.org/10.1371/journal.pone.0129327

95) Seimetz, M., Parajuli, N., Pichl, A., Veit, F., Kwapiszewska, G., Weisel, F. C., Milger, K., Egemnazarov, B., Turowska, A., Fuchs, B., Nikam, S., Roth, M., Sydykov, A., Medebach, T., Klepetko, W., Jaksch, P., Dumitrascu, R., Garn, H., Voswinckel, R., Kostin, S., Weissmann, N. (2011). **Inducible NOS inhibition reverses tobacco-smoke-induced emphysema and pulmonary hypertension in mice**. *Cell*, *147*(2), 293–305. https://doi.org/10.1016/j.cell.2011.08.035

96) Shennan, A. T., Dunn, M. S., Ohlsson, A., Lennox, K., & Hoskins, E. M. (1988). **Abnormal pulmonary outcomes in premature infants: prediction from oxygen requirement in the neonatal period**. *Pediatrics*, *82*(4), 527–532.

97) Shrestha, J., Razavi Bazaz, S., Aboulkheyr Es, H., Yaghobian Azari, D., Thierry, B., Ebrahimi Warkiani, M., & Ghadiri, M. (2020). **Lung-on-a-chip: the future of respiratory disease models and pharmacological studies.** *Critical Reviews in Biotechnology*, *40*(2), 213–230. https://doi.org/10.1080/07388551.2019.1710458

98) Steen, S., Liao, Q., Wierup, P. N., Bolys, R., Pierre, L., & Sjöberg, T. (2003). **Transplantation of lungs from non-heart-beating donors after functional assessment ex vivo**. *The Annals of Thoracic Surgery*, *76*(1), 244–252. https://doi.org/10.1016/s0003-4975(03)00191-7.

99) Strikoudis, A., Cieślak, A., Loffredo, L., Chen, Y. W., Patel, N., Saqi, A., Lederer, D. J., & Snoeck, H. W. (2019). **Modeling of Fibrotic Lung Disease Using 3D Organoids Derived from Human Pluripotent Stem Cells.** *Cell Reports*, *27*(12), 3709–3723.e5. https://doi.org/10.1016/j.celrep.2019.05.077

100) Swan, A. J., & Tawhai, M. H. (2011). **Evidence for minimal oxygen heterogeneity in the healthy human pulmonary acinus.** *Journal of Applied Physiology (Bethesda, Md. : 1985)*, *110*(2), 528–537. https://doi.org/10.1152/japplphysiol.00888.2010

101) T.W. Sadler: Langman's Medical Embryology, 12th edition, Wolters Kluwer, Lippincott Williams & Wilkins (2012), p. 133-161

102) Thébaud, B., & Abman, S. H. (2007). **Bronchopulmonary dysplasia: where have all the vessels gone? Roles of angiogenic growth factors in chronic lung**

disease. *American Journal of Respiratory and Critical Care Medicine*, *175*(10), 978–985. https://doi.org/10.1164/rccm.200611-1660PP

103) Tomashefski J. F., Jr (1990). **Pulmonary pathology of the adult respiratory distress syndrome.** *Clinics in Chest Medicine*, *11*(4), 593–619.

104) Torday, J., Hua, J., & Slavin, R. (1995). **Metabolism and fate of neutral lipids of fetal lung fibroblast origin.** *Biochimica et Biophysica Acta*, *1254*(2), 198–206. https://doi.org/10.1016/0005-2760(94)00184-z

105) Tremblay, L., Valenza, F., Ribeiro, S. P., Li, J., & Slutsky, A. S. (1997). **Injurious ventilatory strategies increase cytokines and c-fos mRNA expression in an isolated rat lung model**. *The Journal of Clinical Investigation*, *99*(5), 944–952. https://doi.org/10.1172/JCI119259

106) Vazquez-Armendariz, A. I., Heiner, M., El Agha, E., Salwig, I., Hoek, A., Hessler, M. C., Shalashova, I., Shrestha, A., Carraro, G., Mengel, J. P., Günther, A., Morty, R. E., Vadász, I., Schwemmle, M., Kummer, W., Hain, T., Goesmann, A., Bellusci, S., Seeger, W., Braun, T., … Herold, S. (2020). **Multilineage murine stem cells generate complex organoids to model distal lung development and disease.** *The EMBO journal*, *39*(21), e103476. https://doi.org/10.15252/embj.2019103476

107) Vila Ellis, L., & Chen, J. (2021). **A cell-centric view of lung alveologenesis.** *Developmental dynamics : an official publication of the American Association of Anatomists*, *250*(4), 482–496. https://doi.org/10.1002/dvdy.271

108) Vogelmeier, C. F., Román-Rodríguez, M., Singh, D., Han, M. K., Rodríguez-Roisin, R., & Ferguson, G. T. (2020). **Goals of COPD treatment: Focus on symptoms and exacerbations.** *Respiratory Medicine*, *166*, 105938. https://doi.org/10.1016/j.rmed.2020.105938

109) Ware, L. B., & Matthay, M. A. (2005). **Clinical practice. Acute pulmonary edema.** *The New England Journal of Medicine*, *353*(26), 2788–2796. https://doi.org/10.1056/NEJMcp052699

110) Watanabe, T., Cypel, M., & Keshavjee, S. (2021). ***Ex vivo* lung perfusion.** *Journal of Thoracic Disease*, *13*(11), 6602–6617. https://doi.org/10.21037/jtd-2021-23

111) Weathington, N. M., Álvarez, D., Sembrat, J., Radder, J., Cárdenes, N., Noda, K., Gong, Q., Wong, H., Kolls, J., D'Cunha, J., Mallampalli, R. K., Chen, B. B., & Rojas, M. (2018). **Ex vivo lung perfusion as a human platform for preclinical small molecule testing.** *JCI insight*, *3*(19), e95515. https://doi.org/10.1172/jci.insight.95515

112) Weissmann, N., Grimminger, F., Walmrath, D., & Seeger, W. (1995). **Hypoxic vasoconstriction in buffer-perfused rabbit lungs.** *Respiration Physiology*, *100*(2), 159–169. https://doi.org/10.1016/0034-5687(94)00133-k

113) Weissmann, N., Kuzkaya, N., Fuchs, B., Tiyerili, V., Schäfer, R. U., Schütte, H., Ghofrani, H. A., Schermuly, R. T., Schudt, C., Sydykov, A., Egemnazarow, B., Seeger, W., & Grimminger, F. (2005). **Detection of reactive oxygen species in isolated, perfused lungs by electron spin resonance spectroscopy**. *Respiratory Research*, *6*(1), 86. https://doi.org/10.1186/1465-9921-6-86

114) Weissmann, N., Lobo, B., Pichl, A., Parajuli, N., Seimetz, M., Puig-Pey, R., Ferrer, E., Peinado, V. I., Domínguez-Fandos, D., Fysikopoulos, A., Stasch, J. P., Ghofrani, H. A., Coll-Bonfill, N., Frey, R., Schermuly, R. T., García-Lucio, J., Blanco, I., Bednorz, M., Tura-Ceide, O., Tadele, E., Barberà, J. A. (2014). **Stimulation of soluble guanylate cyclase prevents cigarette smoke-induced pulmonary hypertension and emphysema.** *American Journal of Respiratory and Critical Care Medicine*, *189*(11), 1359–1373. https://doi.org/10.1164/rccm.201311-2037OC

115) Wiig, H., Opdahl, H., Nicolaysen, A., & Nicolaysen, G. (1985). **Interstitial fluid pressure in the isolated perfused rabbit lung.** *Acta Physiologica Scandinavica*, *125*(4), 601–607. https://doi.org/10.1111/j.1748-1716.1985.tb07761.x

116) Wilson, M. R., Choudhury, S., & Takata, M. (2005). **Pulmonary inflammation induced by high-stretch ventilation is mediated by tumor necrosis factor signaling in mice.** *American Journal of Physiology. Lung Cellular and Molecular Physiology*, *288*(4), L599–L607. https://doi.org/10.1152/ajplung.00304.2004

117) Wolthuis, E. K., Vlaar, A. P., Choi, G., Roelofs, J. J., Juffermans, N. P., & Schultz, M. J. (2009). **Mechanical ventilation using non-injurious ventilation settings causes lung injury in the absence of pre-existing lung injury in healthy mice**. *Critical care (London, England)*, *13*(1), R1. https://doi.org/10.1186/cc7688

118) Xing, Y., Li, C., Li, A., Sridurongrit, S., Tiozzo, C., Bellusci, S., Borok, Z., Kaartinen, V., & Minoo, P. (2010). **Signaling via Alk5 controls the ontogeny of lung** Clara cells. *Development (Cambridge, England)*, *137*(5), 825–833. https://doi.org/10.1242/dev.040535

119) Yaroshenko, A., Pritzke, T., Koschlig, M., Kamgari, N., Willer, K., Gromann, L., Auweter, S., Hellbach, K., Reiser, M., Eickelberg, O., Pfeiffer, F., & Hilgendorff, A. (2016). **Visualization of neonatal lung injury associated with mechanical ventilation**

using x-ray dark-field radiography. *Scientific Reports*, *6*, 24269. https://doi.org/10.1038/srep24269

120) Yoo, H. Y., Zeifman, A., Ko, E. A., Smith, K. A., Chen, J., Machado, R. F., Zhao, Y. Y., Minshall, R. D., & Yuan, J. X. (2013). **Optimization of isolated perfused/ventilated mouse lung to study hypoxic pulmonary vasoconstriction**. *Pulmonary Circulation*, *3*(2), 396–405. https://doi.org/10.4103/2045-8932.114776

121) Zepp, J. A., Zacharias, W. J., Frank, D. B., Cavanaugh, C. A., Zhou, S., Morley, M. P., & Morrisey, E. E. (2017). **Distinct Mesenchymal Lineages and Niches Promote Epithelial Self-Renewal and Myofibrogenesis in the Lung.** *Cell*, *170*(6), 1134–1148.e10. https://doi.org/10.1016/j.cell.2017.07.034

12. List of Tables

13. List of figures:

14. List of Abbreviations and Acronyms

°C - Degree Celsius

ACTA2 – Alpha- smooth muscle actin

ADRP -Adipose differentiation-related protein (Adipophilin or ADFP)

ARDS – Acute respiratory distress syndrome

ALI – Air liquid interface

ANOVA – Analysis of Variance

BPD – Bronchopulmonary dysplasia

BrdU- Bromodeoxyuridine

BSA – Bovine serum albumin

cDNA – complementary deoxyribonucleic acid

CLSM – Confocal laser scanning microscopy

Col4a1 – Collagen alpha – 1 (IV) chain

COPD – Chronic obstructive pulmonary disease

Ct- Cycle threshold

DMEM – Dulbecco's Modified Eagle Medium

E – Embryonic

ECM – Extracellular matrix

EMT – Epithelial to mesenchymal transition

EVLP – *Ex vivo* lung ventilation and perfusion

FC – Fold change

FGF – Fibroblast growth factor

H & E – Hematoxylin and Eosin

H_2O - Water

Hg – Mercury

ILU – Isolated lung unit

Kg – Kilogram

KHB – Krebs-Henseleit Buffer

Mg – milli gram

mL – Milliliter

mm - millimeter

MLI – Mean linear intercept

mRNA – messenger ribonucleic acid

P – Postnatal day

PBS – Phosphate buffered saline

PCLS – Precision cut lung slices

PCR – Polymerase chain reaction

PDGFRA – Platelet-derived growth factor alpha

PECAM – Platelet Endothelial cell adhesion molecule

PEEP – positive end expiratory pressure

PFA – Para formaldehyde

RLT – RNA lysis buffer

RNA – Ribonucleic acid

RR- Respiration rate

RT – PCR – Reverse transcription polymerase chain reaction

RT – Room temperature

rpm – rotations per minute

SD – Standard deviation

SDS – Sodium dodecyl sulfate

SFTPC - Surfactant protein C

TBS – Tris buffered saline

TNF – Tumor necrosis factor

VCM – Ventilation control module

VILI – Ventilator induced lung damage.

VP – Ventilation pressure

Wnt – Wingless/ Integrated

µg- microgram

15. Declaration

"I declare that I have completed this dissertation single-handedly without the unauthorized help of a second party and only with the assistance acknowledged therein. I have appropriately acknowledged and referenced all text passages that are derived literally from or are based on the content of published or unpublished work of others, and all information that relates to verbal communications. I have abided by the principles of good scientific conduct laid down in the charter of the Justus Liebig University of Giessen in carrying out the investigations described in the dissertation."

Reshma Jamal

16. Acknowledgements:

I would like to convey my heartfelt gratitude to each and every person who helped me and were a part of my PhD journey and made the completion of my doctoral study possible.

First of all, I would like to express my deepest thanks to Prof. Werner Seeger, Prof. Rory Morty and to Dr. Dr. Katrin Ahlbrecht and my co-supervisor Prof. Ivan Manzini for believing in me and giving this opportunity to excel and guiding me in each and every stage of the process and providing me all required resources and great mentorship. I would want to extend my thanks to Dominik for helping me set up the negative pressure ventilation set up, Robin for assisting me in gene expression studies and Jonas for lending his helping hand to take over the experiments during long hours and for their continuous support and positivity when I had tough times during my experiments. I would like to acknowledge MBML (Molecular Biology and Medicine of the Lung) program with the best mentors Prof. Rory Morty and Dr. Janine during my first part of the curriculum along with Prof. Elie El Agha and Prof. Ana Ivonne . My lab mates at the Max Planck Institute for Heart and Lung Research, Bad Nauheim Claudio, Despina, Ettore, Misa, Francisco, David ,Francesco, Solmaz, Thjis and Sven. My great appreciation goes to Karin Quanz, senior technician and Dagmar Fenner-Nau in ECCPS (Excellence Cluster of Cardiopulmonary System) for their tremendous technical knowledge and zeal in giving her views and guidance in this project. Many thanks to the Animal House staff Nashia, Laura and Sabrina. I would extend my thanks to Jun.Prof.Miguel in motivating and joining hands in our project.

Family has always been my greatest pillar of support. My father, Mr. Jamal and my mother Mrs. Ameena Jamal for their everlasting love, support, motivation and realized my capabilities even before I knew and constantly stood by me during this journey. My husband, Aneef who supported in this journey and been a supporting hand all through it. Many thanks to my daughter Alaiya for making my life meaningful and for being so understanding! Mumma loves you munna. My other gem, Adyan who recently entered our life bringing in joy and has made our family complete. My extended thanks to the members of TP family (my in-laws, brother-in laws and sister-in laws).

This journey counts the blessings of each and every one of them who has made me stand where I am today and my gratitude and appreciation for this would continue lifelong!